Title
Regulation Of Vascular Stem Cells By Transcription Factor And Microenvironment

Author
Chang, Julia Haewon

Publication Date
2015

Peer reviewed|Thesis/dissertation

Regulation Of Vascular Stem Cells By Transcription Factor And Microenvironment

By

Julia Haewon Chang

A dissertation submitted in partial satisfaction of the requirements

for the degree of

Doctor of Philosophy

in

Molecular and Cell Biology

in the

Graduate Division

of the

University of California, Berkeley

Committee in Charge:

Professor Song Li, Co-Chair

Professor John Ngai, Co-Chair

Professor Richard Harland

Professor Gerard Marriott

Fall 2015

Abstract

Regulation Of Vascular Stem Cells By Transcription Factor And Microenvironment

by
Julia Haewon Chang
Doctor of Philosophy in Molecular and Cell Biology
University of California, Berkeley
Professor Song Li, Co-Chair
Professor John Ngai, Co-Chair

Cardiovascular diseases (CVDs) cause about 31% of all global deaths. As people age, CVD progress due to the accumulation of fatty materials, immune cells, and smooth muscle cells form stabilized fatty plaques in blood vessels through a process known as atherosclerosis. Atherosclerosis plaques affect vessel wall integrity, elasticity, and occlude blood flow, which can result in death. Top risk factors of CVDs include tobacco use, alcohol, blood pressure, and blood cholesterol levels. In order to develop better drug treatment strategies, it is important to elucidate the cellular mechanisms that drive CVD progression within the vessel wall. In healthy blood vessels, smooth muscle cells have a low proliferating rate, low synthesis activity, and high expression of contractility proteins and ion channels important in responding to vessel contraction, tone, and blood pressure.

In chapter one, I discuss current theories on what cells directly contribute to vessel wall repair and/or disease progression. The de-differentiation hypothesis proposes that vascular smooth muscle cells directly contribute to CVDs. This phenotypic switch, or de-differentiation, results in smooth muscle cells that down-regulate expression of contractility proteins, rapidly proliferate and migrate into the damaged area. The heterogeneous population of cells observed in diseased vessels is the result of smooth muscle cell de-differentiation. The isolation and characterization of side populations of vascular stem cells (VSCs) in the vessel wall presents an additional cell source that may also contribute to healthy and diseased vessel wall repair. Previous work from our group characterized a population of multipotent VSCs. In healthy vessel repair, VSCs are activated and differentiate to smooth muscle cell end fates. However, in diseased vessels, aberrant differentiation of VSCs could contribute to the heterogeneous population of fat, bone, and chondrogenic cells.

In chapter two, we characterized how matrix elasticity regulates VSC proliferation, expression of SMC markers, and cellular localization of mechanical signaling factors. We began by confirming trends of previous DNA microarray results when rat VSCs were seeded on polyacrylamide hydrogels (pAAm). While average nuclear area also decreases as matrix elasticity decreases, the rate of cell proliferation was approximately equal compared to glass control. Based on previous work, we tested whether global decreases in nuclear area also led to global chromatin remodeling, primarily detected through histone tail modifications. We did not find global changes in response to matrix elasticity. Instead, we were able to show that smooth muscle marker protein expression decreases as a function of matrix elasticity. As matrix elasticity decreases, F-actin stress fibers decrease, which increases relative pools of G-actin. G-actin can

bind to Myocardin-related transcription factor A, which activates gene transcription of contractile and cytoskeletal proteins, including smooth muscle a-actin.

In chapter three, we describe multiple attempts to characterize the role of Sox family of transcription factor by either targeted knockdown or overexpression. We hypothesized that high expression of two Sox family members, Sox10 and Sox17, in early passage rat VSCs affects vascular stem cell maintenance and/or prevents differentiation. We attempted to use short- and long-term targeted knockdown of Sox protein in rat VSCs. Specifically, we characterized the effects on VSCs proliferation, smooth muscle cell gene expression, cell migration, and directed differentiation. Due to the recovery of Sox gene and protein expression, our results were inconclusive. When we tried to overexpress a GFP-tagged Sox10, we saw dramatic decreases in GFP^+ cells after 7 days in culture.

In this work, we were able to determine: (1) Rat VSCs respond to matrix elasticity, a mechanical signal, and decrease expression of smooth muscle cell markers. (2) Matrix elasticity decreases MRTF-A nuclear localization in rat VSCs. (3) As a result, direct downstream targets of MRTF-A, like SMA, also decrease.

Our data for targeted knockdown of Sox10 and Sox17 in rat VSCs were inconclusive. Rat VSCs showed recovery of Sox protein expression after siRNA transfection. Instead, we tried to generate stable shRNA rat VSC lines, but did not see reduced Sox10 staining compared to scrambled control.

Table of Contents

List of Figures

List of Tables

Commonly Used Abbreviations

ACAN	Aggrecan
ACTA2, SMA	Actin alpha 2, Smooth Muscle Actin
APS	Ammonium Persulfate
bFGF	Basic Fibroblast Growth Factor
Bis	*N,N'*-Methylenebisacrylamide crosslinker
BSA	Bovine Serum Albumin
CD31	Platelet Endothelial Cell Molecule
COL2A1	Collagen, Type II, alpha 1
CVD	Cardiovascular Disease
DAPI	4',6-diamidino-2-phenylindole
dbcamp	N6, 2'-O-Dibutyryladenosine 3',5'-cyclic monophosphate sodium salt
dk	Donkey
DMEM	Dulbecco's Modified Eagle's Media
F98	Polyclonal Rat Glioblastoma Cell Line
GDEC	Glioblastoma-derived Endothelial Cells
gt	Goat
GTIC	Glioblastoma Tumor-Initiating Cells
H342	Hoescht 33342
HEPES	4-(2-hydroxyethyl)-1-piperazineethanesulfonic acid
KLF	Krüppel-like Factor
kPa	Kilopascals
ms	Mouse
MYH11, SM-MHC	Myosin Heavy Chain 11, Smooth Muscle Myosin Heavy Chain
NaCl	Sodium Chloride
P/S	Penicillin/Streptomycin
pAAm	Polyacrylamide
PBS	Phosphate-Buffered Saline, pH 7.4
PVDF	Polyvinylidene Fluoride
rb	Rabbit

RT	Room Temperature
SDS	Sodium Dodecyl Sulfate
SRF	Serum Response Factor
Sulfo-SANPAH	N-Sulfosuccinimidyl-6-(4'-azido-2'-nitrophenylamino) hexanoate
TBST	Tris-Buffered Saline with 0.05% Tween-20 (v/v)
TEMED	Tetramethylethylenediamine
TIE2	Angiopoietin Receptor 2
VEGF	Vascular Endothelial Growth Factor
VSC	Vascular Stem Cell

Acknowledgements

Valerie: A huge thank you for being my possibility model (Thanks for the phrase, Laverne Cox). Your love, patience, creativity and teaching shaped who I am. Thank you for never giving up on me, or letting me give up on myself.

Travis: Thanks to the other half of a dynamic duo. For helping me grow up, late night talks about literature, music, language, and media. I would also like to thank Jim, Ara, Alden, and Susan for welcoming me into your homes.

To my parents: Thank you for doing the best you could from out-of-state, for your support and patience. I am thankful for you giving me space, time, home-cooked meals, peace and quiet.

Dr. Tin Tin Su: Thank you for being my first mentor and providing me with invaluable research experience. Her lab combined my interest in fruit flies and approaching research like a puzzle within a puzzle, waiting to be unraveled. Also thanks to the Su labmates I worked with: Lyle Uyetake, Dr. Kristin Garcia, Dr. Smurti Vidwans, Will and Tony.

Summer in the PNW: Thank you to Dr. Linda Wordeman and Dr. Jason Stumpff for being excellent mentors on my first research internship away from home. Thank you for the invaluable guidance, support, and encouragement early on in my career.

Endless Summer: I want to thank Dr. Elena Pasquale for the years I spent in sunny SD. I want to thank Fatima, Carlos and Eva, Mari and Oscar, Eric and Liem, Kim, Eddie, Victor, and Regina for enriching my life.

The Bay Area: I would like to express my sincere gratitude to my co-advisors, Dr. Song Li and Dr. John Ngai. Together, Song and John stepped in to help me secure lab space to complete my degree after the sudden departure of my PI. I want to thank Dr. Li for welcoming me into his lab during a very stressful time in my graduate career. I want to thank Dr. Ngai for providing me with valuable advice as my MCB advisor. I also want to thank the members of my thesis committee for providing support, advice, and encouragement: Dr. Richard Harland and Dr. Gerard Marriott. I would also like to thank Dr. Don Rio for helping me stay on track.

I would like to thank the Li and Ngai labs for their help and assistance. Thank you for the silly animal pictures, laughs, and conversations about science, non-science, and nonsense: An-Chi, Jen, Sze Yue, Elaine, Weixi, Doug, Dr. Russell Fletcher, Ariane Badhuin, Mary West, Paul Herzmark, and everyone else.

A big thank you to Julia Chu for making the lab run smoothly, her technical expertise and guidance, providing helpful feedback, and answering my endless questions throughout my time in the Li lab. Thank you for your patience and help in providing critical results in the last few months of my degree.

My mentee: I am so lucky and thankful for Alexis (AJ) Seymour, my precocious undergraduate mentee. Thank you for all your patience, kindness, late nights and weekends working tirelessly on characterizing these vascular stem cells on polyacrylamide hydrogels. Thank you for all your

contributions to move the project forward, making me a better mentor, and the lab a more exuberant place.

1st year and beyond: Naeem! I remember commiserating over lost sleep and the long stretch of I-5 between East Bay and SoCal over quick bites. I am so thankful for our long talks, binge-watching Netflix, and for the steady stream of encouragement to finish.

Bay of [Spider] Pigs: Mike, it has been my pleasure to work with you. Thank you for showing me the ropes and reminding me to focus on the task at hand. I have grown so much through our discussions on leadership, race, politics, justice, and history. I am fortunate to have worked beside you as we have both made our way to the finish line.

My sincerest gratitude to the MCB GAO staff: Tanya G., Berta P., Eric B., Mona H., Christina D., and Sarah B. Thank you for helping me make adjustments and all the care in helping me achieve my goals.

Mr. Mayhem: Dr. Aditya Adiredja. What would I have done without you? Thank you so much for your patience, care, and being one of my first friends in the Bay. There are so many memories that encapsulate our friendship. The easiest to recall were always late at night, catching up while alphabetizing exams, teaching trials and tribulations, and bonding over ShondaLand Productions. Thanks for the time and space between beginning and end.

Random acts of non-science: I am so grateful to my friends for all the phone calls, occasional visits, and discussions on politics, pop culture, and queer theory. In no particular order, thank you Shannon O., Ang S., Jen T., Raquel L., Dr. Libby Lewis, Boróka B., Dahlia A., Karl B., Prajit L., Dr. Shoba Rajgopal, Dr. Sabriya Rosemond, and Chris C. (Also, sorry if I missed some of you, you still matter to me!)

I am especially thankful to Tommy Statkiewicz, and his partner Clara M.W., for our writing group. Between opening up his own home as a workspace, delicious meals, delectable teas, and puppy, I could work alongside their brilliance and be encouraged to keep moving forward.

I want to also thank the Gender Equity Resource Center and their staff, Marisa Boyce, Billy Curtis, and CiCi Ambrosio. Their presence was a great comfort in how to build queer community at Cal. I also admire important and necessary work to strengthen, develop, and foster queer communities across campus. Thank you for always being a safe space on campus.

I want to thank all the staff in Stanley Hall and LSA. Calvin and Chris: for always being helpful and insightful remarks in those few moments we could chat. Gloria: thank you for sharing so many wonderful stories, kind words, and a smile during the late nights I spent in Stanley Hall.

Special thanks to the pets in and around my life that have provided unconditional love and/or warm, fuzzy bodies: Creamsicle the snake (RIP), Koya the D.O.G. (RIP), Sherbert the baby snake, Terrance Zoolander and Philip Hans the bunnies, Baron von Snooze, and Juniper the puppy.

Chapter 1: Introduction

1.1 Healthy vascular development

The cardiovascular system in vertebrates consists of the heart, blood vessels, and blood.[3] This system is responsible for the transportation of blood, oxygen, nutrients, and removal of waste products throughout the entire body. A cross-section of a healthy artery shows three distinct layers (Figure 1.1).[4] The innermost layer, or tunica intima, consists of a monolayer of endothelial cells. The tunica media, or middle layer, contains smooth muscle cells (SMCs) embedded in a complex extracellular matrix. The outermost layer is the tunica externa, which contains mast cells, nerve endings, microvessels. This connective tissue is also comprised of collagen and other extracellular matrix proteins that anchor arteries to nearby organs within the body.

In mature adult vertebrates, including humans, the vasculature is subject to hemodynamic forces, including laminar shear stress and blood pressure (Figure 1.2).[5] The frictional fluid force per area, or laminar shear stress (τ), is parallel to blood flow and regulates vascular development in embryonic and adult tissues.[6,7] Endothelial cells cultured *in vitro* and exposed to laminar shear stress and elicit responses that include, longitudinal alignment, growth inhibition, and release of signaling molecules. The role of hemodynamic forces to promote the differentiation of cancer stem cells to vascular cell fates has not been examined.[8] In Appendix III, I show preliminary data to determine whether laminar shear stress-treated Glioblastoma tumor-initiating cells adopt endothelial-like cell fates, and contributes to the leaky tumor vasculature observed *in vivo*.

As the heart pumps blood through blood vessels, a perpendicular force is exerted on the walls of the artery, also known as blood pressure (ρ). Blood pressure stretches the cells within the vessel wall. Vascular SMCs, which reside below the monolayer of endothelial cells, primarily function to regulate and maintain the blood vessel wall. To this end, these vascular SMCs typically have low proliferation and migration rates, little-to-no synthesis of extracellular matrix proteins, and high expression of proteins that aid in cell contractility, including smooth muscle α-actin (SMA), myosin heavy chain 11 (MYH11), calponin1 (CNN1), and SM22α.[9]

1.2 Cardiovascular diseases

Cardiovascular diseases (CVDs) represent about 31% of all deaths worldwide.[1,2,10] CVDs are disorders of the heart and blood vessels, with hardening and/or occlusion of the blood vessel walls leading to high mortality rates. Since CVDs are noncommunicable, intervention costs and strategies often reflect individual management and behavioral changes. Current healthcare cost estimates alone are over $300 billion USD, which includes prescription drugs that lower blood cholesterol and blood pressure. Global studies reveal top risk factors as tobacco use, high blood pressure, and high blood cholesterol. Additional risk factors include physical activity, diet, and diabetes.[i,11]

[i] Re-examination of genome-wide association studies that report CVDs genetic factor(s) fail to account for population-level racial health disparities. Rather, these findings show causal links of health risks to income and education achievement. These reports often over represent significant changes in genetic loci by oversampling for European patients without demonstrating whether these risk patterns hold true for patients from different ethnic and geographic backgrounds.

Atherosclerosis, or hardening of the arteries is a common development to more serious vascular maladies (Figure 1.3).[12,13] This chronic disease progresses from the accumulation of fat, cholesterol, and other substances into the walls of arteries. These sites harden into plaques that disrupt the distinct layers of the blood vessel and thicken the vessel wall. While stabilized, the narrowing of the artery constricts blood flow and results in an increase blood pressure. Ultimately the mortality risk occurs when plaques break off and occlude blood flow. While the inflammatory response is a critical component of disease progression, in these studies we primarily focus on the relationship between early changes in the biophysical properties of the vessel wall and vascular cell response in the early stages of CVDs.

An early symptom and marker of CVD risk and atherosclerosis is hypertension, or high blood pressure. In Figure 1.3, blood pressure increases as vessel walls thicken due to the heterogeneous composition of cells in the disrupted layers of the artery. Unlike animal models of atherosclerosis, mechanical testing of fixed tissue samples pose a number of challenges. In reviews of current techniques, variability can be introduced due to tissue acquisition (e.g., size of excised tissue, delivery time and fixation methods), high variability within plaque architecture, and detection method used (e.g., bulk compression methods, micro-indentations, etc).[14,15]

To address these variations, especially in clinical settings, refinement of non-invasive methods can provide correlative factors that indicate early disease stages in arteries, prior to surgical intervention and tissue acquisition. For instance, D. Liao and colleagues were able to study whether there was a relationship between decreased arterial elasticity and increased hypertension.[16] Through blood pressure, artery diameter, and pulse wave velocity measurements, the data show that increases in vessel stiffening, or marked decreases in arterial elasticity, related to the development of hypertension.

One of the best-utilized models for atherosclerosis is the Apolipoprotein E knockout mouse (ApoE KO).[17] On a standard chow diet, homozygous litters have spontaneous elevation of plasma cholesterol and formation of fatty lesions in vessel walls that exhibit similarities to plaques found in human vessels.[18] When fed a high fat diet, a known CVD risk factor, plaque formation is accelerated. Since additional genes can be assessed in CVD progression through double knockout mice, these mice offer the opportunity to parse the impact of specific genetic and environmental factors that promote atherosclerosis.[19]

In fixed mice tissue samples, invasive techniques can be used to probe the matrix elasticity in atherosclerotic vessels. As expected, the matrix elasticity measurements can confirm differences in regions of the atherosclerosis plaque visible through histology staining. While healthy wild type mouse vessels have mean elasticity of 76 kilopascals (kPa), the mean elasticity of atherosclerotic vessels depended on cellular composition. Atherosclerotic lesions generally have lipid rich, cellular fibrosis, and acellular fibrosis regions. Since these regional categories are heterogeneous, the mean elasticity ranges from 2-9kPa, 5-16kPa, and 12-107kPa respectively.[20,21] Lastly, local changes to the vessel wall of age-matched wild-type and ApoE KO mice can be detected as early as 18 weeks using blood pressure and pulse wave velocity, which can precede atherosclerotic lesions and plaque formation.[22] Taken together, these data show

ApoE KO mice can be used to determine possible cellular source(s) responsible in vascular injury and repair in healthy and diseased blood vessels.

What is the source of the invasive population of smooth muscle cells in damaged blood vessels? Do they originate from the local vessel wall or differentiate from circulating progenitor cells? To address this, J.F. Benzton and colleagues repeated previous work using sex-mismatched bone marrow transplants with $eGFP^+$ ApoE KO mice into ApoE KO mice.[23] While they recovered circulating GFP^+ cells in their irradiated ApoE KO mice in equal proportions to the $eGFP^+$ ApoE KO control, they could not detect GFP^+ SMA^+ and/or Y $chromosome^+$ smooth muscle cells in the fatty lesions of the irradiated ApoE KO blood vessels. Similar results were also observed in transplanted carotid artery grafts. These observations alongside work by other groups suggest the local vessel wall is the source of the invasive SMCs in the progression of atherosclerosis.

Although atherosclerosis plaques are composed of cells from the immediate area, segments of the vessel wall do not contribute equally to atherosclerotic development. Regions exposed to disturbed laminar shear stress, like in the aortic arch or arterial branches, are the most susceptible to atherosclerosis.[24,25] One way to assess whether vessel wall position is sufficient to develop atherosclerosis was to perform homograft aortic transplant experiments.[26] In reviewing published work, M.W. Majesky summarizes that contrary to expectations, atherosclerosis-prone regions developed lesions in the relocated atherosclerosis-resistant area. Surprisingly, atherosclerosis-resistant areas flanking the transplant did not develop lesions. Similarly, atherosclerosis-resistant artery transplants did not develop lesions in areas that typically develop atherosclerosis. Together, these studies highlight the cells within the vessel wall, and not just the position, determines the distribution and progression of diseased vessels.

1.3 Cellular mechanisms of cardiovascular disease progression

As outlined above, current theories about CVD progression depend on the cells in close proximity to the site of vessel damage and fat accumulation. The following sections and Figure 1.4 discuss current theories of the cellular mechanisms that drive healthy and diseased vessel development in adults.

1.3.1 De-differentiation of smooth muscle cells

In vivo, the primary function of SMCs is to respond to vessel contraction, tone, blood pressure, and distribution.[12,24,27] Characterization of these vascular SMCs reveals a low proliferation rate, low synthesis activity, and high expression of contractility proteins and ion channels that maintain blood vessels. Contractility proteins like CNN1, MYH11, SMA, and SM22α are used to as markers of mature SMCs.

Isolation and characterization of vascular cells from arterial tissue *in vitro* have observed a distinct population of highly proliferative, migratory cells that synthesize ECM proteins.[28,29] In cell culture, these cells do not express typical contractility markers and undergo morphology changes. Since these proliferative/synthetic cells emerge from freshly isolated arterial tissue, researchers proposed that the mature SMCs in the vessel wall de-differentiated to the proliferative/synthetic population (Figure 1.4).

The de-differentiation hypothesis of vascular SMCs offers the following explanation of healthy vessel repair.[30,31] The complex interplay of mechanical signals and soluble factors that maintain the elasticity of the blood vessel, in turn, regulate vascular SMC expression of contractility proteins and dampens cell proliferation and ECM protein synthesis. Vessel wall remodeling can stimulate SMCs to undergo a phenotypic switch, where cells proliferate, migrate, and repair the damaged area. Over time, vascular SMCs increase expression of contractility proteins and cease proliferation and synthesis.

In atherosclerotic plaque regions, like Figure 1.3, the proliferative/synthetic SMCs are morphologically distinct from mature SMCs, and occupy the neointima layer. However, there is no direct evidence that mature SMCs undergo this phenotypic change and contribute to the pool of proliferative/synthetic SMCs. Surgical damage to vessel walls varies among experimental animals and research groups, which affects forming definitive conclusions about the sole contribution of vascular SMCs. Even so, one challenge that persists in both mouse and human models of atherosclerosis is the inability to lineage-trace mature SMCs after vessel injury or damage.

1.3.2 Vascular stem cells

In available literature the term "vascular stem cells" recovers less than 50 articles. Typical usage refers to stem or stem-like cells in the vascular system. In their literature review, C-S Lin and T.F. Lue define vascular stem cells as "cells that reside within the blood vessel wall that can differentiate into all of the cell types that constitute a functional blood vessels."[32] This definition is then used to discuss the evidence of side populations of vascular stem cells.

Early evidence showed that SMCs in atherosclerotic plaques are monoclonal, and that a rare cell population within the vessel wall could explain these results.[33,34] One side population of $Sca1^+$ cells from wild-type mice were isolated and characterized to differentiate to endothelial and SMC cell fates.[35] In ApoE-deficient mice, the adventitial layer of arteries also shows a $Sca1^+$ $c\text{-}kit^+$ side population of cells.[36] In 2012, our group reported the isolation and characterization of a population of adult multipotent vascular stem cells (VSCs) from both normal and surgically injured blood vessels.[37] These VSCs were isolated from the media and adventitial layer of rodent and human tissues, and maintained in a custom maintenance media. These data show that initial populations of VSCs are $Sca1^-$ and $ckit^-$, do not have the typical mature SMC morphology, and are not positive for mature SMC markers, like MYH11 and CNN1.

Protocols to isolate and characterize vascular SMCs from animal tissue *in vitro* expose cells for up to 3 weeks in high serum cultures (10-20% FBS).[27,28] The above culturing conditions cannot rule out the possibility of dormant stem cell populations in the vessel wall also contributing to vessel wall remodeling. When VSCs are cultured in high serum media for weeks, as established protocols for SMC isolation describe, the morphology changes to expected mature SMCs, with larger cell bodies, long fibers, and positive staining for mature SMC markers. Finally, *ex vivo* tissue explant cultures also show that RFP-labeled $Sox10^+$ cells emerge from the tunica media and tunica adventitia of mouse thoracic aortas.[38] Other groups have been able to use VSC markers (e.g., Sox10, Sox17, S100β) to isolate and characterize migrating cell populations from tissue explant cultures and commercially available vascular SMCs.[39-41]

As an alternative hypothesis to the de-differentiation theory, aberrant differentiation of VSCs may also contribute to the heterogeneous composition of atherosclerotic plaques. In normal vessel wall remodeling, a VSC niche is within the medial and/or adventitial layers. Once activated, VSCs begin to proliferate and adopt SMC end fates. After the repair has been made, VSCs become quiescent. Similarly, at early stages of atherosclerosis, lipid and cholesterol accumulates in the vessel wall and affects local arterial wall stiffness. Since VSCs are multipotent, aberrant differentiation could contribute to heterogeneous populations of adipogenic, osteogenic, and chondrogenic cells observed. In chapter two, we use an *in vitro* approach to characterize rat VSCs seeded on different matrix elasticity.

1.4 Stem cells

A stem cell is defined as a cell that exhibits self-renewal and unrestricted fate potential.[42] In the adult, stem cell populations usually have more restricted lineage differentiation capabilities, but retain self-renewal *in vitro*.

1.4.1 Sox family members in vascular stem cells

The Sex-determining region Y-related HMG box (Sox) transcription factor family members are best characterized for controlling cell fate and differentiation in a multitude of processes, such as sexual differentiation, stem cell maintenance, neurogenesis, and skeletogenesis.[43] In mammals, the Sox family has 20 members in 9 groups (A-H) based on sequence homology. [44] Here we focus on Sox10 and Sox17, in Sox groups E and F respectively, due to their high expression in VSCs.[37] When cultured in high serum media (10% FBS), VSCs lose Sox10 and Sox17 protein expression and up regulate mature SMC markers, like SMA, CNN1, and MYH11. The absence of Sox genes may allow for lineage commitment or affect VSC maintenance.

Sox10

Sox10 is a well-known marker of neural crest stem cells.[45] Sox10 knockout mice are embryonic lethal, with defects in neural crest stem cells migration.[46,47] Further characterization has shown Sox10 is required for undifferentiated neural crest stem cells survival, lineage commitment, and melanocyte pigmentation.[48-50] Constitutive expression of Sox10 preserves glial and neuronal differentiation in cultured neural crest stem cells compared to controls.[45]

During development, the vascular SMCs of the thoracic artery have different embryonic cell origins.[51] Our VSCs are isolated from the aorta that is patterned from cardiac neural crest stem cells, we hypothesized that Sox10 may have a similar role in vascular stem cell maintenance and/or prevents differentiation.

Sox17

Sox17, along with Sox7 and Sox18, are SoxF group members, with some functional redundancy between member roles in cardiogenesis and angiogenesis.[52] Sox17 knockout mice are embryonic lethal with defects in the definitive endoderm and heart development.[53,54] In hematopoietic stem cells, Sox17 knockout affects fetal, but not adult, hematopoietic stem cell pools.[55] Ectopic expression of Sox17 in adult progenitor cells causes them to exhibit properties restricted to fetal hematopoietic stem cell.[56]

Based on these known roles in stem cell maintenance or preventing differentiation, we proposed that Sox proteins were good candidate genes to further investigate in VSCs differentiation. In Chapter 3, we characterize the effects of Sox protein knockdown in VSCs.

1.5 Matrix elasticity regulates stem cell differentiation and self-renewal *in vitro*

Cells, tissue, and organs from the body exhibit different matrix elasticity (Figure 1.5).[57] As mentioned in Section 1.1, mechanical forces regulate and maintain blood flow and healthy vessels. While cells inside the body experience matrix elasticity up to hundreds of kilopascals (kPa), isolation and culturing *in vitro* are on the gigapascals range. Seminal work performed by A.J. Engler and colleagues in 2006 demonstrated how mechanical signals alone could regulate mesenchymal stem cell differentiation.[58] Matrix elasticity corresponding to brain, muscle, or bone directed differentiation to neurogenic, myogenic, and osteogenic cells *in vitro*. Chemical inhibition that disrupts the cytoskeletal relay of matrix elasticity eliminates the directed differentiation effects observed.

These results highlight that biophysical factors are a critical component in the culture and maintenance of stem cells *in vitro*. Controlling the stem cell biophysical microenvironment can circumvent the ongoing challenge with current culturing methods in maintaining high expression of stem cell markers, heterogeneous populations of stem cells, preventing spontaneous differentiation, or directing differentiation to a specific terminal fate. These effects have been documented for embryonic stem cells, [59,60] neural stem cells,[61] mesenchymal stem cells,[62,63] and in cell reprogramming.[64,65] Since biophysical factors can replace soluble and/or chemical factors required in stem cell maintenance and/or differentiation media recipes, exploiting mechanical signaling pathways could decrease overall culturing time and still ensure purity and enrichment of desired cell fates.

1.6 Conclusion

Early detection and effective drug treatment strategies are critical steps to address the high mortality rate of CVDs. As stated earlier, there is no exclusive marker of SMCs to coincide with specific differentiation state(s). De-differentiation is defined by the down-regulation or absence of cytoskeletal and contractile proteins. While our current isolation protocol for rat VSCs is still comprised of a heterogeneous pool of cells, serial passaging enriches for the faster growing population of cells, which are also Sox10 and Sox17-positive.

Since we were able to narrow the VSC niche to the medial and adventitial layers of the blood vessel, we are specifically interested in further characterization of VSCs in response to local change sin the biophysical microenvironment. We hypothesize that aberrant differentiation of VSCs in cardiovascular disease progression. In this work we aim to show that rat VSCs seeded onto varying matrix elasticity *in vitro* can direct differentiation to terminal fates that more closely resemble cells of the same elasticity *in vivo*. This presents potential therapeutic target for cells that may directly contribute to vessel wall disorganization.

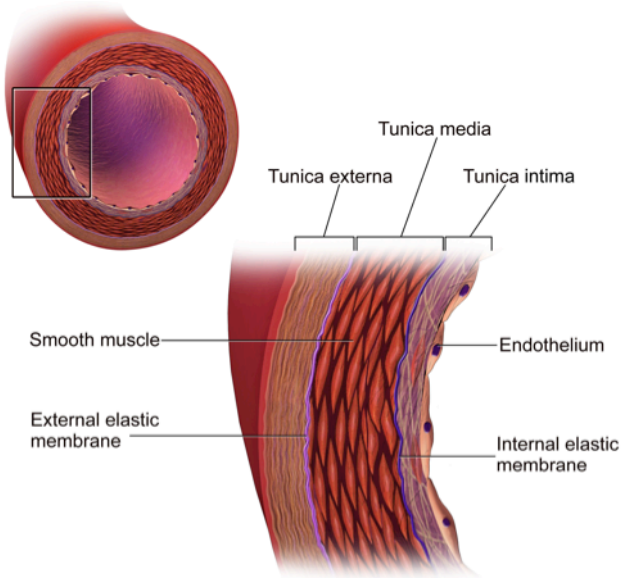

Figure 1.1 The Structure Of An Artery Wall. [ref. 4] The inner layer, or tunica intima, consists of a monolayer of endothelial cells. The next layer, or tunica media, contains smooth muscle cells (SMCs). The outermost layer, or tunica externa, has mast cells, nerve endings, and microvessels. Collagen and other extracellular matrix proteins are also present and help anchor arteries to nearby organs within the body.

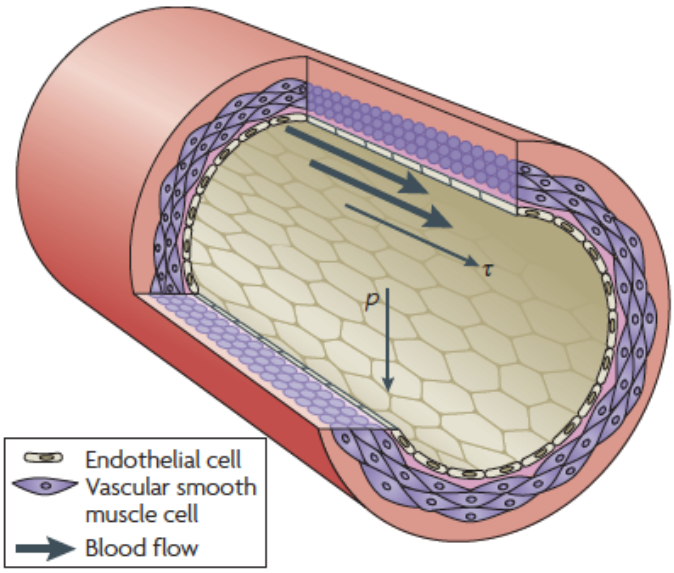

Figure 1.2. Mechanical forces on the vessel wall. A section of an artery wall shows the endothelial cells that form the inner lining and align longitudinally, and vascular smooth muscle cells that form the outer layers and align circumferentially. Pressure (ρ) is normal to the vessel wall, which results in circumferential stretching of the vessel wall. Shear stress (τ) is parallel to the vessel wall and is exerted longitudinally in the direction of blood flow. [ref. 5]

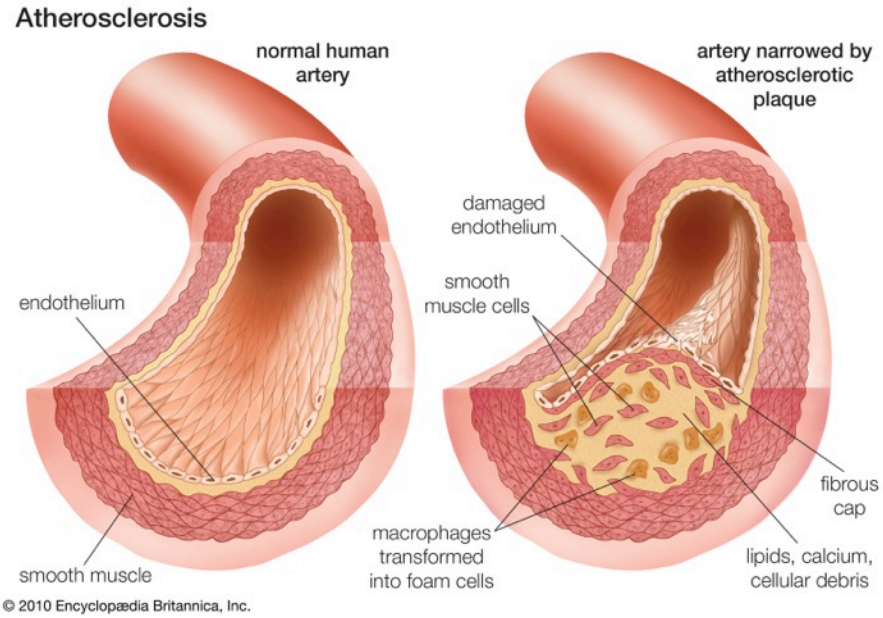

Figure 1.3. Normal And Atherosclerotic Human Artery Cross-Sections. Normal human arteries have three distinct layers that facilitate blood flow throughout the body. As atherosclerosis progresses, the diseased vessel have a disrupted vessel wall. In the figure, there are no longer three distinct ordered layers. The intima layer is disrupted and shows damaged endothelial cells. The medial layer has a heterogeneous accumulation of lipids, calcium, debris, immune and SMCs. This vessel wall thickening constricts blood flow through the artery, resulting in increased blood pressure. [ref. 12]

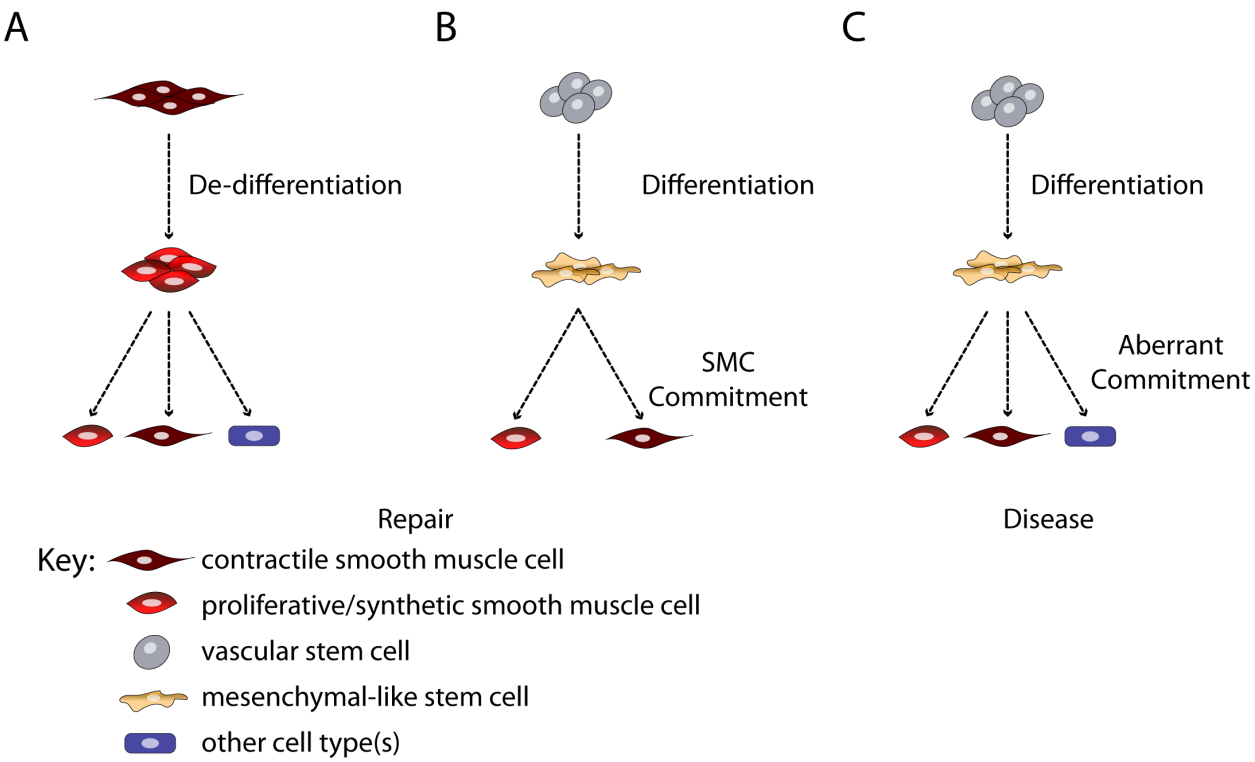

Figure 1.4. Schematic comparing the cellular source(s) involved in healthy and diseased vessel repair in adults. *A,* De-differentiation of contractile smooth muscle cells to a proliferative/synthetic smooth muscle cell. Vessel repair includes differentiation and maturation of contractile and proliferative/synthetic smooth muscle cells, as well as other cell type(s). *B,* Differentiation of vascular stem cells may occur as a step-wise process, first to a mesenchymal-like stem cell, then to smooth muscle cell end fates. *C,* Other cell type(s) visible in diseased vessels, like adipogenic, chondrogenic or osteogenic lineages, may result from aberrant differentiation of vascular stem cells. [Modified from refs. 30,32]

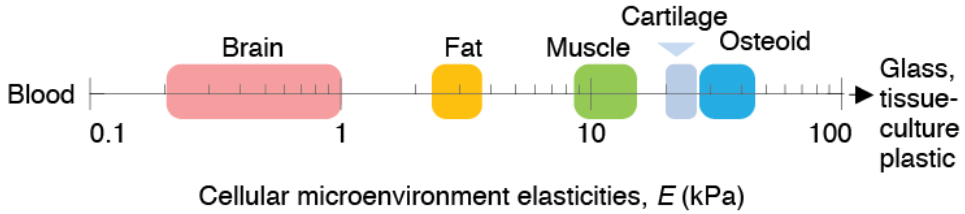

Figure 1.5. Matrix Elasticity Scale Range For Soft Tissues In The Body. The scale shows the matrix elasticity, in kilopascals, from blood to pre-calcified bone. Conventional tissue culture plastic and glass have values greater than 10^6 kilopascals. [ref. 42]

References

1. World Health Organization. (2014). *Global Status Report on Noncommunicable Diseases 2014*. Geneva, Switzerland: World Health Organization.
2. Mozaffarian D, *et al*. (2015). Heart Disease and Stroke Statistics–2015 Update: A Report From the American Heart Association. *Circulation* 131: e29-e322.
3. Russell PJ, Hertz PE, McMillan B. *Biology: The Dynamic Science* (Brooks/Cole, Canada, ed. 2, 2011), pp. 956-957.
4. Blausen.com staff. "Blausen gallery 2014". Wikiversity Journal of Medicine. DOI: 10.15347/wjm/2014.010. ISSN 20018762. - Own work. Licensed under CC BY 3.0 via Wikimedia Commons - http://commons.wikimedia.org/wiki/File:Blausen_0055_ArteryWallStructure.png#/media/File:Blausen_0055_ArteryWallStructure.png Accessed on 30 April 2015.
5. Hahn C and Schwartz MA. (2009). Mechanotransduction in vascular physiology and atherogenesis. *Nat. Rev. MCB* 10: 53-62.
6. Davies PF. (1995). Flow-Mediated Endothelial Mechanotransduction. *Physiol. Rev.* 75(3): 519-560.
7. Jain RK. (2003). Molecular Regulation of Vessel Maturation. *Nature Medicine*. 9(6): 685-693.
8. Stolberg S and McCloskey KE. (2009). Can Shear Stress Direct Stem Cell Fate? *Biotechnol. Prog.* 25(1): 10-19.
9. Shi Z-D and Tarbell JM. (2011). Fluid Flow Mechanotransduction in Vascular Smooth Muscle Cells and Fibroblasts. *Annals Biomed. Eng.* 39(6): 1608-1619.
10. Center for Disease Control and Prevention: Division for Heart Disease and Stroke Prevention. (20 June 2014). Heart Disease Frequently Asked Questions. http://www.cdc.gov/heartdisease/index.htm Accessed 30 April 2015.
11. For further reading, see Kaufman JS, *et al* (2015). The Contribution of Genomic Research to Explaining Racial Disparities in Cardiovascular Disease: A Systematic Review. *Am J Epidemiol.* 181(7): 464-472; Braveman PA, *et al* (2010). Socioeconomic Disparities in Health in the United States: What the Patterns Tell Us. *Am J Public Health* 100(S1): S186-S196.
12. "Atherosclerosis: Comparison of Arteries." Art. *Encyclopædia Britannica Online*. Web. Retrieved on 03 May. 2015 from http://www.britannica.com/EBchecked/topic/40908/atherosclerosis/images-videos/95216/atherosclerosis-comparison-of-arteries
13. Libby P, Ridker PM, Hansson GK. (2011). Progress and Challenges in Translating the Biology of Atherosclerosis. *Nature* 473: 317-325.
14. Chai C-K, Speelman L, Oomens CWJ, Baaijens FPT. (2014). Compressive Mechanical Properties of Atherosclerotic Plaques-Indentation Test to Characterise the Local Anisotropic Behavior. *Journal of Biomechanics* 47: 784-792.
15. Kohn JC, Lampi MC, Reinhart-King CA. (2015). Age-Related Vascular Stiffening: Causes and Consequences. *Frontiers in Genetics* 6: 112. doi 10.3389/fgene.2015.00112

16. Liao D, *et al*. (1999). Arterial Stiffness and the Development of Hypertension: The ARIC Study. *Hypertension* 34: 201-206.
17. Meir KS and Leitersdorf E. (2004). Atherosclerosis in the Apolipoprotein E-Deficient Mouse: A Decade of Progress. *ATVB* 24: 1006-1014.
18. Zhang SH, Reddick RL, Piedrahita JA, Maeda N. (1992). Spontaneous Hypercholesterolemia and Arterial Lesions in Mice Lacking Apolipoprotein E. *Science* 258(5081): 468-471.
19. Zhang SH, Reddick RL, Burkey B, Maeda N. (1994). Diet-Induced Atherosclerosis in Mice Heterozygous and Homozygous for Apolipoprotein E Gene Disruption. *J. Clin. Invest.* 94: 937-945.
20. Tracqui P, *et al*. (2011). Mapping Elasticity Moduli of Atherosclerotic Plaque *in situ* via Atomic Force Microscopy. *Journal of Structural Biology* 174: 115-123.
21. Broisat A, *et al*. (2011). Assessing Low Levels of Mechanical Stress in Aortic Atherosclerotic Lesions from Apolipoprotein E-/- Mice–Brief Report. *ATVB* 31: 1007-1010.
22. Gotschy A, *et al*. (2013). Local Arterial Stiffening Assessed by MRI Precedes Atherosclerotic Plaque Formation. *Circ. Cardiovasc. Imaging* 6: 916-923.
23. Bentzon JF, *et al*. (2006) Smooth Muscle in Atherosclerosis Originate From the Local Vessel Wall and Not Circulating Progenitor Cells in ApoE Knockout Mice. *ATVB* 26: 2696-2702.
24. Chiu JJ and Chien S. (2012). Effects of Disturbed Flow on Vascular Endothelium: Pathophysiological Basis and Clinical Perspectives. *Physiol. Rev.* 91: 327-387.
25. Leroux-Berger M, *et al*. (2011). Pathological Calcification of Adult Vascular Smooth Muscle Cells Differs on their Crest or Mesodermal Embryonic Origin. *JBMR* 26(7): 1543-1553.
26. Majesky MW. (2007). Developmental Basis of Vascular Smooth Muscle Diversity. *ATVB* 27: 1248-1258.
27. Owens GK, Kumar MS, Wamhoff BR. (2004). Molecular Regulation of Vascular Smooth Muscle Cell Differentiation in Development and Disease. *Physiol. Rev*. 84: 767-801.
28. Thyberg J, *et al*. (1990). Regulation of Differentiated Properties and Proliferation of Arterial Smooth Muscle Cells. *ATVB* 10: 966-990.
29. Churchman AT and Siow RCM. (2009). Isolation, Culture, and Characterisation of Vascular Smooth Muscle Cells. In Martin S, Murray C, editors. *Methods in Molecular Biology, Angiogenesis Protocols*. Vol. 467 2nd ed. New York; London: Humana Press. pp.127-138.
30. Miano JM. (2012). Vascular Smooth Muscle Cell Phenotypic Adaptation. In Hill JA and Olson EN, editors. *Muscle: Fundamental Biology and Mechanisms of Disease. Volume 2.* Oxford: Academic Press. pp. 1269-1278.
31. Gomez D and Owens GK. (2012). Smooth Muscle Cell Phenotypic Switching in Atherosclerosis. *Cardiovascular Research* 95: 156-164.
32. Lin C-S and Lue TF. (2013). Defining Vascular Stem Cells. *Stem Cells Dev* 22(7): 1018-1026.
33. Benditt EP and Benditt JM. (1973). Evidence for a Monoclonal Origin of Human Atherosclerotic Plaques. *PNAS* 70(6): 1753-1756.

34. Murry CE, *et al*. (1997). Monoclonality of Smooth Muscle Cells in Human Atherosclerosis. *Am J Pathol*. 151(3): 697-705.
35. Sainz J, *et al*. (2006). Isolation of "Side Population" Progenitor Cells from Healthy Arteries of Adult Mice. *ATVB* 26: 281-286.
36. Hu Y, *et al*. (2004). Abundant progenitor cells in the adventitia contribute to atherosclerosis of vein grafts in ApoE-deficient mice. *J Clin Invest* 113: 1258-1265.
37. Tang Z, *et al*. (2012). Differentiation of Multipotent Vascular Stem Cells Contributes to Vascular Diseases. *Nat Commun* 3: 875.
38. Tang Z, *et al*. (2013). Smooth Muscle Cells: To Be Or Not To Be? *Circulation Res* 112:23-26.
39. Leach DF, *et al*. (2014). The Sources of Synthetic Vascular Smooth Muscle Cells Revisited. *Austin J Anat* 1(2): 1007.
40. Curtis BM, *et al*. (2014). Slow And Sustained Nitric Oxide Releasing Compounds Inhibit Multipotent Vascular Stem Cell Proliferation And Differentiation Without Causing Cell Death. *BBRC* 450: 208-212.
41. Kennedy E, *et al*. (2014). Embryonic Rat Vascular Smooth Muscle cells Revisited – A Model For Neonatal, Neoinitmal SMC Or Differentiated Vascular Stem Cells? *Vascular Cell* 6:6.
42. Stem Cell Basics: Introduction. In *Stem Cell Information*. Bethesda, MD: National Institutes of Health, U.S. Department of Health and Human Serives, 2015. Web. Accessed 16 May 2015. Available at http://stemcells.nih.gov/info/basics/pages/basics1.aspx
43. Lefebvre V, *et al*. (2007). Control of Cell Fate and Differentiation by Sry-Related High-Mobility-Group Box (Sox) Transcription Factors. *Int J Biochem Cell Biol* 39(12): 2195-2214.
44. Schepers GE, *et al*. (2002). Twenty Pairs of *Sox*: Extent, Homology, and Nomenclature of the Mouse and Human *Sox* Transcription Factor Gene Families. *Developmental Cell* 3: 167-170.
45. Herbarth B, *et al*. (1998). Mutation of the Sry-related Sox10 gene in Dominant megacolon, a mouse model for human Hirschsprung disease. *PNAS* 95: 5161-5165.
46. Southard-Smith EM, Kos L, and Pavan WJ. (1998). Sox10 mutation disrupts neural crest development in Dom Hirschsprung mouse model. *Nat. Genet.* 18: 60-64.
47. Mollaaghababa R and Pavan WJ. (2003). The Importance Of Having Your SOX On: Role Of SOX10 In The Development of Neural Crest-Derived Melanocytes And Glia. *Oncogene* 22: 3024-3034.
48. Britsch S, *et al*. (2001). The Transcription Factor Sox10 Is A Key Regulator Of Peripheral Glial Development. *Genes Dev*. 15: 66-78.
49. Paratore C, *et al*. (2001). Survival And Glial Fate Acquisition Of Neural Crest Cells Are Regulated By An Interplay Between The Transcription Factor Sox10 And Extrinsic Combinatorial Signaling. *Development* 128: 3949-3961.

50. Kim J, *et al*. (2003). SOX10 Maintains Multipotency And Inhibits Neuronal Differentiation Of Neural Crest Stem Cells. *Neuron* 38: 17-31.
51. Hirschi KK and Majesky MW. (2004). Smooth Muscle Stem Cells. *The Anatomical Record Part A* 276A: 22-33.
52. Francois M, Koopman P, Beltrame M. (2010). *SoxF* Genes: Key Players In The Development Of The Cardio-Vascular System. *Int. J. Biochem. Cell Biol.* 42: 445-448.
53. Kanai-Azuma M, *et al*. (2002). Depletion of Definitive Gut Endoderm in *Sox17*-Null Mutant Mice. *Development* 129: 2367-2379.
54. Pfister S, *et al*. (2011) *Sox17*-Dependent Gene Expression And Early Heart And Gut Development In *Sox17*-Deficient Mouse Embryos. *Int. J. Dev. Biol*. 55: 45-58.
55. Kim I, Saunders TL, Morrison SJ. (2007). *Sox17* Dependence Distinguishes the Transcriptional Regulation of Fetal from Adult Hematopoietic Stem Cells. *Cell* 130: 470-483.
56. He S, Kim I, Lim MS, Morrison SJ. (2011). Sox17 expression confers self-renewal potential and fetal stem cell characteristics upon adult hematopoietic progenitors. *Genes Dev* 25: 1613-1627.
57. Sun Y, Chen CS, Fu J. (2012). Forcing Stem Cells To Behave: A Biophysical Perspective Of The Cellular Microenvironment. *Annu. Rev. Biophys*. 41: 519-542.
58. Engler AJ, *et al*. (2006). Matrix Elasticity Directs Stem Cell Lineage Specification. *Cell* 126: 677-689.
59. Chowdhury F, *et al*. (2010). Soft Substrates Promote Homogeneous Self-Renewal of Embryonic Stem Cells via Downregulating Cell-Matrix Tractions. PLoS ONE 5(12): e15655.
60. Chen W, *et al*. (2012). Nanotopography Influences Adhesion, Spreading, and Self-Renewal of Human Embryonic Stem Cells. ACS Nano 6(5): 4094-4103.
61. Saha K, *et al*. (2008). Substrate Modulus Directs Neural Stem Cell Behavior. *Biophysical Journal* 95: 4426-4438.
62. Li Y, *et al.* (2011). Biophysical Regulation of Histone Acetylation in Mesenchymal Stem Cells. *Biophysical J* 100: 1902-1909.
63. Huebsch N, *et al*. (2010). Harnessing Traction-Mediated Manipulation of the Cell-Matrix Interface to Control Stem Cell Fate. *Nat Mater* 9(6): 518-526.
64. Downing TL, *et al*. (2013). Biophysical regulation of epigenetic state and cell reprogramming. *Nat Mater* 12: 1154-1162.
65. Yoo J, *et al*. (2015). Nanogrooved substrate promotes direct lineage reprogramming of fibroblasts to functional induced dopaminergic neurons. *Biomaterials* 45: 36-45.

Chapter 2: Matrix Elasticity Regulates Vascular Stem Cell Smooth Muscle α-Actin Expression By Myocardin-Related Transcription Factor A Translocation

In this chapter, experiment design, data collection and analysis was work performed by myself, Alexis J. Seymour, Julia Chu, and Song Li. I will submit parts of this chapter as a first author manuscript at a future date.

2.1 Introduction

Rat vascular stem cells (VSCs) present an additional cell population that may contribute to atherosclerosis and cardiovascular disease. We have narrowed the VSC niche to the medial and adventitial layers of the blood vessel wall.[1] Direct and indirect measurements of rodent and human vessels show heterogeneous matrix elasticity, ranging from two to hundreds of kilopascals (kPa) (See Chapter 1). We hypothesize that these heterogeneous regions act as biophysical cues to prime VSCs to differentiate to cell fates with the same matrix elasticity. As matrix elasticity decreases within the vessel wall, these mechanical signals may affect cell morphology and proliferation. As a result, decreases in nuclear area may remodel chromatin, and previously suppressed genes could be accessible to transcription factors to promote gene expression to different cell fates.

The Myocardin-related transcription factor (MRTF) family are important in the expression of cytoskeletal and contractile proteins in cardiovascular development and vascular SMCs.[2,3] The serum response factor (SRF) promoter sequence motif, CArG, is bound by SRF and MRTF family members to activate gene expression (Figure 2.10). The founding member, Myocardin, is critical in early cardiac development and vascular SMC differentiation in the embryo. But, is later restricted to the heart in adults.[4,5] Unlike Myocardin, the remaining family members, MRTF-A and MRTF-B, are expressed throughout adult tissues.

In adult tissues, MRTF-A and -B nuclear translocation and activity are regulated by the actin cytoskeleton.[6-8] G-actin in the cytoplasm can bind MRTF-A/B, which sequesters localization to the cytoplasm. As G-actin polymerizes into F-actin, the pool of G-actin decreases and MRTF-A/B is released. MRTF-A/B is imported into the nucleus to promote gene expression.

Recent work demonstrates that biophysical cues, like matrix elasticity and cyclic stretching, regulate a number of transcription factors. Upstream of these mechanical signaling pathways are changes in the ratio of G- and F-actin inside a cell. In fibroblasts experiencing cyclic stretching forces, MRTF-A nuclear translocation promotes cell survival on soft substrates.[9] Changes to tension can downregulate the SRF-MRTF-A mechanical signaling pathway by increasing the G-actin in fibroblasts.[10] Lastly, fibroblasts show that increasing matrix elasticity promotes upregulation of SMA by increasing MRTF-A nuclear translocation.[11]

In this chapter, we isolate and characterize vascular stem cells response to changes in matrix elasticity. We were specifically interested in whether decreases in matrix elasticity affect expression of SMC proteins through MRTF-A nuclear translocation. We show that as matrix elasticity decreases, average nuclear area, SMA expression, and MRTF-A nuclear localization decrease in rat VSCs. Targeted knockdown of MRTF-A decreases SMA expression in rat VSC,

especially on soft (~1kPa) pAAm gels. Finally, Blebbistatin-treatment affects MRTF-A localization and SMA expression on stiff (glass) but not soft (~1kPa) pAAm gels.

2.2 Materials and Methods

Isolation of Rat Vascular Stem Cells and Cell Culture

We previously reported a tissue explant method protocol to isolate and culture VSCs.[12] Thoracic aortas were harvested from Sprague-Dawley rats 3-6 months in age were removed and stored in plain DMEM + 1% P/S for up to 4 hours at 4ºC. In a sterile tissue culture hood, aortas were submerged in sterile 1X PBS + 5% P/S. All excess muscle, fat, and tissue were removed and the aortas were cut lengthwise. Once opened, the endothelial layer was scraped with a sterile surgical blade (No.10) for 30 seconds. After thorough rinsing with 1X PBS + 5% P/S, the aorta was dissected into smaller pieces and evenly distributed across a 10cm tissue culture plate, pre-treated with CellSTART® (Life Technologies) for at least 2 hours at 37ºC. All emergent cells were cultured for up to 7 days in VSC maintenance media, with media exchange on every third day (see Figure 2.1). After testing for mycoplasma (Lonza MycoAlert™), all cells were collected using 1X TrypLE (Invitrogen) and passaged onto 1% CellSTART-coated 10cm tissue culture plate. After cell expansion, second passage VSCs were stained for expression of Sox10, Sox17, and p75 to confirm the undifferentiated state of VSCs.

VSC maintenance media consists of Dulbecco's Modified Eagle Medium (Corning) supplemented with 2% Chicken Embryo Extract (MP Biomedicals, LLC), 2.5% Fetal Bovine Serum (Thermo Fisher Scientific), 1% N2, 1% B27, 1% P/S (Invitrogen), 100nM Retinoic Acid, 100μM 2-Mercaptoethanol [βME] (Sigma-Aldrich), and 20ng/mL basic fibroblast growth factor (R&D Systems).

For all experiments, rat VSCs (Passages 3-6) with 70-80% confluency were used. Unless otherwise stated, rat VSCs were seeded at 2,000 cells per cm^2 for experiments in 1% FBS (low-serum media) or 1,000 cells per cm^2 for experiments in 10% FBS (high-serum media). For all drug-treated samples, culturing media was supplemented with either DMSO or 10μM Blebbistatin.

Fabrication of Polyacrylamide Hydrogels

Polyacrylamide (pAAm) hydrogels were polymerized based on methods used by R. Pelham and Y-L Wang with modifications made by A-C Tsou.[13,14] Glass coverslips were submerged in 70% ethanol and sonicated for 15 minutes at room temperature. Air-dried coverslips were oxygen-plasma treated for 2 minutes. Silane-treated glass coverslips with a solution of 1% 16-methyltrimethoxysilane, 94% anhydrous methanol, 5% distilled water, and 57nM glacial acetic acid for 5 minutes at room temperature. Silane-treated glass coverslips were rinsed 3 times in anhydrous methanol for 1 minute at room temperature, then baked dry for 30 minutes at 110ºC. Hydrogel solutions were prepared on the silane-treated coverslips using desired rations of acrylamide monomer and bis crosslinker solutions, ammonium persulfate, and TEMED (see Table 2.1), approximately 8.3μL solution per cm^2. Separate glass slides were coated with a hydrophobic Gel-Slick® solution (Lonza) and used to prevent oxygen from inhibiting the polymerization reaction, as well as creating a uniform surface for each sample (see Figure 2.2). Hydrogels were cross-linked in a 2mg/mL solution of Sulfo-SANPAH (Thermo Fisher

Scientific) protected from light, for 30 minutes, the activated under ultraviolet light for 5 minutes at room temperature. Hydrogels were washed 3 times in 200mM HEPES, pH 8.5 for at least 5 minutes per wash at room temperature, before applying ~8.3μg/cm^2 Rat Tail Collagen I (BD Biosciences) by passive adsorption for at least 60 minutes to allow for cell attachment. All samples were sterilized using 70% ethanol for 30 minutes and washed thoroughly with sterile 1X PBS + 5% P/S, pH 7.4 prior to cell seeding.

Isolation of RNA and Quantitative Reverse-Transcription Polymerase Chain Reaction (qPCR)
The manufacturer's recommended protocol for Trizol® (Invitrogen) was used to isolate RNA. In brief, samples on each pAAm hydrogel were lysed in Trizol® after removing culturing media. Total RNA was collected using Chloroform and Phenol extractions, followed by precipitation in isopropanol overnight at -20ºC. The following day, the RNA pellet was washed in 70% ethanol (-20ºC) and air-dried for up to 10 minutes at room temperature. The RNA pellet was resuspended in nuclease-free water. RNA concentration and purity was measured on a NanoDrop™ (Thermo Scientific).

For cDNA synthesis, the Maxima 1st strand cDNA Synthesis Kit (Thermo Fisher Scientific) was used. Appendix I: Table A has a detailed list of qPCR primer sequences of the genes of interest used in this study. All qPCR primers were designed using the ABI Prism Primer Express Software version 2.0 (Applied Biosystem). The iQ5 Optical System (Bio-Rad) was used with the Maxima SYBR green/Fluorescein reagent (Thermo Fisher Scientific) to perform qPCR. RNA from rat heart, lung, liver, and bone were used to generate standard curves for genes. Gene expression levels were normalized to 18S Ribosomal RNA of each sample. Data were analyzed using iQ5 software.

Whole Cell Lysis and Immunoblotting
All samples were collected on ice and washed twice in cold 1X PBS. Approximately 100μL buffer was used for every 12cm^2 of pAAm hydrogel. For 1X RIPA buffer lysis: 50mM Tris-HCl, pH 8.0, 150mM NaCl, 1% Triton-X-100, 0.5% Sodium Deoxycholate, 0.1% SDS in diH2O was kept at 4ºC. Protease inhibitors were added to a final concentration of 1mM Sodium Orthovanadate, 1mM PMSF, 10μg/mL Leupeptin (Sigma-Aldrich) just prior to cell lysis. A DC protein assay (Bio-Rad) was used to determine relative protein concentration of each sample. Approximately 30μg of protein were loaded into each well. For 1X Sample buffer lysis: The 4X sample buffer (200mM Tris-HCl pH 6.8, 8% SDS, 40% glycerol, 0.04% Bromophenol blue) was diluted in 1X RIPA buffer with protease inhibitors (see above) (1XSB+). For each sample, 1X SB+ was pipet twice before collecting in a labeled 1.5mL tube on ice. A cell scraper was used to carefully scrape the pAAm gel for any remaining whole cell lysate. All samples were boiled for 5 minutes at 100ºC, then centrifuged at 13,000 rpm for 10 minutes at 4ºC. Equal volumes of whole cell lysates were loaded into Mini-Protean® TGX Pre-Cast gels (Bio-Rad). Gels were transferred at 4ºC overnight in 1X Transfer Buffer (25mM Tris-base, 192mM Glycine, 20% Methanol) at 30V (constant) onto PVDF membranes, pre-treated with 100% Methanol. PVDF membranes were blocked in 3% BSA (w/v) in 1X TBST (50mM Tris, pH 7.5, 120mM NaCl, 0.05% Tween-20) for 2 hours at room temperature. Primary antibodies (see Appendix II: Table A. Primary Antibodies) were diluted in 1X TBST and incubated on a rocking platform overnight at 4ºC. The following day, membranes were incubated with corresponding HRP-conjugated IgG secondary antibodies (see Appendix II: Table B. Secondary Antibodies) for 1 hour at room

temperature. Three washes in 1X TBST were performed between antibody incubations. Housekeeping proteins, like GAPDH, Lamins, and Histone proteins, were analyzed and volumes adjusted to equalize loading across samples.

Membranes were stripped and re-probed using Restore™ PLUS Western Blot Stripping Buffer (Pierce). Stripping buffer was applied to membranes for 15 minutes at room temperature on a rocking platform. Membranes were washed once in 1X TBS for 10-15 minutes followed by blocking and antibody incubation listed above.

Immunoblot Analysis

Protein bands were visualized using Western Lightning™ Plus Enhanced Chemiluminescence Substrate (PerkinElmer) and Quantity One Digital Developer software (Bio-Rad). Images were exported and quantified using ImageJ software (National Institutes of Health).[15]

For analysis, exported images from the Digital Developer software were opened and measured in ImageJ. The densities of each protein were normalized to the mean density of multiple loading controls before being normalized to glass control slide.[7,16] These data are presented as mean density normalized to glass control slide, plus one standard deviation for at least 2 separate experiments.

Fluorescent Immunocytochemistry Staining of Cells on Coverslips

All samples were placed on ice and washed twice in cold 1X PBS. Each glass coverslip was submerged in cold 4% PFA for 10 minutes at RT. Samples were rinsed 3 times with cold 1X PBS, then submerged in cold 0.2% Triton-X-100 for 15 minutes at room temperature. Samples were rinsed 3 times with 1X PBS to remove excess detergent. A blocking solution of heat-denatured BSA (0.1% w/v) was applied for two hours at room temperature. Primary antibodies (Appendix II: Table A. Primary Antibodies Used) were diluted in 1X PBS. Coverslips were placed on ParafilmM® in a humidified container overnight at 4ºC. The following morning, the coverslips were incubated in corresponding Alexa Fluor-488, -546, or -633 secondary antibodies (Life Technologies™) for 1 hour at room temperature. Samples were washed 3 times in 1X PBS for 5 minutes between antibody incubations. Fluoromount-G® (Southern Biotech) was used to mount coverslips onto slides. Epifluorescence images were taken on a Zeiss Axio Observer.A2 using Zen 2012 software. Confocal images were taken on a Zeiss LSM700 using Zen 2009 software. Images were exported and further processed using NIH ImageJ software.

Cell Proliferation Assay

The cell proliferation was quantified using Click-iT® EdU Alexa Fluor®-488 or -647 Imaging Kit (Invitrogen) according to manufacturer's protocol. Briefly, one hour prior to cell fixation, culturing media was exchanged with media containing 10μM EdU. After cell fixation and membrane permeabilization (see *Immunocytochemistry*), coverslips were rinsed twice in 0.1% heat-denatured BSA (w/v) and placed evenly on ParafilmM®. Due to surface tension and hydrophobicity of Parafilm, the Click-iT reaction volume was reduced to 200μL per coverslip. Coverslips were covered in foil and incubated for 30 minutes at room temperature. Coverslips were washed in 1X PBS for 5 minutes before proceeding with blocking and primary antibody staining (see *Immunocytochemistry*). A macro was written to automate the quantification of EdU staining and total Hoescht33342 staining of an image.

Transient Transfection of rat siRNA

For all siRNA experiments, rat VSCs were seeded at ~60-70% confluency in CEE media in a 6-well plate. In a sterile hood, rat siMRTF-A (Dharmacon, L-081405-02-0005) was resuspended to 20μM in nuclease-free water, and stored at -20ºC until use. siRNA and Lipofectamine 2000 were diluted separately in pre-warmed Opti-MEM I (Invitrogen) media for 5 minutes at room temperature. The diluted siRNA and Lipofectamine 200 were combined and mixed gently for 20 minutes at room temperature. During second incubation step, rat VSCs were rinsed two times with plain DMEM. Wells were filled with 1.5mL of plain DMEM and kept at 37ºC. 500μL siRNA-Lipofectamine 2000 complexes were added drop-wise to each well. The final concentration of siRNA is 100nM in 2mL transfection volume. After 6 hours, the transfetction media was removed and replaced with CEE. For qPCR, cells were allowed to recover 24 hours after transfection at 37ºC before harvesting RNA. For immunoblot, cells were lysed in 1XSB+ either 48 or 72 hours post transfection. For seeding onto pAAm gels, after siRNA transfection cells were collected and seeded onto pAAm gels in high serum media.

Statistical Analysis

Statistical analysis was performed using GraphPad Prism (GraphPad Software Inc., La Jolla, CA, USA). Data is presented as mean ± SD unless otherwise stated. One-way ANOVA multiple comparisons was used to test significance of differences in mean nuclear area, circularity, and SMA^+ cells on different matrix elasticities. Two-way ANOVA Dunnett's multiple comparisons test was used to determine significance of siRNA or Blebbistatin-treated cells seeded on different matrix elasticities.

2.3 Results

Rat vascular stem cells (VSCs) isolated from the thoracic aorta were cultured in VSC maintenance media (CEE) using the standardized timeline shown in Figure 2.1a. After VSC isolation (Figure 2.1b), a subset of cells were fixed and stained to confirm VSC marker expression of Sox10, Sox17, p75 (Figure 2.1c) and diffuse to no expression of differentiated SMC markers, SMA, CNN1, and MYH11 (Figure 2.1d).

Uniform polyacrylamide hydrogels (pAAm gels) were fabricated across glass surfaces through capillary action, as previously reported (Figure 2.2).[15,16] Rat VSCs were allowed to settle on pAAm gels for up to 120 minutes before filling sterile secondary containers with culturing media (Figure 2.3a,b). We determined an optimal seeding density to recover enough cells per samples at sub-confluency. We confirmed preliminary microarray results that show down-regulation of SMC markers on rat VSCs cultured on soft (~1kPa) pAAm gels compared to glass controls (Table 2.2). We show that F-actin staining (Figure 2.3c), and average nuclear area (Figure 2.3d) decrease as matrix elasticity decreases. Other components of nuclear shape, like circularity and aspect ratio (S.Figure 2.4) do not statistically differ across samples. We also pulsed samples with EdU prior to cell fixation and found proliferation rates to be similar across all samples (Figure 2.3f).

Since we observed significant decreases in nuclear area on the softest (1kPa) versus stiffest (glass) pAAm gels, we wanted to determine whether gene expression is regulated due to global

chromatin remodeling. We expected to see increases in epigenetic markers that correspond to sites of active transcription as matrix elasticity decreased. Therefore, we chose to focus on di- and tri-methylation of Lysine 4 on Histone 3, acetylation of Lysine 9 on Histone 3, and acetylation of Lysine 5 on Histone 4. Using conventional lysing conditions, cells were harvested in cold 1X RIPA buffer supplemented with protease inhibitors. Results from these samples were inconsistent, where significant changes observed fluctuated with efficient recovery of total Histone proteins.

Therefore, we modified our protocol for whole cell lysis for western blot analysis (see *Methods*). In brief, rat VSCs were lysed in 1X Sample Buffer with 5% βME. Equal volumes of each sample were loaded into wells and common loading controls (GAPDH and β-tubulin, nuclear Lamin B1, and/or total Histone 3) were stained and relative protein density measured. If necessary, subsequent immunoblot well volumes were adjusted to ensure equal protein loading (Figure 2.4 a). With full recovery of total Histone 3 and 4 proteins, no global differences were observed in rat VSCs in response to changes in matrix elasticity (Figure 2.6b). Parallel experiments were fixed and fluorescent staining for tri-methyl Lys4 or acetyl Lys9 on Histone 3 tail modifications confirm no significant changes in these markers (Table 2.4).

Next, we examined whether matrix elasticity affected expression of SMC contractile protein marker in rat VSCs (Figure 2.5a). We see that as matrix elasticity decreased, rat VSCs expression of SMC contractile proteins, SMA and CNN1, also decrease (Figures 2.5b). In Figure 2.6, representative images show MRTF-A and SMA staining of actin fibers in higher matrix elasticity samples (yellow arrowheads, glass). On soft (~1kPa) pAAm gels, MRTF-A has diffuse and/or cytoplasmic staining (white arrows). Since antibody host species for CNN1 and transcription factors are shared, we could not quantify co-staining in $CNN1^+$ cells. Samples stained for SMA and CNN1 show double-positive staining (S.Figure 2.3).

To determine whether MRTF-A regulates SMA^+ expression in rat VSCs on pAAm gels, we transfected cells with siRNA against MRTF-A, a scrambled sequence, or water control. MRTF-A gene expression significantly decreases compared to scrambled sequence (Figure 2.7a, left) and water control (data not shown). YAP, another known mechanical signaling protein, is not affected in MRTF-A knockdown samples (Figure 2.7a, right). MRTF-A knockdown also significantly decreases SMC genes, CNN1, SMA, and MYH11 (Figure 2.7b). We also confirmed MRTF-A siRNA knockdown downregulates MRTF-A and SMA expression by immunoblot (Figure 2.7c).

For our knockdown experiments, we scored MRTF-A localization and fraction of SMA^+ cells on pAAm gels compared to glass controls. In Figure 2.8a, the average fraction of SMA^+ cells decreases in MRTF-A knockdown samples, with the most pronounced affect on rat VSCs on 1kPa (blue bars). Average nuclear area (Figure 2.8b), circularity (S.Figure 2.5a), and aspect ratio (S.Figure 2.5b) are not affected by siRNA treatment on any pAAm gels. Scrambled siRNA controls show MRTF-A localization is similar to untreated controls (S.Figure 2.4a and Figure 2.6, bottom row). MRTF-A knockdown also shows an increase in cytoplasmic and/or diffuse staining (S.Figure 2.4b, bottom row) across all pAAm gels.

Lastly, we treated rat VSCs with Blebbistatin, a non-motile myosin chemical inhibitor.[17] It is commonly used to disrupt the upstream cytoskeletal relay of matrix elasticity and gene expression. Blebbistatin-treatment (black bars) dampens SMA^{+} expression in rat VSCs seeded on stiff (glass) pAAm gels (Figure 2.9a, left). Mean proliferation rate (Figure 2.9b), nuclear area (Figure 2.9c), circularity (Figure 2.9d), and aspect ratio (data not shown) are not affected by drug treatment or matrix elasticity. Figure 2.9e-h are representative images of DMSO- and Blebbistatin-treated rat VSCs on glass or 1kPa pAAm gels. Rat VSCs stained for SMA (green) and MRTF-A (red) show changes in overall cell morphology (spindle-like structures) and pancellular MRTF-A staining (Figure 2.9f,h bottom row).

2.4 Discussion and Conclusions

Preliminary DNA microarray results show matrix elasticity dependent expression of smooth muscle cell markers in rat VSCs cultured on polyacrylamide hydrogels (pAAm). Here we confirmed that as matrix elasticity decreases, expression of SMA, an early SMC marker, is downregulated. Consistent with other studies, we show that matrix elasticity affects nuclear area and cell spreading.

Interestingly, while overall nuclear area and cell spreading are affected by matrix elasticity, average cell proliferation rates are not reduced. These results are in contrast to other groups who report softer matrix elasticity suppresses cell proliferation.[18-20] Initially, I thought that the high serum concentration (10%) may mask any small fluctuations in cell proliferation rates on soft versus stiff pAAm gels. When we culture rat VSCs in low serum concentrations (1%), proliferation rates drop by about 50% (S.Figure 2.2). However, we do not see significant differences in overall rates across pAAm gels.

In work published by our group, changes in nuclear shape led to global chromatin remodeling and enhanced cell reprogramming.[21] We wanted to determine whether global chromatin remodeling was the reason for changes in contractile protein expression. We used two separate approaches to observe these changes, immunoblot and fluorescence staining. When we stained for Histone 3 tail modification of fixed rat VSCs on pAAm gels, we found no differences in total fluorescence across all samples. After modifying our cell lysis protocols, we confirmed approximately equal Histone tail modifications exist.

Previously, we characterized how in the presence of high serum, VSCs spontaneous differentiate to smooth muscle cells. We can identify these cells through upregulation of SMC markers, like CNN1, SMA, and MYH11. In healthy vessel wall repair, VSCs proliferate and then commit to SMC end fates. By contrast, disease blood vessels have varying elastic properties, and the medial layer is disrupted due to heterogeneous regions of accumulated fat, immune cells, and other secreted matrix proteins. We hypothesize that VSCs differentiate to other cell fates in response to the differences in matrix elasticity. We confirmed that expression of SMC markers, like CNN1, SMA, and MYH11, are down-regulated in rat VSC seeded on soft (1kPa) pAAm gels.

Previous studies show MRTF-A is a strong coactivator of the SRF pathway in regulating contractile and cytoskeletal protein expression. Targeted knockdown of MRTF-A in rat VSCs

shows significant decreases in SMC gene and protein expression. Consistent with other findings, we are able to show MRTF-A depletion downregulates SMA and CNN1 expression.

The interplay between MRTF-A and other transcription factors, like YAP, has been shown specifically in response to different mechanical signals.[13,22] In response to cyclic stretching, MRTF-A depletion also affects YAP expression in mouse embryonic fibroblasts. In our work, we did not see YAP gene or protein expression depleted by MRTF-A knockdown.

In response to matrix elasticity, MRTF-A localization and activity is sequestered in the cytoplasm due to changes in G-actin concentration (Figure 2.10). On average, there is a 50% reduction of SMA^+ cells when rat VSCs are seeded on soft (1kPa) compared to stiff (glass). These cells also show increased MRTF-A localization in the cytoplasm.

Targeted knockdown of MRTF-A has a more potent effect in decreasing overall SMA^+ cells. These values decrease to 10-15% of the scrambled control on glass. This likely represents the cells already committed to SMC protein expression. There may be alternative signaling factors that may direct SMC lineage commitment in the absence of MRTF-A. In untreated samples, MRTF-A nuclear localization increases as matrix elasticity increases. In contrast, MRTF-A knockdown causes an increased fraction of diffuse and weak staining in the cytoplasm.

Typical chemical inhibitors of cells on pAAm gels affect the cytoskeletal relay of the matrix elasticity to biochemical outcomes. Only in glass controls does Blebbistatin-treatment reduce the total number of SMA^+ cells, while it does not affect cell proliferation, nuclear shape, and area. Unlike targeted knockdown, Blebbistatin-treated cells do not affect MRTF-A nuclear localization.

In our simplified signaling pathway, matrix elasticity is a biophysical factor that regulates SMA and contractile protein expression in rat VSCs through MRTF-A localization (Figure 2.10). Here we propose that stiff surfaces (e.g., glass or 40 kPa) cause cells to spread, which requires more stable F-actin fibers, and decreases the pool of G-actin. MRTF-A is then released from G-actin, and can be imported into the nucleus. MRTF-A, with its co-activator SRF, begins transcription of target genes, like SMA. By contrast, on soft surfaces (e.g., 1 kPa), cells spreading and F-actin fibers decrease, and greater amounts of G-actin are available. This increase in G-actin binds and sequesters MRTF-A to the cytoplasm, where it is inactive. Since MRTF-A is required to transcribe SRF genes, downstream gene expression is decreased.

pAAm gel (kPa):	Glass (>10^6)	40	15	8	1
Acrylamide (% final)	0	8	6	6	6
Bis (% final)	0	0.05	0.50	0.25	0.05

Table 2.1 Formulation of Polyacrylamide (pAAm) Hydrogels.[15,16]

Gene	Cell Marker	$\frac{\text{1 kPa}}{\text{Glass}}$ ($\log_2$)	Fold change
Calponin 1 (CNN1)	SMC marker	-4.08	0.06
Smooth Muscle Myosin Heavy Chain (MYH11)	SMC marker	-2.34	0.20
Smooth muscle α-actin (SMA)	SMC marker	-2.00	0.25
Aggrecan (ACAN)	Chondrogenic marker	1.51	2.85
SOX10	VSC marker	-0.16	0.90
SOX17	VSC marker	-0.09	0.94

Table 2.2 Preliminary DNA microarray data show differential gene expression of smooth muscle cell and chondrogenic markers for Rat VSCs seeded on 1kPa and Glass matrix elasticity. Undifferentiated Rat VSCs were grown on pAAm gels of varying matrix elasticity (1 kPa, Glass) for 3 days in high serum media (10% FBS). There is down-regulation of smooth muscle cell markers (CNN1, SMA, MYH11) on soft (1kPa) surfaces compared to glass controls (>10^6 kPa). Conversely, there is up-regulation of a chondrocyte marker on soft surfaces compared to glass controls. VSC markers, Sox10 and Sox17, did not change on soft surfaces compared to glass controls.

Matrix elasticity:	Glass	15 kPa	8 kPa	1 kPa
Histone 3 acetyl K9	1.52±0.81	1.30±0.60	1.42±0.62	1.15±0.57
Histone 3 K4me3	1.18±0.57	1.16±0.61	1.13±0.55	1.17±0.57

Table 2.3 No significant differences in corrected total cell fluorescence of Histone 3 tail modifications of rat VSCs on pAAm gels confirms immunoblot results. Rat VSCs were cultured on pAAm gels for 2 days in high serum media. A nuclear area mask was generated from the DAPI channel of each image. Then, the corrected total cell fluorescence was calculated based on average pixel intensity minus background pixel intensity. Values represent the mean corrected total cell fluorescence ± SD for at least 2 experiments. Total cells counted for Histone 3 acetyl Lys9 are 1941 (glass), 1938 (15kPa), 1549 (8kPa), and 2173 (1kPa). Total cells counted for Histone 3 tri-methyl Lys4 are 5972 (glass), 5410 (15kPa), 5044 (8kPa), 7044 (1kPa).

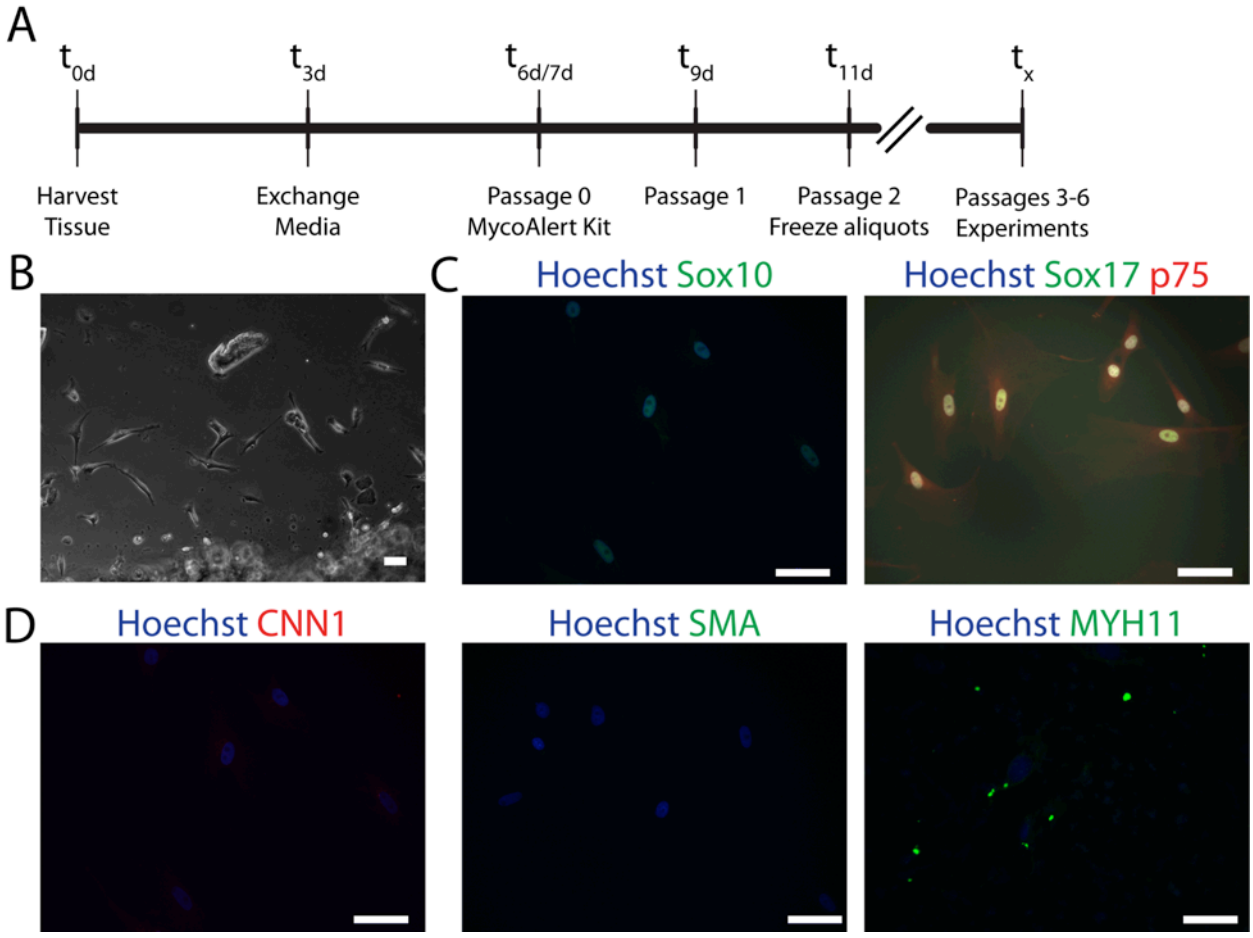

Figure 2.1 Rat vascular stem cells isolated *in vitro* using tissue explant culturing method. *A*, Timeline for rat thoracic aorta tissue explant method. *B*, Brightfield image of emerging rat vascular stem cells (VSCs) at day 4. *C*, Rat VSCs after passage 1 fixed and stained for nuclei (Hoechst33342, Hoechst) and VSC markers (Sox10, Sox17, p75) or *D,* SMC markers (CNN1, SMA, MYH11). Color labels above images correspond to fluorescent probe wavelength. Scale bar represents 50 microns.

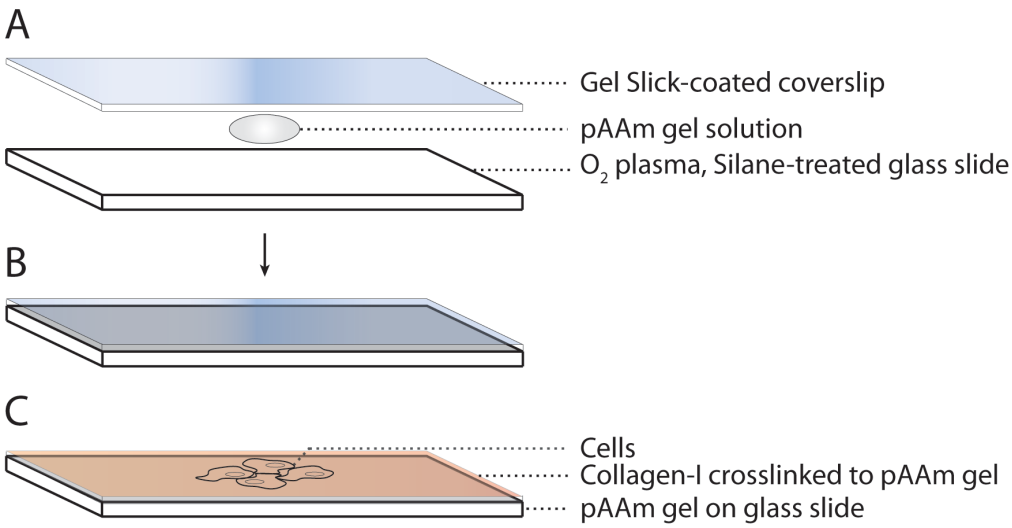

Figure 2.2 Schematic of pAAm hydrogel fabrication. *A*, pAAm hydrogel solutions are placed onto O_2-plasma and Silane-treated glass coverslips. Gel Slick-coated glass coverslips create a uniform pAAm hydrogel surface through capillary action. *B*, pAAm gels polymerize for 15 minutes before the Gel Slick-coated coverslips are removed. pAAm gels were stored in 200mM HEPES for up to 3 weeks at 4ºC prior to use. *C*, Collagen-I is crosslinked to pAAm gels to allow cell adhesion.

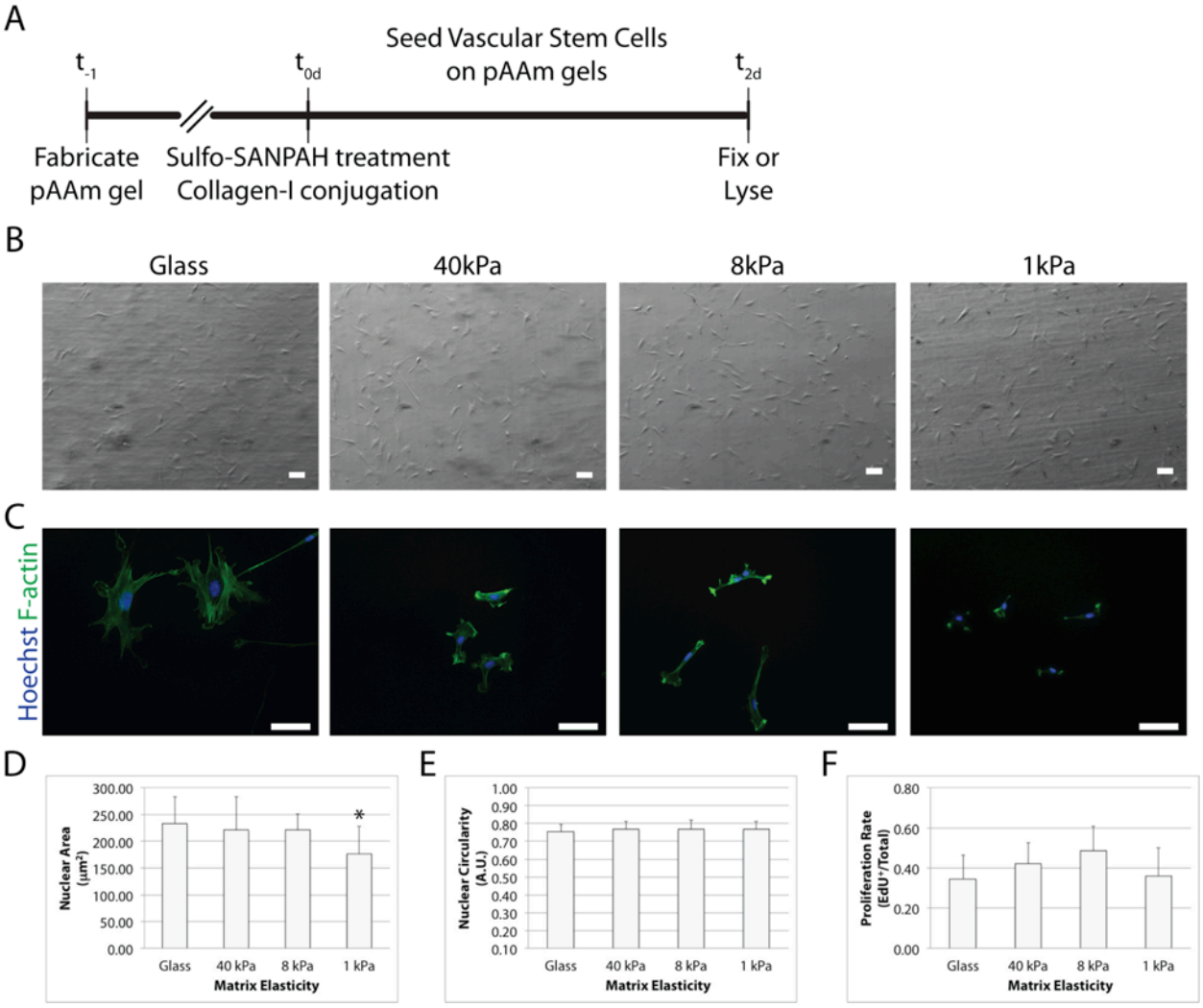

Figure 2.3 Rat VSC nuclear area and cell spreading but not cell proliferation rates decrease as matrix elasticity decreases. *A*, Experiment timeline. *B,* Representative Phase contrast images of cells at day 0. *C*, Nuclei (Hoechst) and F-actin (green) staining at day 2. Quantification of rat VSC *D,* nuclear area, *E,* nuclear circularity, and *F,* proliferation rate on pAAm gels. For *D-F,* data are presented as mean ± SD of at least 3 separate experiments. Total cells counted are 950 (glass), 1085 (40kPa), 1094 (8kPa), and 1277 (1kPa). Matrix elasticity values are given in kPa or glass control. Scale bar represents 50 microns. * $p = 0.0423$

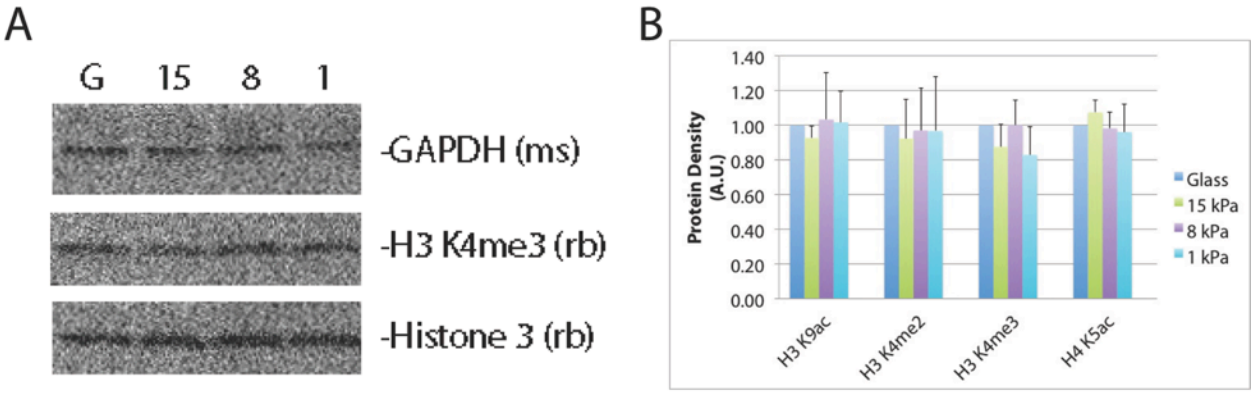

Figure 2.4 No global epigenetic changes observed in rat VSCs cultured on different pAAm gels. *A,* Representative immunoblot of rat VSCs cultured on pAAm gels lysed in 1X sample buffer + 5% βME. Equal volumes of lysate were loaded into each well. *B,* Compiled quantification of Histone 3 acetyl Lys9, di-methyl Lys4, tri-methyl Lys4, or Histone 4 acetyl Lys5. Data are mean density ± SD, for at least 3 experiments. Density normalized to mean loading control densities, then to glass control (See *Methods*). Data do not significantly differ between samples for all antibodies tested. Matrix elasticity shown are glass (G, blue), 15kPa (green), 8kPa (purple) and 1kPa (cyan).

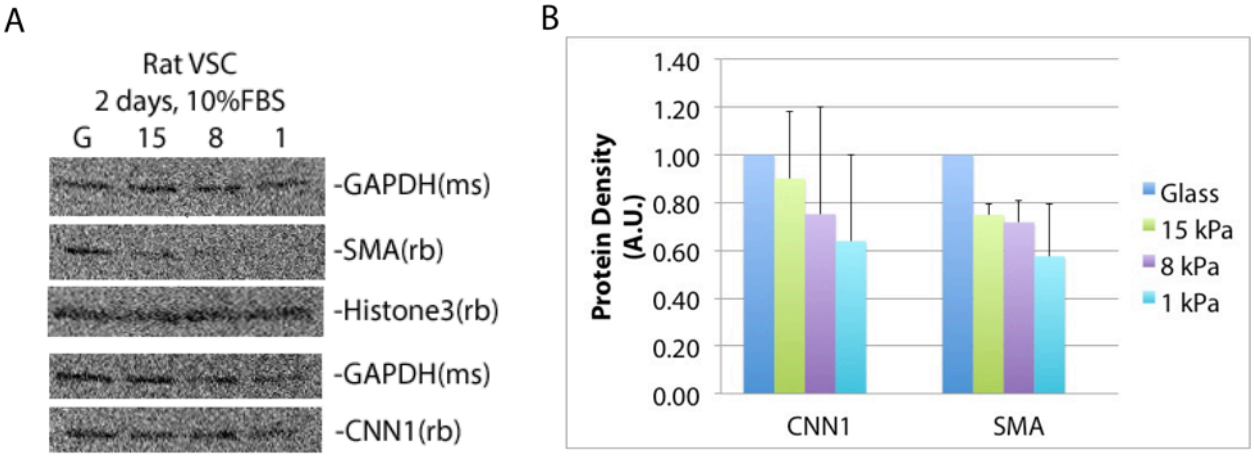

Figure 2.5. As matrix elasticity decreases, SMA protein expression, an early SMC marker, significantly decreases in rat VSCs. *A,* Immunoblot of rat VSCs whole cell lysis in 1XSB+ and probed for early SMC markers (SMA, CNN1) and loading controls (GAPDH, Histone 3). *B,* CNN1 and SMA protein expression cultured on glass (blue), 15kPa (green), 8kPa (purple), and 1kPa (cyan) pAAm gels. Data is mean density ± SD, for 2 experiments. Data is normalized to mean of loading controls, then normalized to glass. Matrix elasticity values are given in kPa or glass control, G.

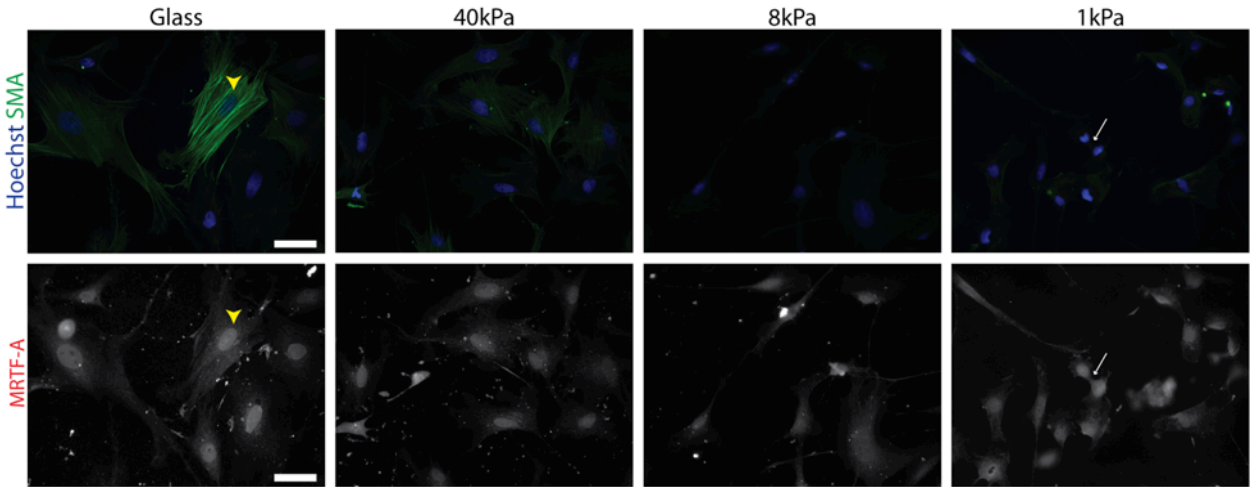

Figure 2.6 MRTF-A nuclear localization decreases as matrix elasticity decreases in rat VSCs cultured in high serum. Representative images of rat VSC stained for nuclei (Hoescht), SMA, and MRTF-A. Cell scoring for SMA^{+} staining with actin fibers is illustrated in glass and 40 kPa samples. Yellow arrowheads point out cells with strong nuclear MRTF-A staining (glass). White arrows highlight cells with diffuse and/or cytoplasmic staining (1kPa). Scale bar represents 50 microns.

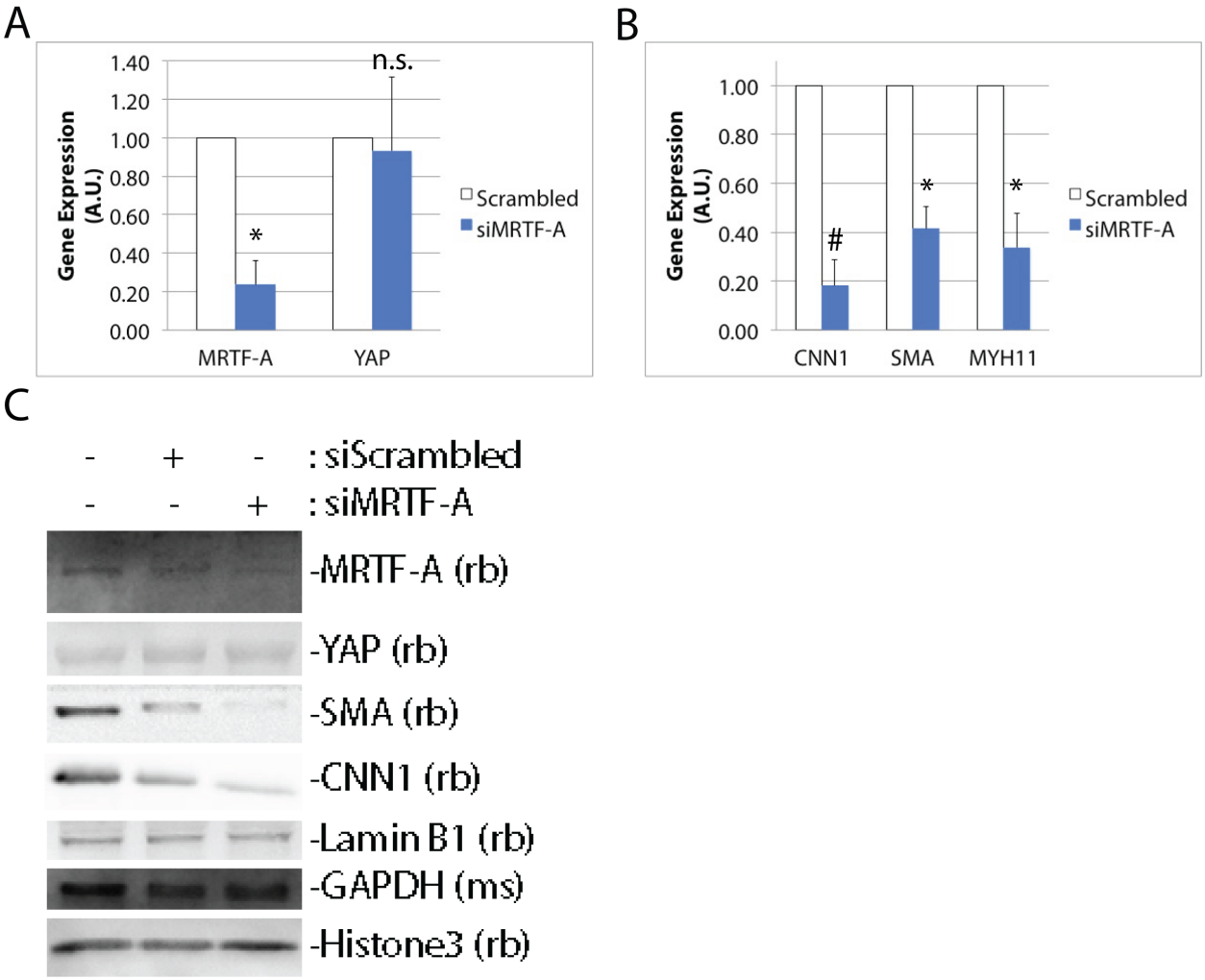

Figure 2.7 MRTF-A knockdown decreases SMC marker gene and protein expression in rat VSCs. *A,* qPCR results confirm MRTF-A mRNA knockdown (left panel, blue) does not affect YAP gene expression (right panel, blue). *B,* Only MRTF-A siRNA treated samples (blue) show down-regulation of SMC markers, CNN1, SMA, and MYH11 compared to scrambled controls (white). *C,* MRTF-A knockdown also affects SMA protein expression 48 hours after siRNA transfection. For *A-B,* data ± SD were normalized to 18S rRNA, then to siRNA scrambled control for at least 2 experiments. n.s. = not significant * $p = 0.03$ # $p = 0.002$

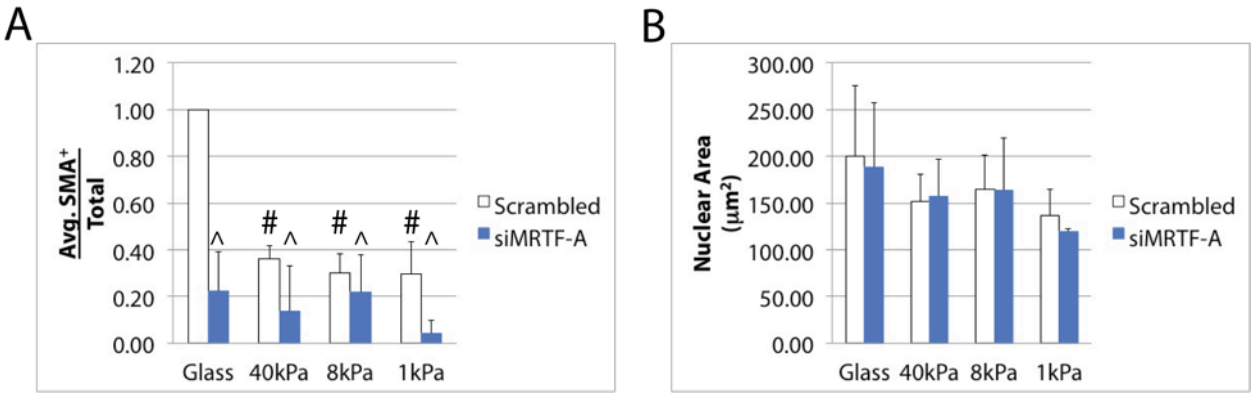

Figure 2.8 MRTF-A knockdown significantly decreases SMA$^+$ cells compared to scrambled control. *A,* Average fraction of SMA$^+$ cells normalized to glass control in scrambled control (left) or MRTF-A siRNA (right) treated cells. *B,* Mean nuclear area in scrambled or MRTF-A siRNA treated cells. Total cells scored for scrambled control are 340 (glass), 229 (40kPa), 214 (8kPa), and 194 (1kPa). Total cells scored for MRTF-A siRNA are 336 (glass, 206 (40kPa), 216 (8kPa), and 205 (1kPa). Scale bar represents 50 microns. Two-way ANOVA multiple comparison analysis were compared to scrambled glass control # $p = 0.003$ ^ $p = 0.0002$

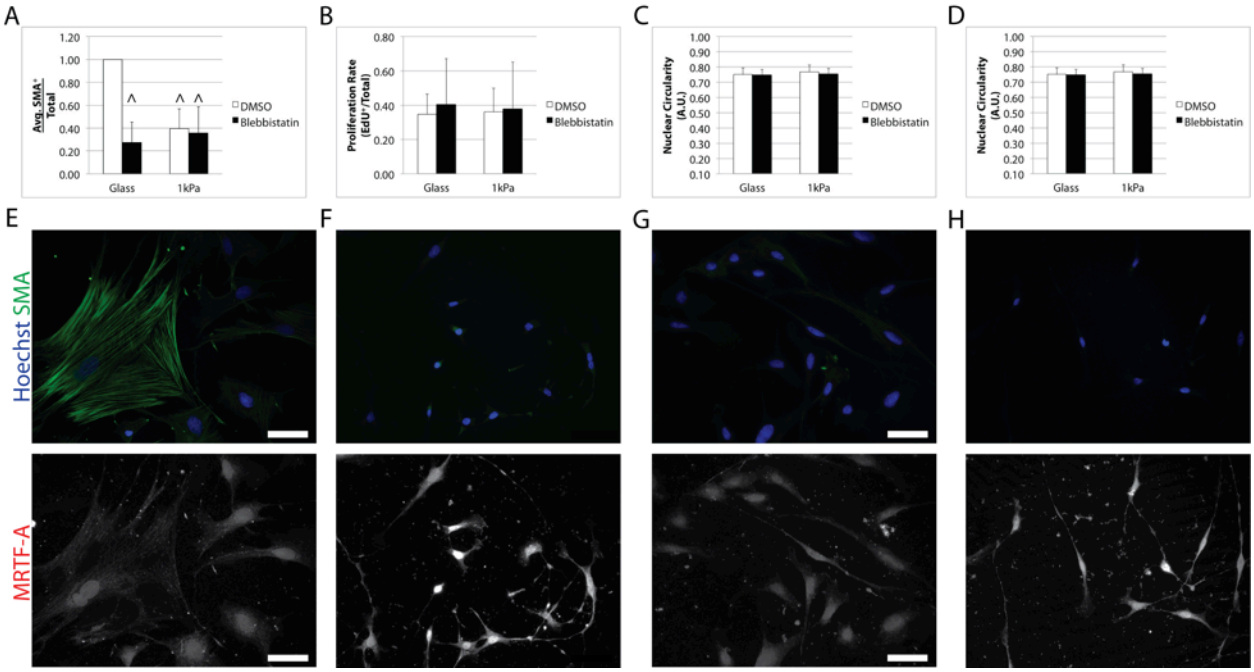

Figure 2.9 Blebbistatin-treated rat VSCs significantly decreases SMA expression in rat VSCs cultured on glass and 1kPa pAAm gels compared to DMSO-treated glass controls. *A,* Relative fraction of SMA$^+$ cells scored in DMSO (white) or 10μM Blebbistatin (black) on Glass (left) and 1kPa (right) pAAm gels. *B,* Mean cell proliferation, C, nuclear area and *D,* nuclear circularity are not significantly affected in Blebbistatin-treated cells compared to DMSO controls. *E-H,* Representative images of drug-treated rat VSCs on glass and 1kPa pAAm stained for nuclei (Hoechst), SMA (green), and MRTF-A (bottom row). Rat VSCs on glass control pAAm gels cultured in DMSO, *E,* or 10μM Blebbistatin, *F*. Rat VSCs on 1kPa pAAm gels cultured in DMSO, *G,* or 10μM Blebbistatin, *H*. Data represent mean values ± SD for at least 2 experiments.

For *A-D,* total cells counted in Blebbistatin-treated samples are 521 (glass) and 535 (1kPa). Scale bar represents 50 microns. ^ $p = 0.004$

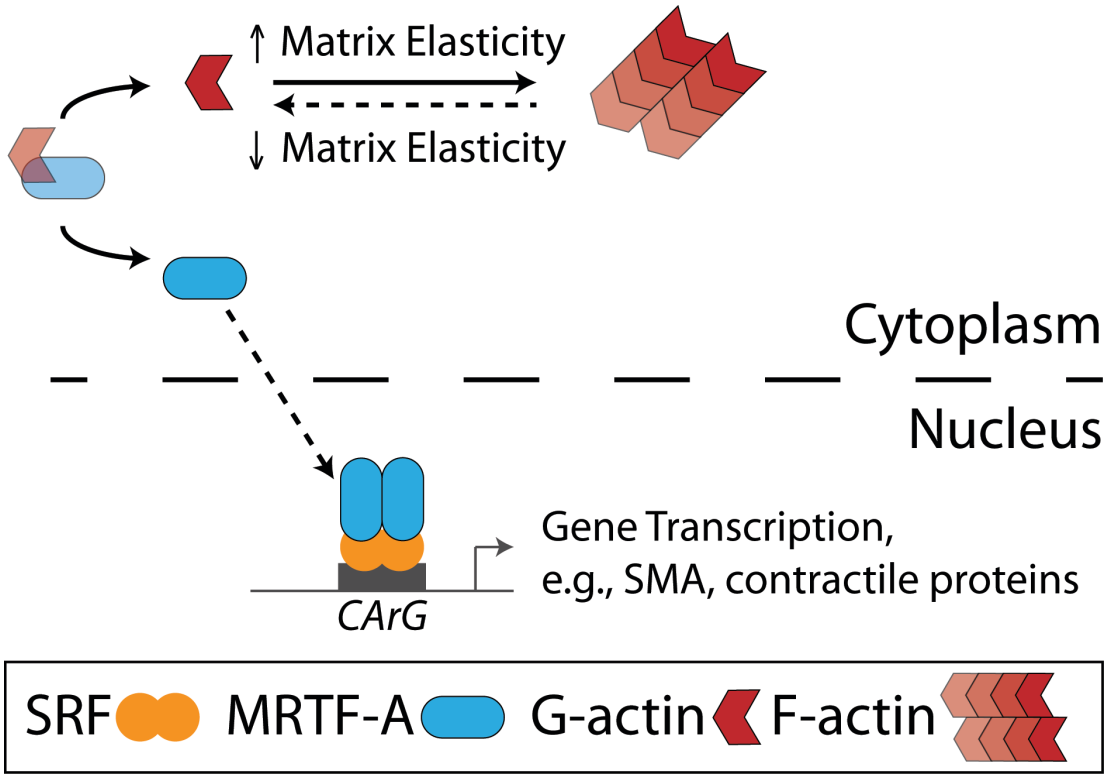

Figure 2.10 Model of how matrix elasticity regulates MRTF-A localization via actin binding and results in decreased SMA gene expression.[4,5] MRTF-A activity is regulated by its localization within a cell. In high serum media, serum response factor (SRF) is present. On soft surfaces with low matrix elasticity, cell spreading and F-actin fibers decrease. This increase in G-actin can bind to MRTF-A, which sequesters MRTF-A in the cytoplasm. As matrix elasticity increases, F-actin is formed from G-actin. MRTF-A is released from G-actin, and is imported into the nucleus. SRF and MRTF-A are co-activators whose downstream gene targets include SMA, and other contractile proteins. The shift in MRTF-A localization to the cytoplasm prevents gene transcription and results in lower total SMA^+ cells.

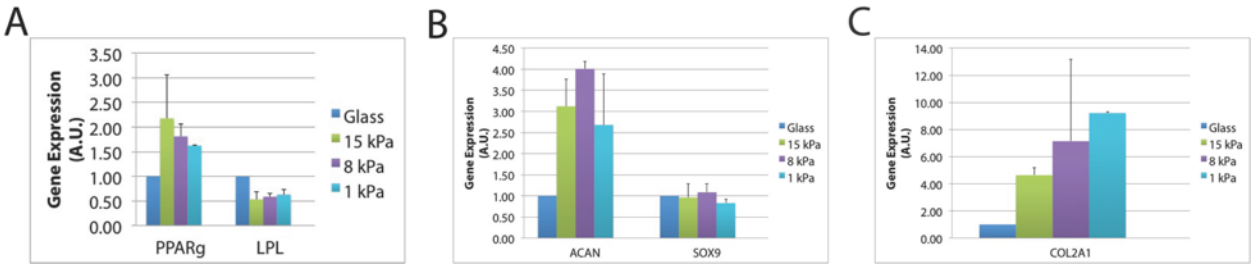

Supplemental Figure 2.1 Rat VSCs cultured in high serum on various pAAm gels confirm DNA microarray trends. qPCR results of *A,* adipogenic cell markers, PPARγ and LPL, or chondrogenic cell markers, *C,* ACAN and SOX9, and *D,* COL2A1. Data are mean expression ± SD, for 2 experiments. Data are normalized to 18S rRNA, then to glass control. Matrix elasticity represented are glass (blue), 15 kPa (green), 8 kPa (purple), and 1 kPa (cyan).

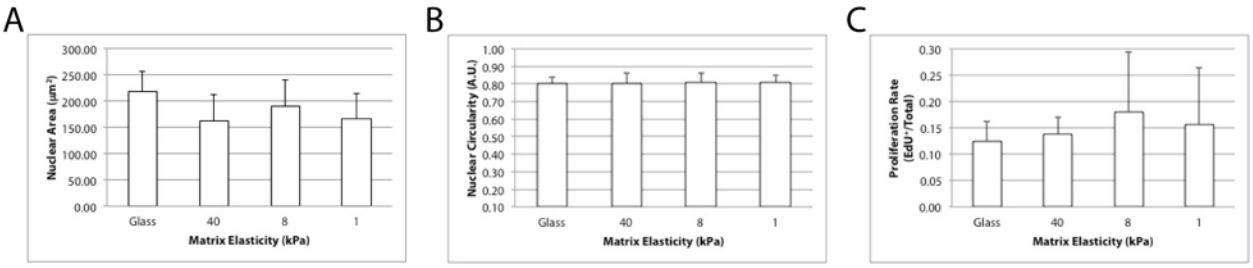

Supplemental Figure 2.2 Rat VSCs average nuclear area, circularity and proliferation rates in low serum media. Quantification of rat VSC *A*, nuclear area, *B*, nuclear circularity, and *C*, proliferation rate on pAAm gels. Data represent mean ± SD, for at least 3 experiments. For *A-B*, total number of cells counted is 3298 (glass), 2096 (40kPa), 3258 (8kPa), and 3165 (1kPa). For *C*, total number of cells counted is 1497 (glass), 1731 (40kPa), 1838 (8kPa), and 1615 (1kPa).

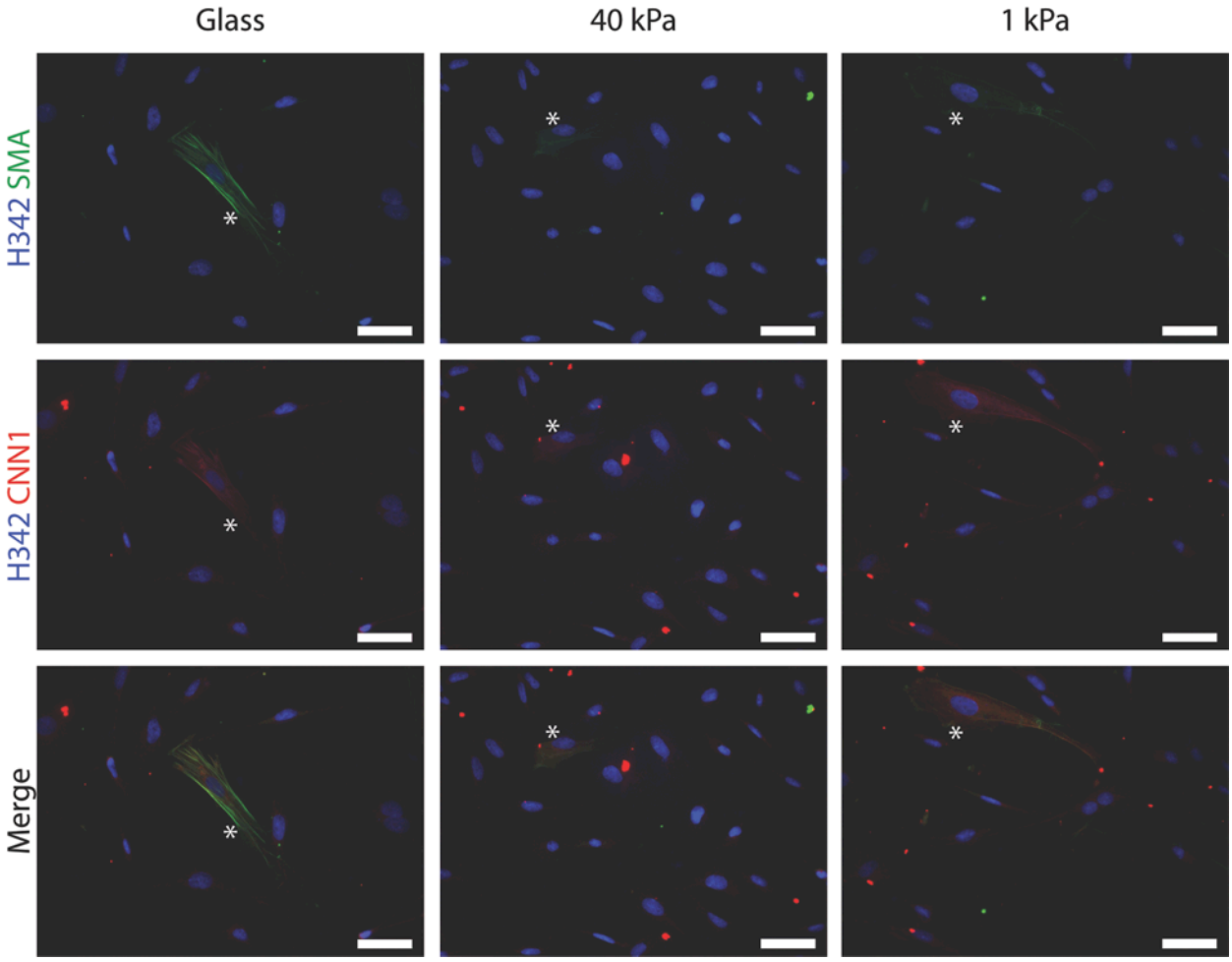

Supplemental Figure 2.3 SMA and CNN1-positive rat VSCs cultured in high serum on pAAm gels. Images of SMA and CNN1-positive staining of rat VSCs on glass, 40 kPa, and 1 kPa polyacrylamide hydrogels. Scale bar represent 50μm. Asterisk shows double-positive staining of actin fibers.

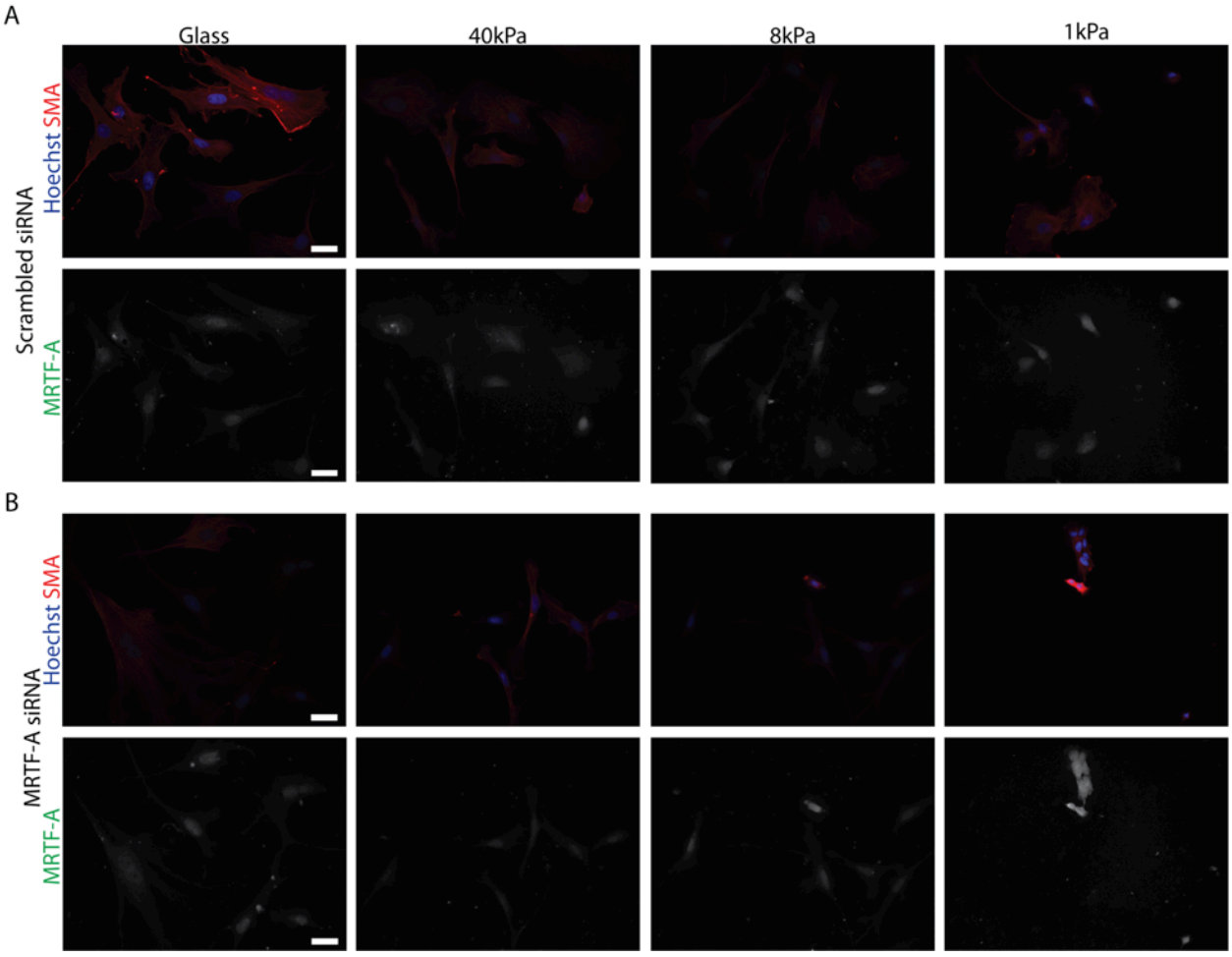

Supplemental Figure 2.4 MRTF-A knockdown show diffuse cytoplasmic staining on all pAAm gels. *A,* Scrambled and *B,* MRTF-A siRNA transfected rat VSCs stained for nuclei (Hoechst), SMA (red), and MRTF-A (bottom row). Scale bar represents 50 microns.

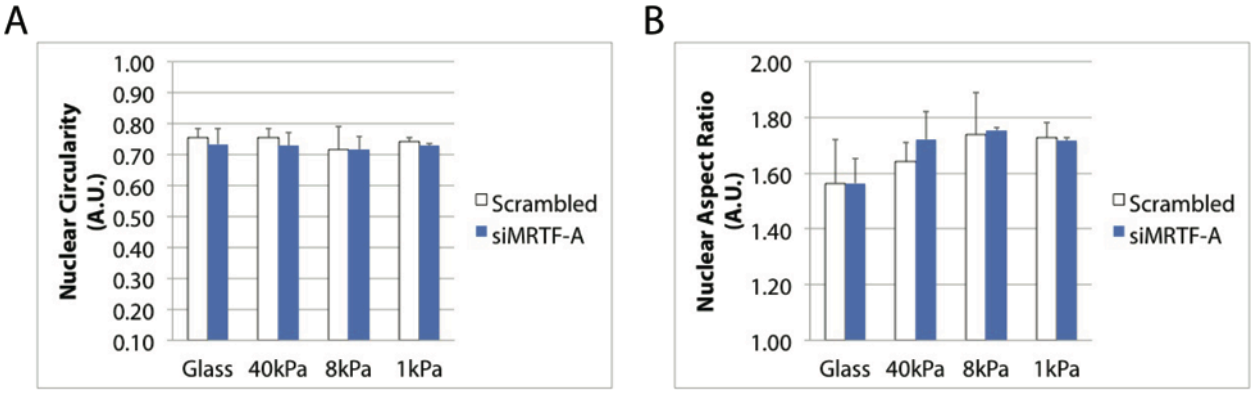

Supplemental Figure 2.5 No significant changes in nuclear circularity or aspect ratio in siRNA-treated samples. *A,* Average nuclear circularity and *B,* nuclear aspect ratio of scrambled (white) or siMRTF-A (blue) cells. Data represent mean ± SD for Figure 2.9.

References

1. Tang Z, et al. (2013). Smooth Muscle Cells: To Be Or Not To Be? *Circ. Res.* 112: 23-26.
2. Parmacek MS. (2007). Myocardin-Related Transcription Factors: Critical Coactivators Regulating Cardiovascular Development and Adaptation. *Circ. Res.* 100: 633-644.
3 Posern G, Treisman R. (2006). Actin' together: serum response factor, its cofactors and the link to signal transduction. *TRENDS in Cell Biol.* 16(11): 588-596.
4 Wang D-Z, et al. (2001). Activation of Cardiac Gene Expression by Myocardin, a Transcriptional Cofactor for Serum Response Factor. *Cell* 105: 851-862.
5 Du KL, et al. (2003). Myocardin Is a Critical Serum Response Factor Cofactor in the Transcriptional Program Regulating Smooth Muscle Cell Differentiation. *Mol. Cell. Biol.* 23(7): 2425-2437.
6 Wang D-Z, et al. (2002). Potentiation of serum response factor activity by a family of myocardin-related transcription factors. *PNAS* 99(23): 14855-14860.
7 Cen B, et al. (2003). Megakaryoblastic Leukemia 1, a Potent Transcriptional Coactivator for Serum Response Factor (SRF), Is Required for Serum Induction of SRF Target Genes. *Mol. Cell. Biol.* 23(18): 6597-6608.
8 Mirralles F, Posern G, Zaromytidou A-I, Treisman R. (2003). Actin Dynamics Control SRF Activity by Regulation of Its Coactivator MAL. *Cell* 113: 329-342.
9 Cui Y, et al. (2015). Cyclic stretching of soft substrates induces spreading and growth. *Nat. Commun.* 6: 6333.
10 McGee KM, et al. (2011) Nuclear transport of the serum response factor coactivator MRTF-A is downregulated at tensional homeostasis. *EMBO J.* 12(9): 963-970.
11 Huang X, et al. (2012). Matrix Stiffness-Induced Myofibroblast Differentiation Is Mediated by Intrinsic Mechanotransduction. *Am. J. Respir. Cell. Mol. Biol.* 47(3): 340-348.
12 Tang Z, et al. (2012). Differentiation of Multipotent Vascular Stem Cells Contributes to Vascular Diseases. *Nat. Commun.* 3: 875.
13 Pelham RJ and Wang Y-L. (1997). Cell Locomotion and Focal Adhesions are Regulated by Substrate Flexibility. *PNAS* 94: 13661-13665.
14 Tsou, D A-C. (2012). Engineering Cell and Tissue Mechanical Microenvironments for Regenerative Medicine (Doctoral Dissertation). UC Berkeley: Bioengineering. Retrieved from http://escholarship.org/uc/item/90s569kq
15 Abramoff MD, Magalhaes PJ, and Ram SJ. (2004). Image Processing with ImageJ. *Biophotonics International* 11(7): 36-42. Retreived from http://rsb.info.nih.gov/ij/docs/menus/analyze.html#gels on 15 June 2013.
16 Janes KA. (2015) Methods: An Analysis Of Critical Factors For Quantitative Immunoblotting. *Science Signaling* 8(371): rs2. doi: 10.1126/scisignal.2005966.
17 Kovács M, et al. (2004) Mechanism of Blebbistatin Inhibition of Myosin II. *JBC* 279(34): 35557–35563.
18 Mih JD, et al. (2012). Matrix stiffness reverses the effect of actomyosin tension on cell proliferation. *JCS* 125: 5974-5983.
19 Guilak F, et al. (2009). Control of Stem Cell Fate by Physical Interactions with the Extracellular Matrix. *Cell Stem Cell* 5: 17-26.
20 Mammoto A, Ingber DE. (2009). Cytoskeletal control of growth and cell fate switching. *Curr. Opin. Cell Biol.* 21:864–870.
21 Downing TL, et al. (2013). Biophysical regulation of epigenetic state and cell

reprogramming. *Nature Materials* 12: 1154-1162.
22 Dupont S, *et al.* (2011). Role of YAP/TAZ in mechanotransduction. *Nature* 474: 179-183.

Chapter 3: Role of Sox Family Proteins in Vascular Stem Cell Maintenance

In this chapter, experiment design, data collection and analysis was performed by myself, in collaboration with Julia Chu and Song Li.

3.1 Introduction

Members of the Sox family of transcription factors have been shown to be critical for embryonic development, sex differentiation, stem cell maintenance, and differentiation (Chapter 1).

In this chapter, we used several knockdown strategies to determine whether Sox protein expression affects the differentiation or maintenance of rat vascular stem cells (VSCs). In our first report and characterization of rat VSCs, long-term cultures in high serum media (>4 weeks in 10%FBS) results in loss of Sox10 and Sox17 expression and up-regulation of known smooth muscle cell markers, CNN1, SMA, and MYH11.[1] Directed differentiation to smooth muscle cells in serum-free media with TGFβ1 also produces similar results in rat VSCs.

We hypothesized that the high expression of Sox family members in early passage VSCs may have a similar role in either preventing VSC differentiation or VSC maintenance. To determine whether knockdown affects stem cell maintenance, we characterized the effects on VSC proliferation, smooth muscle cell gene expression, cell migration, and directed differentiation.

3.2 Materials and Methods

Isolation of Rat Vascular Stem Cells and Cell Culture
See Chapter 2 Methods.

Isolation of Mouse Vascular Stem Cells and Cell Culture
For mouse vascular stem cell isolation, culturing timeline follows Chapter 2 methods, except for a Collagenase type II digestion for 20 minutes at 37ºC. After digestion, VSC maintenance media and tissue were centrifuged at 1000rpm for 4 minutes at RT. Tissue explants were cut similar to rat tissue and equally distributed across 6cm tissue culture plates pre-treated with CellSTART. Mouse VSC culturing was similar to rat VSC in Chapter 2 Methods.

Immunoblot Analysis
See Chapter 2 Methods.

Fluorescent Immunocytochemistry Staining of Cells on Coverslips
See Chapter 2 Methods. For all images using the ImageXpress Micro (IXM, Molecular Devices) system, software settings were designed to take multiple images equally distributed across each sample using the same exposure and gain. To quantify cell proliferation by EdU^{+}-staining, the MetaXpress software (Molecular Devices) first scores all cell nuclei through Hoescht33342 staining. Positive cells are when immunofluorescent staining thresholds overlap between the assigned channels (e.g., Hoescht33342 and EdU-AF488).

Isolation of RNA and Quantitative Reverse-Transcription Polymerase Chain Reaction (qPCR)

See Chapter 2 Methods.

Cell Proliferation Assay
See Chapter 2 Methods.

Transient Transfection of rat siRNA
See Chapter 2 Methods.

Rat siRNA Sox10 (Dharmacon, L-090803-02-0005; Ambion, s131239) and rat siRNA Sox17 (Dharmacon, L-090803-02-0005; Ambion s162077). Mouse siRNA Lamin A/C (Santa Cruz Biotechnology, Inc. sc-29385), mouse Sox10 (Dharmacon, L-049957-01-0005), and mouse Sox17 (Dharmacon, L-059106-01-0005). Rat VSCs were allowed to recover in VSC maintenance media post transfection.

Rat shRNA Plasmid Purification and G418 Selection
Each rat SureSilencing shRNA Sox10 (SA Biosciences, KR45102N) and Sox17 (SA Biosciences, KR43961N) stock plasmids were amplified in DH5α competent cells. From single clones, DNA plasmids were purified using the NucleoBond® Xtra Maxi Plasmid DNA Purification kit (Clontech) following manufacturer's instructions. The DNA pellet was resuspended in nuclease-free water. DNA concentration and purity was measured on a NanoDrop™ (Thermo Scientific). *PstI* restriction digests also confirmed the shRNA insert and antibiotic resistance (S.Fig.3.2).

DNA plasmids were transfected with Lipofectamine2000 (Invitrogen) for 6 hours, then changed to VSC maintenance media. After 6 days in culture, cells were grown in selection media (VSC maintenance media supplemented with 200μg/mL G418) for up to 7 days before experimental use.

G418 selection was determined by seeding $1x10^4$ rat VSCs per mL in duplicate wells of a 24-well plate. The following day, VSC maintenance media was supplemented with 0, 100, 200, 400, or 800 μg/mL G418. Media was exchanged every other day for up to 1 week. Cells were fixed and stained in 0.5% crystal violet (50mg crystal violet powder in 25% methanol) for 20 minutes at RT. Wells were washed 3 times in distilled water and allowed to air dry at RT. On a shaking platform, 500μL of 10% acetic acid was added to each well for 20 minutes at RT. Absorbance at 595nm was measured to determine optimal antibiotic selection based on cell survival. (S.Fig.3.3)

GFP-tagged mouse Sox10 DNA Plasmid Purification
FLAG-tagged mouse Sox10 cDNA was a generous gift from Dr. Yick Fong (R. Tjian lab). The cDNA was shuffled to the pEGFP-N1 plasmid (Karl Banta, A. Winoto lab) using the *EcoRI, BamHI* restriction enzyme sites. A double restriction enzyme digest confirmed the insert was ligated into the pEGFP-N1 vector (S.Fig.3.8). The sequence was verified using the UCB Sequencing Facility.

Directed Differentiation Assay
For adipogenic differentiation, DMEM with 10% FBS, 1% P/S, 500μM 3-isobutylmethylxanthine, 1μM Dexamethasone (Sigma-Aldrich), and 10μg/mL Insulin

(Invitrogen) was exchanged every 3 days for at least 2 weeks. Lipid accumulation was confirmed through Oil Red O staining. In brief, rat VSCs were washed and fixed (see *Immunocytochemistry*). Cells were rinsed in 60% isopropanol, then stained in freshly prepared Oil Red O working solution for 15 minutes at RT. Mix 6mL 0.05% Oil Red O in 4mL distilled water for 10 minutes at RT, then pass solution through a 0.22μm filter before use. Rinse samples in 60% isopropanol once, then rinsed with distilled water until excess dye particles are removed (2-3X). Keep samples in distilled water and image immediately.

For osteogenic differentiation, DMEM with 10% FBS, 1% P/S, 10mM β-glycerophosphate, 0.1μM Dexamethasone, and 200μM Ascorbic Acid (Sigma-Aldrich), was exchanged every 3 days for at least 3 weeks. Calcium deposits were stained using Alizarin Red S stain. In brief, rat VSCs were washed and fixed (see Chapter 2 Methods). 2% Alizarin Red S, pH 4.1 was stained for up to 5 minutes at RT. Excess dye was blot dry. For TC plates, scan and image immediately. For cells seeded on pAAm gels, were dehydrated in 100% acetone, then in 1:1 acetone-xylene, and cleared in Xylene. A synthetic mounting media (Permount) was used to preserve staining.

For smooth muscle cell differentiation, DMEM, 1% P/S, and 20ng/mL TGF-β1 was exchanged every other day for up to 2 weeks. For spontaneous smooth muscle cell differentiation, DMEM, 10% FBS, and 1%P/S was exchanged every other day for up to 2 weeks. See *Immunocytochemistry* for cell fixation and staining.

Statistical Analysis
See Chapter 2 Methods.

3.3 Results

Preliminary experiments with Sox10 and Sox17 siRNA did not show knockdown of gene expression 24 hours post transfection (Fig. 3.1a, S.Fig. 3.1). After 3 days post-transfection, Sox10 siRNA-treated rat VSCs does show ~50% knockdown of gene expression (Fig. 3.1c, left green bar) without affecting Sox17 expression (Fig. 3.1c, right green bar). In these samples, SMA and MYH11 expression does increase, but not significantly (Fig.3.1d, middle and right green bars). However, when we fixed siRNA-transfected cells, there is no loss of Sox10 nuclear localization compared to scrambled controls (Fig.3.2a-b). We also do not see significant decreases in proliferation rates of Sox10 siRNA-treated rat VSCs.

We used commercially available shRNA plasmids against rat Sox10 or Sox17 for long-term stable knockdown in rat VSCs (S.Fig.3.2). We established an optimal antibiotic selection concentration (S.Fig.3.3). Rat VSCs were allowed to recover for 6 days post-shRNA plasmid transfection, and then selection media was exchanged for up to 7 days before cells were used. Initial experimental results show shSox10#3 had >50% knockdown of Sox10 without affecting Sox17 gene expression (S.Fig.3.4a). None of the shSox17 plasmids showed robust knockdown of Sox17 (S.Fig.3.4b). We proceeded with shSox10#3 in our shRNA experiments. Repeated experiments using stable rat shSox10#3 cell lines do not exhibit significant changes in Sox10 gene expression, SMC marker expression, or proliferation rates (Fig.3.3). Similar to siRNA results, rat VSC shSox10 cell lines show robust Sox10 nuclear staining (Fig.3.4c), while Sox17 expression appears diffuse and/or cytoplasmic (Fig.3.4f).

Spontaneous differentiation of stable rat VSC shSox10 cell lines (Fig.3.5f) in high serum media does not show increased SMA expression compared to parent (Fig.3.5d) or scrambled shRNA cell lines (Fig.3.5e). We produced similar results when 20ng/mL TGF-β1 was supplemented in basal media (Fig.3.6).

When shSox10#3 rat VSCs cell lines were passaged, Sox10 gene expression is recovered (S.Fig.3.5a, green bars). Directed differentiation of shSox10#3 cell lines to smooth muscle, adipogenic, and osteogenic cell fates did not show significant differences compared to parental or scrambled shRNA cell lines (S.Fig.3.6).

In overexpression experiments, we found that GFP-tagged Sox10 could be expressed in rat VSCs and localizes to the nucleus (Fig.3.7b). However, after 7 days in culture, we were unable to maintain or increase total GFP-positive cells in culture (Fig.3.7d,e). We concluded that the overexpression of Sox10-GFP was toxic to cells.

3.4 Discussion and Future Directions

Isolation and characterization of vascular stem cells show high expression of Sox family members. Our working hypothesis was that loss of either protein affects the multipotency of rat VSCs, and that culturing in high serum media would increase expression of SMC markers, like SMA and CNN1. We tried a number of approaches to knockdown either Sox10 or Sox17 expression in rat VSCs. First, we transfected rat VSCs with Sox10 and/or Sox17 siRNA for short-term studies. Instead, data were inconclusive due to insufficient knockdown of Sox proteins and recovery within 5 days. We also tried to use siRNA to knockdown expression of Sox proteins in mouse VSCs (S.Fig.3.7) and got similar inconclusive results. In contrast, mouse Lamin A/C siRNA-treated VSCs did show gene knockdown for up to three days in culture (data not shown).

Our next approach was to generate stable cell lines expressing shRNA against Sox10 or Sox17. We used commercially available shRNA plasmids to generate these long-term knockdown cell lines. Our initial results determined shSox10#3 knocked down Sox10 mRNA without affecting Sox17 expression levels. However, even after antibiotic selection, we still see the remaining cells in culture stain positively for Sox10.

Using early passage shSox10 cell lines, we expected to see an increase in SMC marker expression, especially in high serum media. Although Sox10 expression is greatly reduced in shSox10 cell lines compared to scrambled control, this reduction is comparable to expression lost in parental cell lines (S.Fig.3d-f). In directed differentiation to adipogenic, osteogenic, and smooth muscle cell fates, shSox10 cell lines also did not significantly increase compared to controls.

Sox10 is known to play a key role in cell migration and metastasis of melanoma cells.[2] We did not see significant differences in transwell migration in rat VSCs with targeted knockdown of Sox10 (data not shown).

I transfected a GFP-tagged Sox10 to determine whether overexpression of Sox10 affects rat VSC maintenance. GFP-tagged Sox10 shows strong nuclear localization compared to ubiquitous GFP expression of the empty vector control. However, we saw dramatic decreases in total GFP-positive cells after 7 days in culture. Since we were unable to maintain these rat VSCs, we concluded that overexpression of GFP-tagged Sox10 is toxic to rat VSCs.

Taken together, these data suggest that targeted knockdown of Sox proteins in early passage rat VSCs recover expression of Sox10 and Sox17. As previously stated (see Chapter One), there is no exclusive marker of SMCs to coincide with specific differentiation state(s). In our work, we were able to use Sox10 and Sox17 as early rat and human VSC markers. While our current isolation protocol for rat VSCs is still a heterogeneous pool of cells, other groups have since used $Sox10^+$ staining to isolate and characterize migrating cell populations from tissue explant and enzyme digestion cultures.[3] Some commercially available rat smooth muscle have also shown $Sox10^+$ nuclear staining.[4]

Curiously, when I used *in situ hybridization* (ISH) in uninjured blood vessels, I could not detect Sox expression within the medial or adventitial layers of the vessel wall (data not shown). In order to address which cells directly contribute to cardiovascular disease, it is necessary to identify and characterize the vascular stem cell niche.

G.K. Owens and colleagues, sought to identify "de-differentiated" SMCs in single cells and tissue samples, even as antibodies do not detect SMC proteins like MYH11.[5] Their report combined ISH of a biotin-labeled DNA probe to target the Myh11 promoter with Histone 3K4me2 antibody staining using a proximal ligation assay (PLA).

While tissue sections stain weakly against MYH11, they show that ~66% of cells were Myh11 H3K4me2 PLA^+ efficiency being similar to that of other ISH methods for tissue samples. Based on the identification of potential epigenetic signatures, a similar method would be useful to know what fraction, if any, of Myh11 H3K4me2 PLA^+ cells are also Sox10 and/or Sox17 positive. Curiously, in their images of single SMC staining, not all SMA^+ cells are PLA^+.

A similar lineage-tracing method developed in our lab combines *in situ* PCR and Histone3K4me2 antibody staining (Danny Huang, unpublished data). Early results show that VSCs isolated from tissue explant culture are negative for Myh11 labeling. Consistent with antibody staining, these VSCs are positive for Sox10 labeling. Clarification of separate populations of cells within the healthy and damaged vessel wall, including VSCs and/or de-differentiated SMCs will help broaden development of new therapeutic approaches to cardiovascular disease.

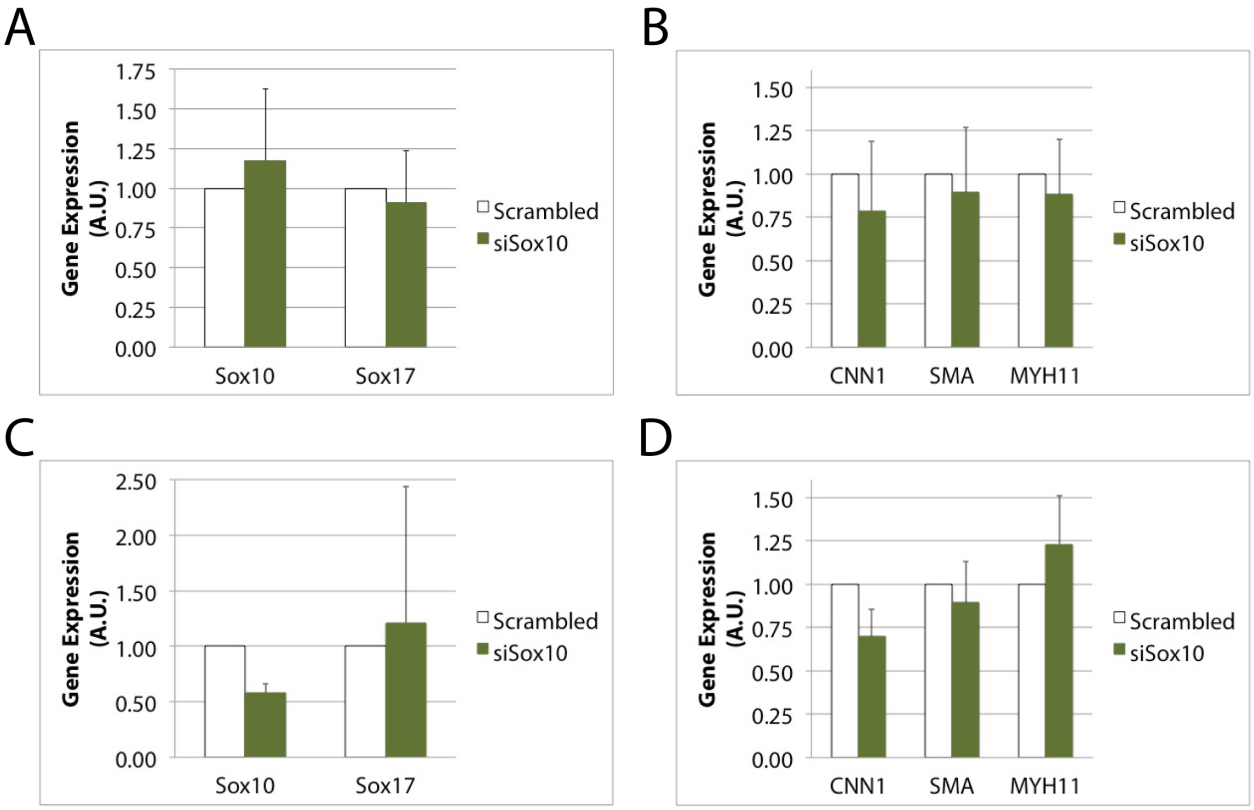

Figure 3.1 Three days after targeted knockdown of Sox10 in rat VSCs does not significantly increase expression of SMC markers. One day post-transfection, Sox10 siRNA (green bars) do not show changes in *A,* Sox10 (left) or Sox17 (right) gene expression compared to scrambled siRNA controls (white bars). *B,* SMC markers, CNN1 (left), SMA (middle), MYH11 (right) also do not show significant increase in gene expression. *C,* Three days post-transfection, Sox10 siRNA (green, left) show decreased expression of Sox10, but not Sox17 gene expression compared to controls. *D,* Only MYH11 shows increased expression in rat VSCs with decreased Sox10 expression compared to scrambled control. Data ± SD were normalized to 18S rRNA, then to siRNA scrambled control for at least 3 experiments.

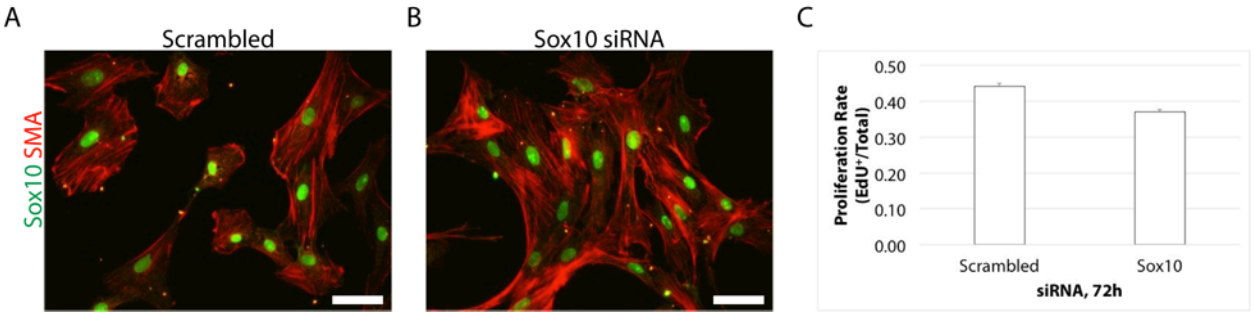

Figure 3.2 Targeted Sox10 knockdown in rat VSCs does not significantly decrease Sox10 protein expression, SMA$^+$ staining, or proliferation rates compared to scrambled control. Representative images of rat VSCs transfected with *A,* scrambled or *B,* Sox10 siRNA recovered in VSC maintenance media for three days. *C,* Mean proliferation rate does not significantly decrease in Sox10 siRNA-treated rat VSCs compared to scrambled controls. Data are mean ± SD

from multiple images taken per well, using the automated IXM workstation at the Shared Stem Cell Facility. Total cells counted are 48,998 (scrambled) and 40,928 (Sox10 siRNA).

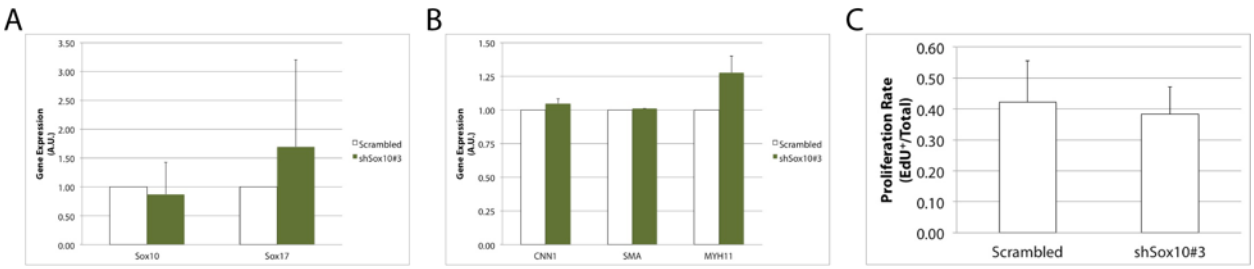

Figure 3.3 Stable rat Sox10 shRNA cell lines does not significantly decrease Sox10 gene expression or proliferation rates. *A,* shSox10#3 cell lines do not show consistent loss of Sox10 expression over time (left, green) compared to scrambled control (white). *B,* SMC markers, CNN1 (left), SMA (middle), MYH11 (right) also do not show significant increase in gene expression. *C,* Proliferation rates of shSox10#3 cell lines compared to scrambled controls. For *A-B,* data ± SD were normalized to 18S rRNA, then to siRNA scrambled control for at least 2 experiments. For *C,* data are mean ± SD from multiple images taken per well, using the automated IXM workstation at the Shared Stem Cell Facility. Total cells counted are 29,318 (scrambled) and 29,846 (Sox10 #3 shRNA).

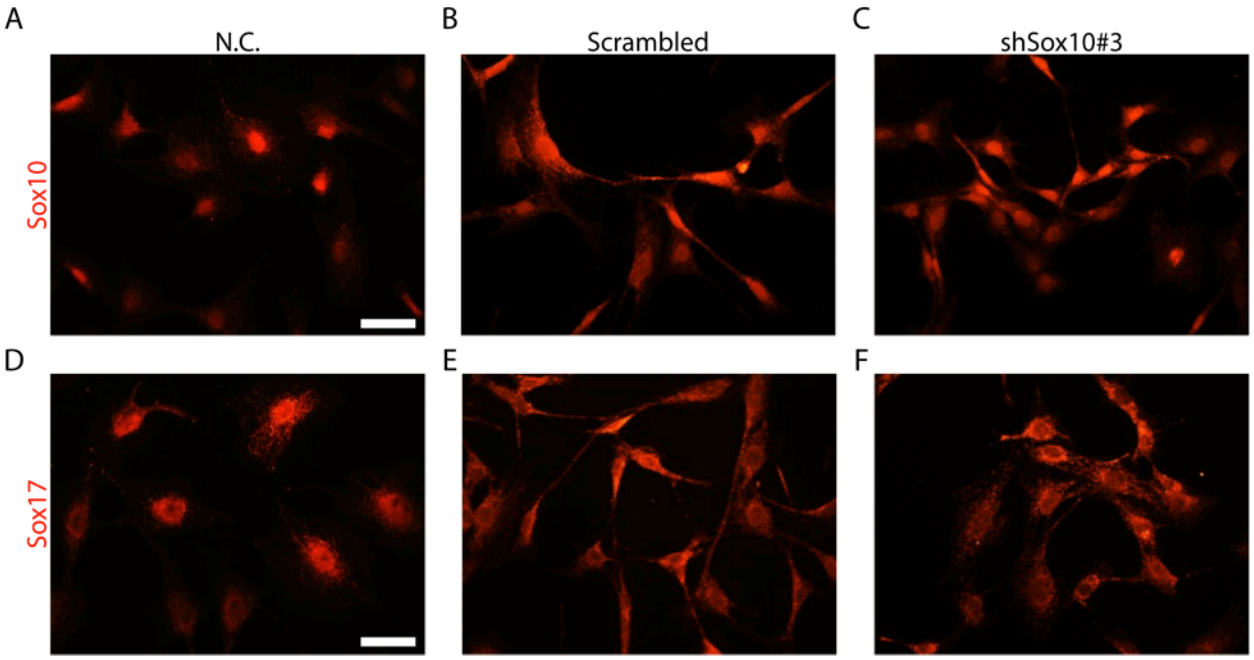

Figure 3.4 Both rat Sox10 shRNA and scrambled control cell lines maintain Sox10 protein expression even after antibiotic selection. *A-C,* Sox10 protein expression in parent cell lines, scrambled shRNA, and shSox10#3, respectively. *D-F,* Sox17 protein expression is lost in cell lines transfected with shRNA plasmids. Scale bar represents 50 microns. N.C., negative control

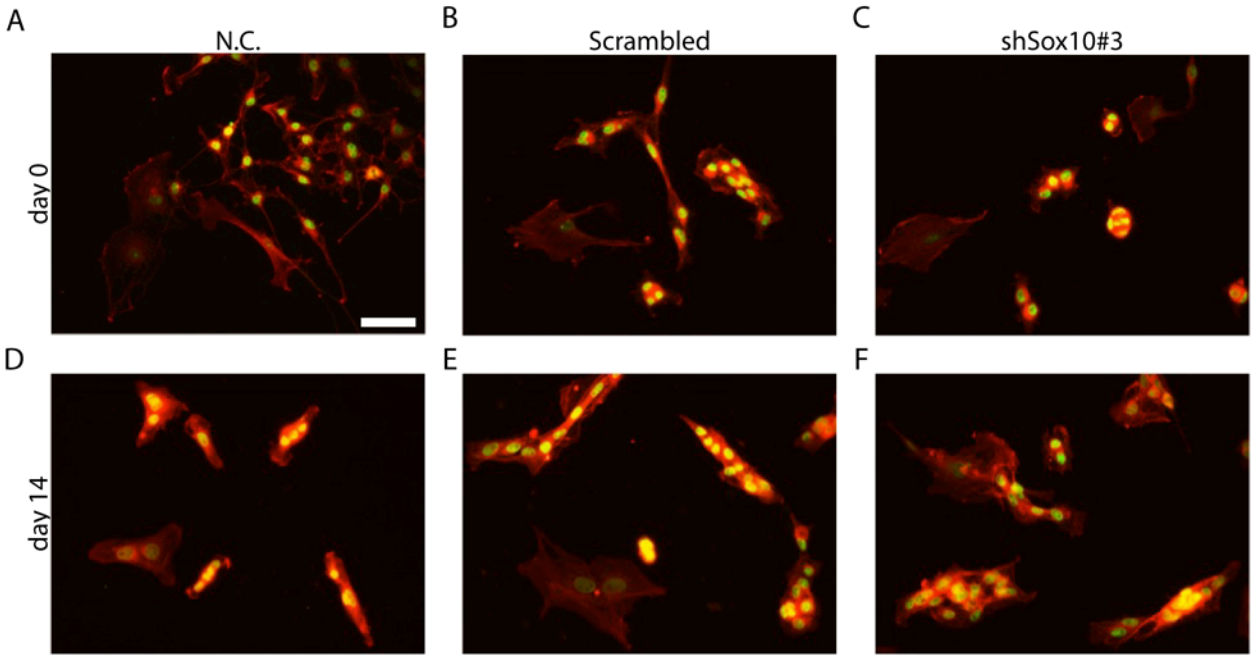

Figure 3.5 Spontaneous differentiation of stable rat Sox10 shRNA cell lines do not show significant decreases in Sox10 protein expression. Rat VSC cell lines were cultured in 10%FBS DMEM for up to 14 days. Sox10 (green) and SMA (red) protein expression at day 0, *A-C,* and day 14, *D-F*, in parent cell lines, scrambled shRNA, and shSox10#3, respectively. Scale bar represents 50 microns. N.C., negative control

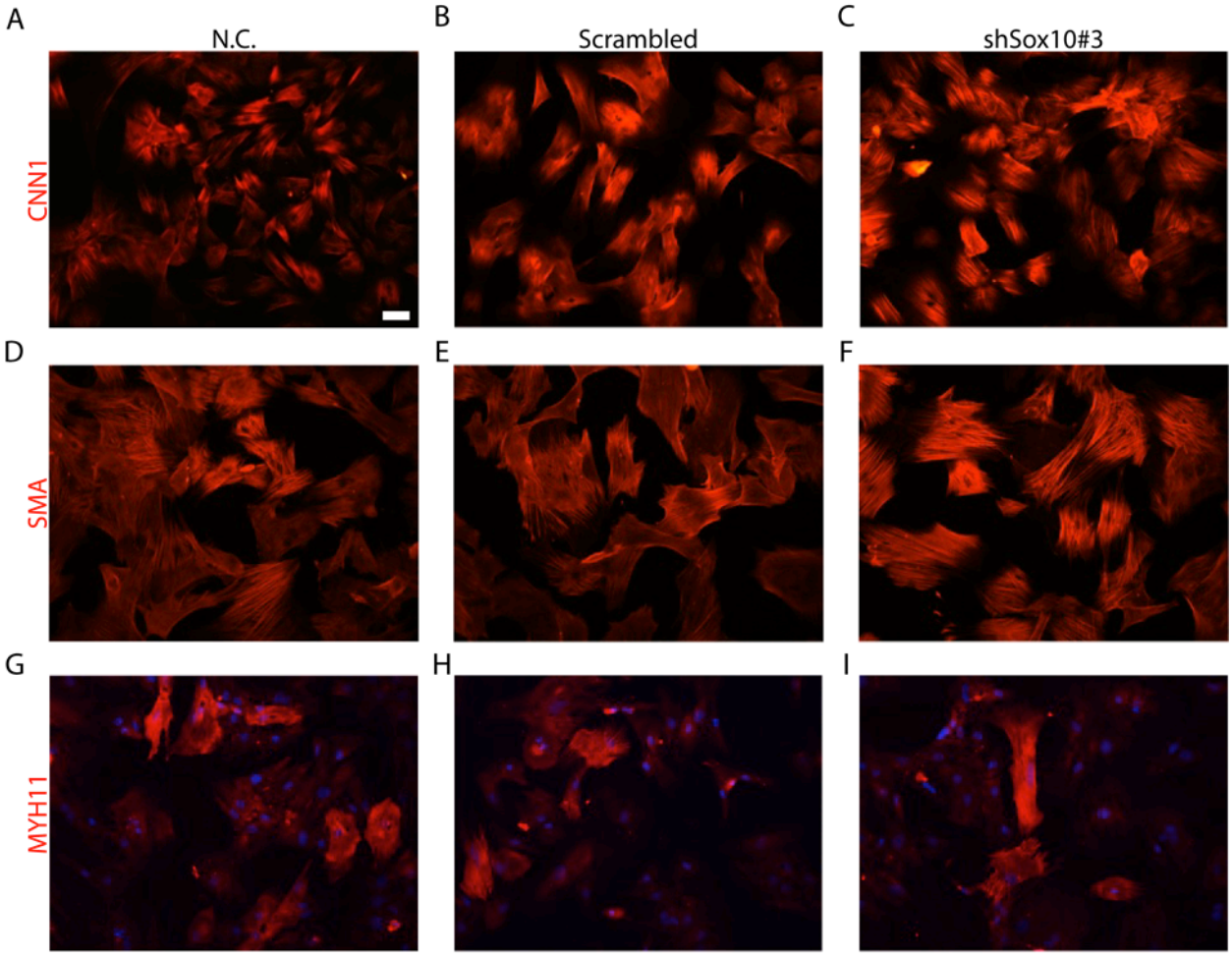

Figure 3.6 Directed differentiation with TGF-β does not significantly increase expression of SMC markers in stable rat Sox10 shRNA cell lines. Rat VSC cell lines were cultured in DMEM with TGF-β for up to 14 days. *A-C,* CNN1 (red) and nuclei (blue) staining in rat VSC parent cell lines, scrambled shRNA, and shSox10#3, respectively. *D-F,* SMA (red) and nuclei (blue). *G-I,* MYH11 (red) and nuclei (blue) staining. Scale bar represents 50 microns. N.C., negative control.

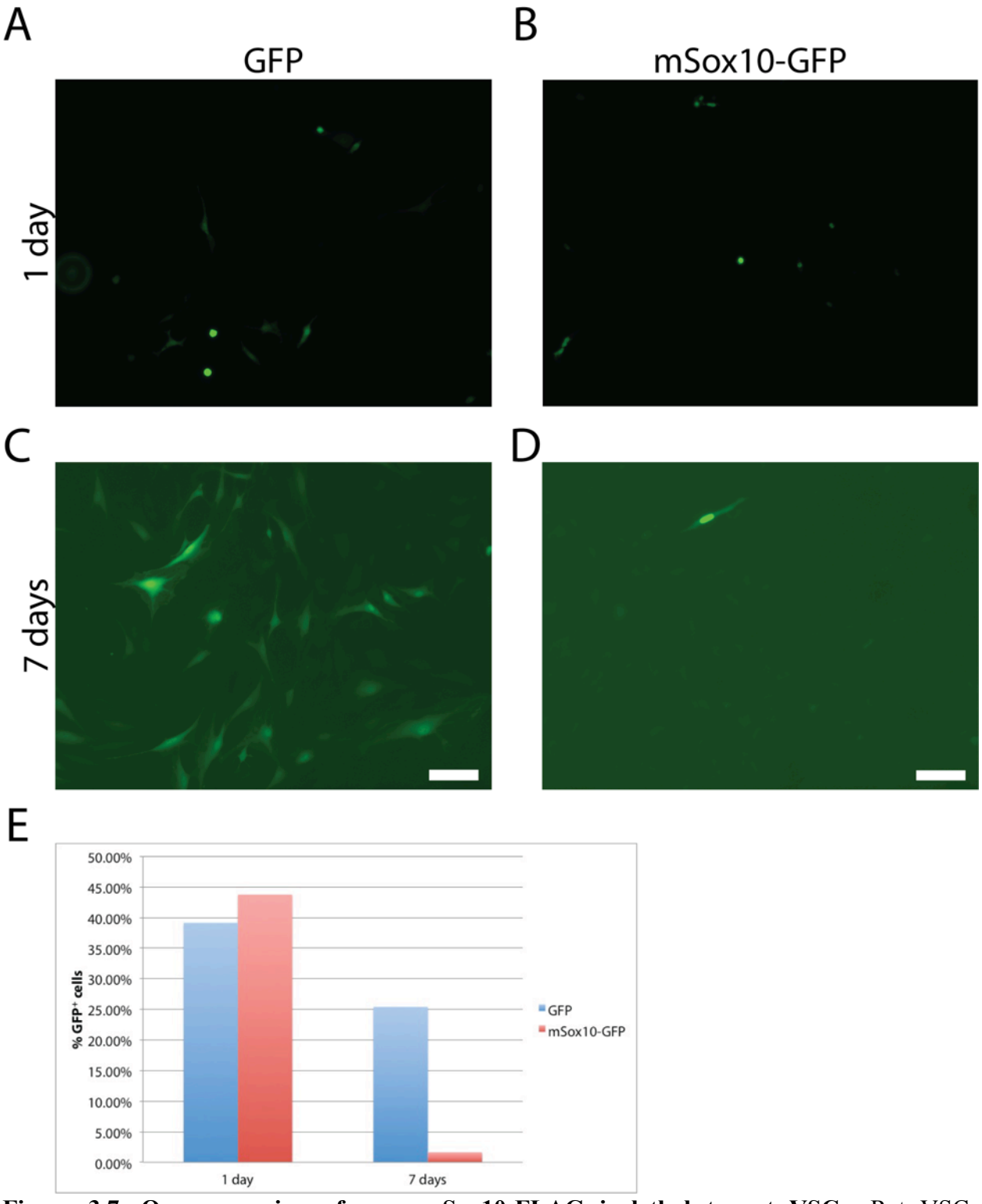

Figure 3.7. Overexpression of mouse Sox10-FLAG is lethal to rat VSCs. Rat VSCs transfected with empty GFP vector or mSox10-GFP show 40-50% transfection efficiency. Live imaging of rat VSCs 24 hours post-transfection of *A,* GFP empty vector or *B,* GFP-tagged Sox10. Live imaging of rat VSCs 7 days post-transfection of *C,* GFP, or *D*, GFP-tagged Sox10. *E,* GFP-

positive cells in either GFP (blue) or GFP-tagged Sox10 (red) at 1 day (left) or 7 days (right) post-transfection. Scale bar represents 100 microns.

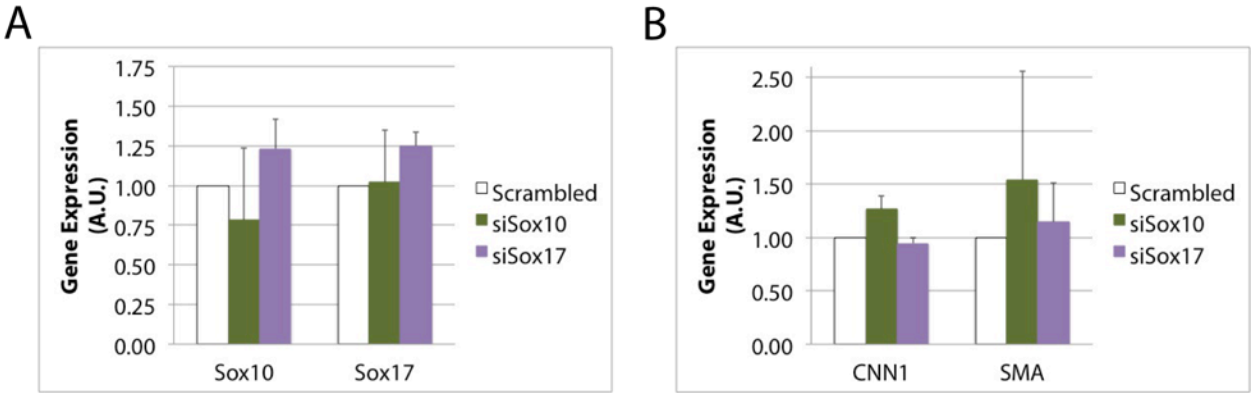

Supplemental Figure 3.1 Preliminary experiments show pooled siRNA against Sox10 or Sox17 do not show robust knockdown in rat VSCs. Rat VSCs transfected with Sox10 (green) and Sox17 siRNA (purple) do not show significant decreases in gene expression. *A,* qPCR results show Sox10 siRNA does not affect Sox17 gene expression (purple) and no significant decrease in Sox10 (left) gene expression. *B,* Early SMC markers also show high variability in Sox10 siRNA (green) samples compared to scrambled control. For *A-B,* data ± SD were normalized to 18S rRNA, then to siRNA scrambled control for at least 2 experiments.

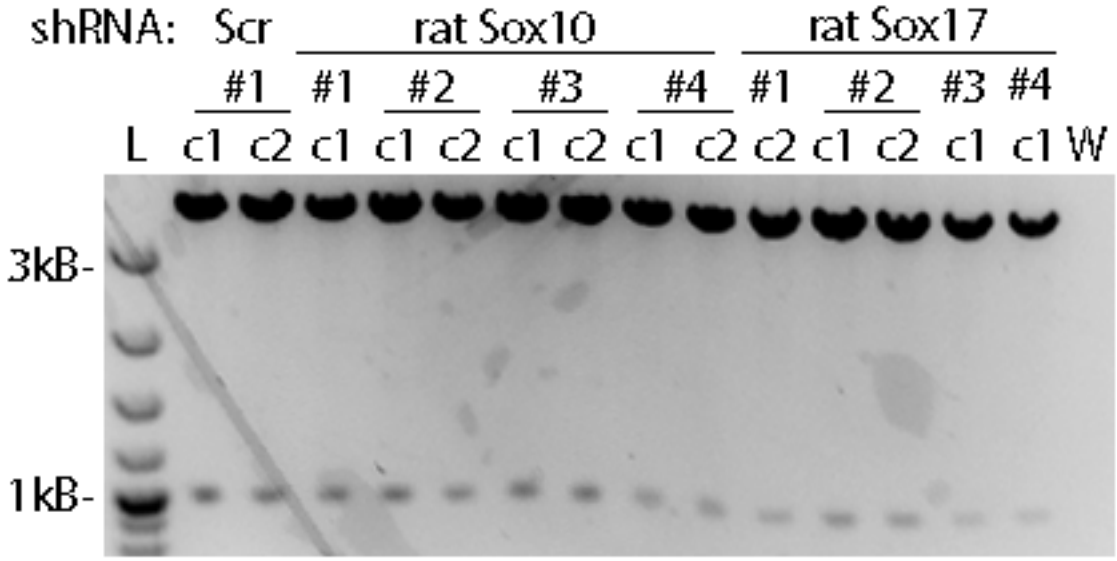

Supplemental Figure 3.2 *PstI* restriction enzyme digest confirm presence of ~1kB shRNA and Neomycin selection cassette. For each shRNA DNA plasmid, 1-2 colonies were picked and purified using NucleoBond MaxiPrep kit instructions (c#). *PstI* restriction enzyme digests were performed for 1 hour at 37ºC, then run on 0.8% SYBRsafe-agarose gel. Images were taken using a digital developer with a UV filter (see Chapter 2 Methods), and then processed in Photoshop CC (Adobe). L, DNA Ladder, c, colony, W, water.

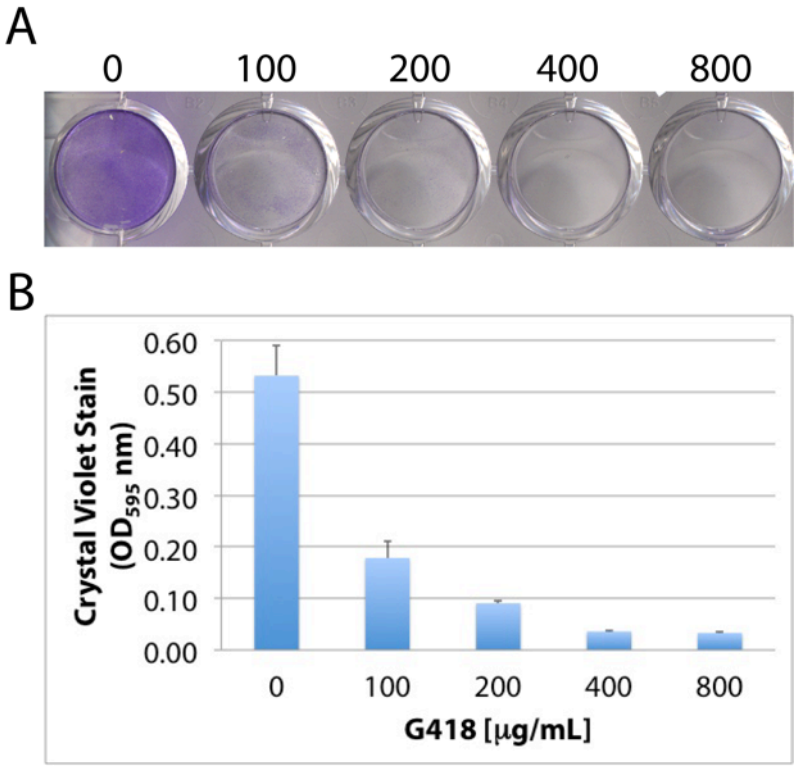

Supplemental Figure 3.3 G418 titration kill curve used to determine optimal antibiotic selection concentration of rat VSCs. *A,* Representative scan of crystal violet stained rat VSCs cultured in VSC maintenance media supplemented with G418. Numbers above well reflect final concentration of G418 in µg/mL. *B,* Average crystal violet stain absorbance measured to determine optimal antibiotic selection concentration to use.

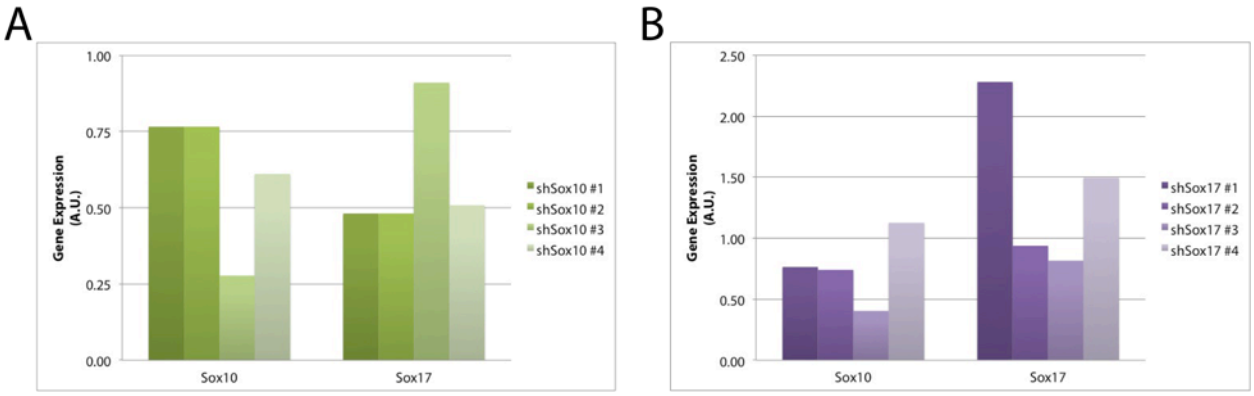

Supplemental Figure 3.4 Preliminary results of Sox10 and Sox17 gene expression after shRNA plasmid transfection and G418 selection. Sox10 and Sox17 expression levels in rat VSCs transfected with SureSilencing shRNA DNA plasmids targeting *A,* Sox10 and *B,* Sox17. For shRNA experiments, shSox10#3 shows consistent knockdown of Sox10 (*A,* 3rd bar on left) without affects on Sox17 gene expression (*A,* 3rd bar on right). Stable rat Sox17 shRNA cell lines do not show significant knockdown of Sox17 gene expression (*B,* right). For *A-B,* data ± SD were normalized to 18S rRNA, then to shRNA scrambled control.

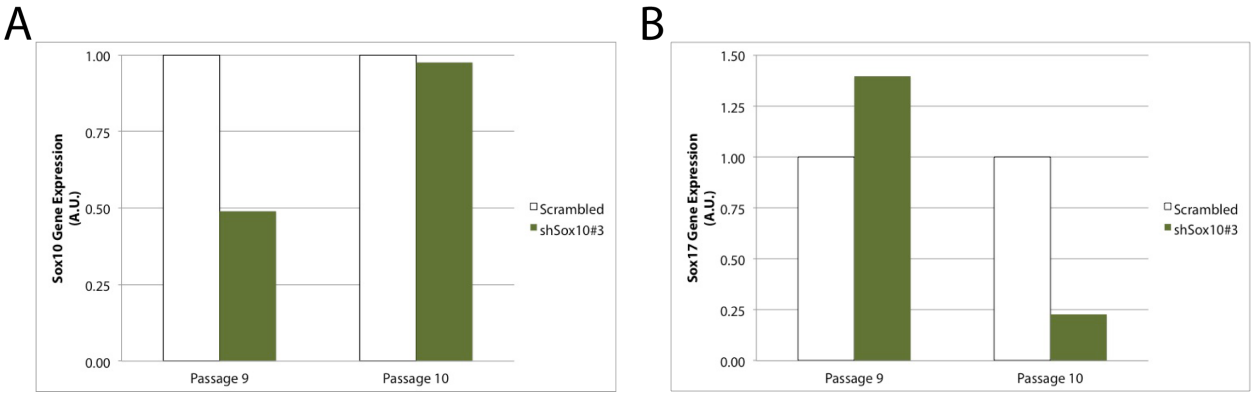

Supplemental Figure 3.5 Stable cell lines of shRNA Sox10 in rat VSCs do not show stable knockdown of Sox10 after 1 passage. *A,* Sox10 and *B,* Sox17 expression levels in rat VSCs transfected with scrambled shRNA (white bars) or shSox10#3 (green bars). While rat VSC shSox10#3 passage 9 show at least 50% reduction of Sox10 mRNA compared to scrambled control (*A,* left), an additional passage in cell culture shows Sox10 mRNA recovers (*A,* right). Sox17 mRNA shows the opposite pattern of Sox10; initially, shSox10#3 cell lines show Sox17 mRNA is about 1.4 times greater than scrambled controls (*B,* left), but then reduces to less than 25% as Sox10 expression levels increase (*B,* right).

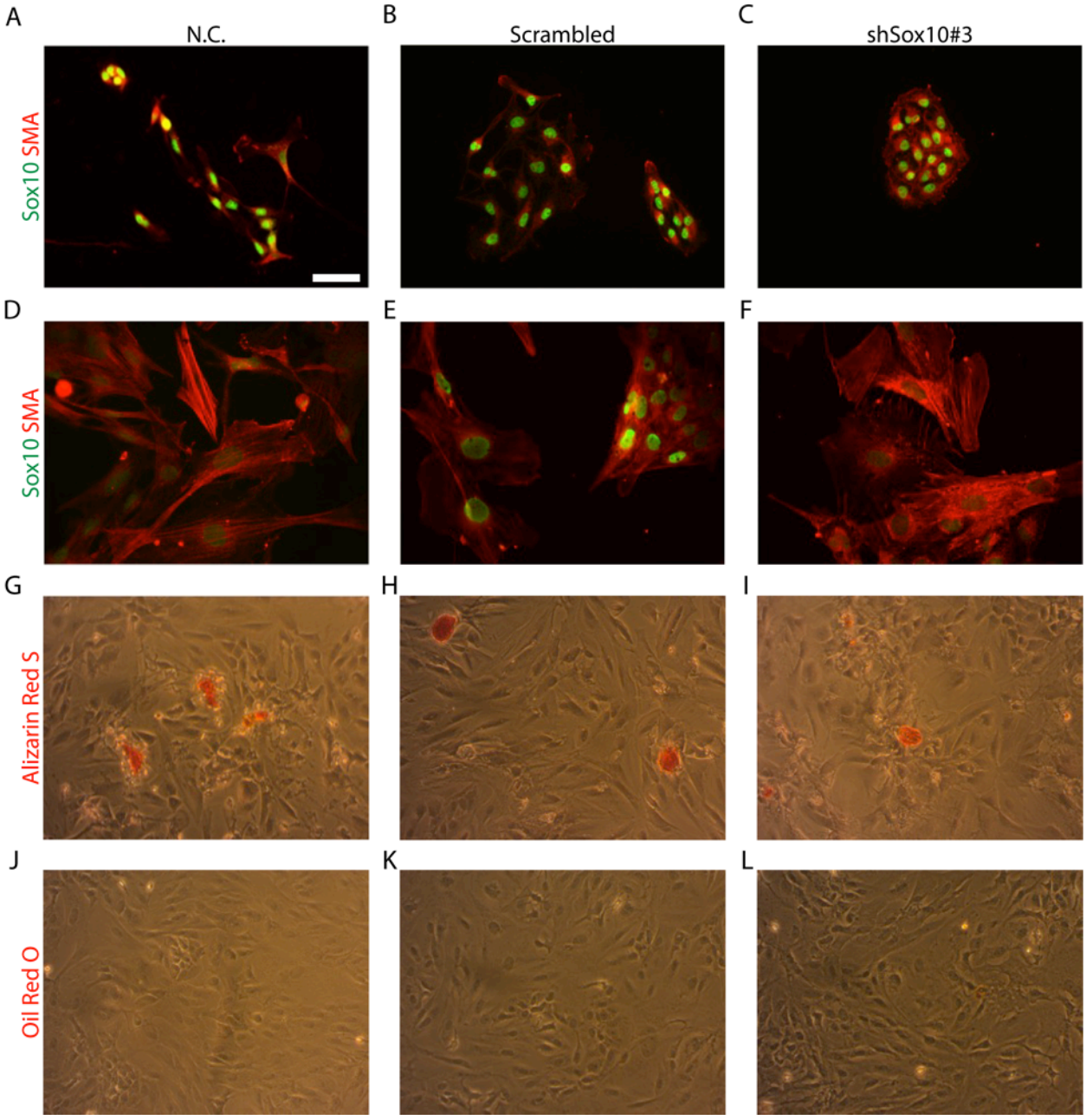

Supplemental Figure 3.6 Directed differentiation of stable rat Sox10 shRNA cell lines does not significantly increase compared to controls. Rat VSC cell lines cultured in directed differentiation media for up to 14 days. Sox10 (green) and SMA (red) protein expression in rat VSC parent cell lines, scrambled shRNA, and shSox10#3, respectively, at day 2 (*A-C*) and day 12 (*D-F*). *G-I,* Alizarin Red S stain. *J-L*, Oil Red O stain. Scale bar represents 50 microns. N.C., negative control.

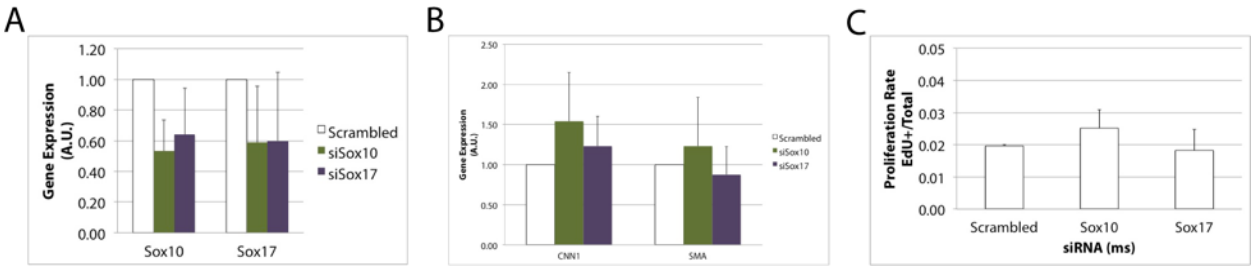

Supplemental Figure 3.7 Preliminary experiments with pooled siRNA against Sox10 or Sox17 also do not show significant knockdown in mouse VSCs. Mouse VSCs transfected with Sox10 (green) and Sox17 siRNA (purple) do not show significant decreases in gene expression after 3 days. *A,* qPCR results show Sox10 siRNA does not affect Sox17 gene expression (purple) and no significant decrease in Sox10 (left) gene expression. *B,* Early SMC markers also show high variability in Sox10 siRNA (green) samples compared to scrambled control. *C,* Proliferation rates for siRNA-treated mouse VSCs. For *A-B,* data ± SD were normalized to 18S rRNA, then to siRNA scrambled control for at least 3 experiments. For *C,* data are mean ± SD from multiple images taken per well, using the automated IXM workstation at the Shared Stem Cell Facility. Total cells counted are 3,307 (scrambled), 3,426 (Sox10 siRNA), and 3,343 (Sox17 siRNA).

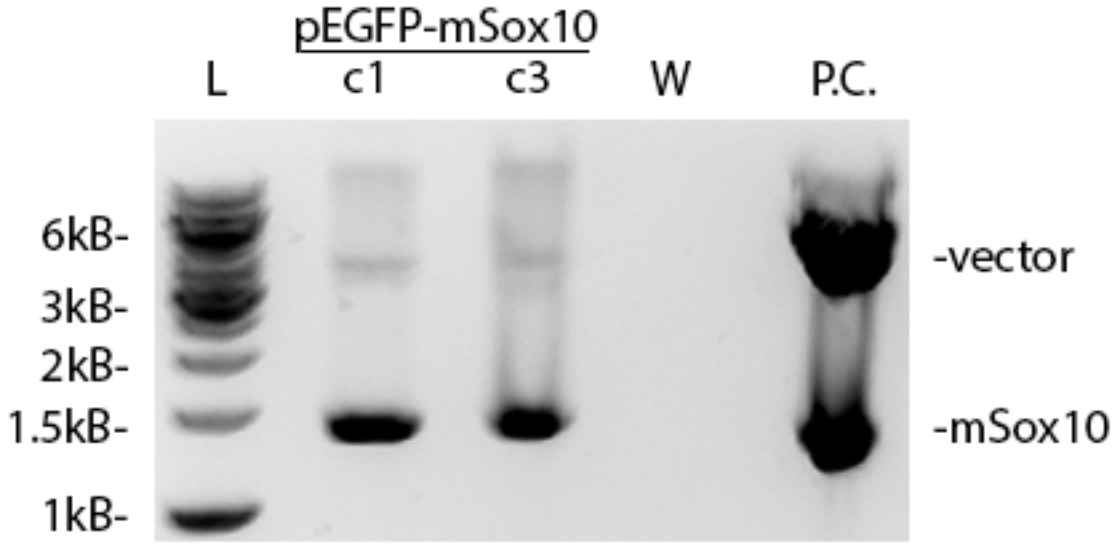

Supplemental Figure 3.8 *EcoRI, BamHI* double digest confirms presence of ~1.4kB Sox10 cDNA in GFP-tagged Sox10 colonies. For each DNA plasmid, 3 colonies were picked and purified using NucleoBond MaxiPrep kit instructions (c#). *EcoRI, BamHI* restriction enzyme digest were performed overnight at 37ºC, then run on 1% SYBRsafe-agarose gel. Images were taken using a digital developer with a UV filter (see Chapter 2 Methods), and then processed in Photoshop CC (Adobe). L, DNA Ladder, kB, kilobases, c, colony, W, water.

References

1. Tang Z, *et al.* (2012). Differentiation of Multipotent Vascular Stem Cells Contributes to Vascular Diseases. *Nat Commun* 3: 875.
2. Seong I, *et al*. (2012). Sox10 Controls Migration of B16F10 Melanoma Cells through Multiple Regulatory Target Genes. *PLoS ONE* 7(2): e31477.
3. Leach DF, *et al*. (2014). The Sources of Synthetic Vascular Smooth Muscle Cells Revisited. *Austin J Anat* 1(2): 1007.
4. Kennedy E, *et al* (2014). Embryonic rat vascular smooth muscle cells revisited – a model for neonatal, neointimal SMC or differentiated vascular stem cells? *Vasc Cell* 6:6.
5. Gomez D, Shankman LS, Nguyen AT, Owens GK (2013). Detection of histone modifications at specific gene loci in single cells in histological sections. *N. Meth* 10(2): 171-177.

Appendix I: qPCR Primers Used

Primer Sequence Name	Sequence (5' → 3')	Full Gene Name
18S rat-962F	GCCGCTAGAGGTGAAATTCTTG	Rat 18S rRNA
18S rat-1027R	CATTCTTGGCAAATGCTTTCG	
ACTA2 rat-254F	TCCTGACCCTGAAGTATCCGATA	Rat α-Actin 2
ACTA2 rat-325R	GGTGCCAGATCTTTTCCATGTC	
CNN1 rat-122F	AGAACAAGCTGGCCCAGAAA	Rat Calponin 1
CNN1 rat-189R	CACCCCTTCGATCCACTCTCT	
COL2A1#2 rat-4176F	CCAGGGCTCCAATGATGTG	Rat Collagen Type II, alpha 1
COL2A1#2 rat-4260R	GTGTTTCGTGCAGCCATCCT	
GFAP rat-763F	GCTAGCCCTGGACATCGAGAT	Rat Glial Fibrillary Acidic Protein
GFAP rat-834R	GGAATGGTGATGCGGTTTTC	
MKL1 rat-2440F	GTCTCTCCACCAGTAGCAGC	Rat Myocardin Related Protein Factor A
MKL1 rat-2576R	CTTCAGCTCTGCCACCTTCA	
MYH11 rat-1759F	TTCCGGCAACGCTACGA	Rat Myosin Heavy Chain 11, Smooth Muscle
MYH11 rat-1818R	TCCATCCATGAAGCCTTTGG	
p75#2 rat-869F	CATTCCTGTCTATTGCTCCATCTTG	Rat p75
p75#2 rat-946R	CTGTTCCACCTCTTGAAAGCAATAT	
S100a rat-84F	GCTGAGCAAGAAGGAGCTGAA	Rat S100α Calcium Binding Protein A1
S100a rat-165R	CACAGCATCTGCATCCTTCTG	
S100b rat-45F	CTGTCTACCCTCCTAGTCCTTGGA	Rat S100β Calcium Binding Protein B
S100b rat-116R	GAGGCTCCTGGTCACCTTTTG	
SM22a rat-23F	CACAAACGACCAAGCCTTTTC	Rat SM22α, Transgelin
SM22a rat-89R	CACGGCTCATGCCATAGGAT	
SOX10 rat-1005F	CTGGAGGTTGCTGAACGAGAGT	Rat Sox10
SOX10 rat-1092R	GTCCGGATGGTCTTTTTTGTG	
SOX17 rat-565F	AGAACCCGGATCTGCACAAC	Rat Sox17
SOX17 rat-615R	AGGATTTGCCTAGCATCTTGCT	
YAP rat-936F	ACGGAATATCAATCCCAGCACA	Rat Yes Associated Protein
YAP rat-990R	CGCTCTGACGGTCTGACAT	

Appendix II. Table 1: Primary Antibodies Used

Antibody (Host Species)	Company	Catalog Number	IB Dilution	IF Dilution
Aggrecan (ms)	Millipore	MABT84	1:1000	1:200
ANGPTL4 (gt)	Santa Cruz Biotechnology, Inc.	sc-32184	1:3000	1:50
β-Actin (gt)	Santa Cruz Biotechnology, Inc.	sc-1616	1:2000	N.A.
CCR1 (rb)	Abcam	ab1681	1:1000	1:200
CNN1 (rb)	Abcam	ab46794	1:2000	1:100
Collagen II (rb)	Abcam	ab53047	N.A.	1:200
Erk 1/2 (rb)	Cell Signaling Technology	4695	1:500	1:200
GAPDH (ms)	Santa Cruz Biotechnology, Inc.	sc-32233	1:1000	N.A.
HDAC 1 (rb)	Santa Cruz Biotechnology, Inc.	sc-7872	1:2000	N.A.
HDAC 2 (rb)	Santa Cruz Biotechnology, Inc.	sc-7899	1:1000	N.A.
HDAC 4/5/7 (rb)	Santa Cruz Biotechnology, Inc.	sc-11421	1:1000	N.A.
Histone 3 (rb)	Abcam	ab1791	1:3000	N.A.
Histone 3 K4me2 (rb)	Abcam	ab32356	1:1000	1:100
Histone 3 K4me3 (rb)	Millipore	07-473	1:1000	1:100
Histone 3 K9ac (rb)	Cell Signaling Technology	C5B11	1:1000	1:100
Histone 4 (rb)	Abcam	ab7311	1:2000	N.A.
Histone 4 K5ac (rb)	Cell Signaling Technology	9672S	1:500	N.A.
Lamin A/C (gt)	Santa Cruz Biotechnology, Inc.	sc-6215	1:1000	N.A.
Lamin A/C (ms)	Santa Cruz Biotechnology, Inc.	sc-7292	1:500	1:200
Lamin B1 (rb)	Abcam	ab16048	1:1000	1:200
MRTF-A (H-140) (rb)	Santa Cruz Biotechnology, Inc.	sc-32909	1:500	1:100
MYH11 (rb)	Biomedical Technologies	562	1:1000	1:100
Phospho-Erk 1/2 (rb)	Cell Signaling Technology	9102	1:500	1:200
Phospho-Smad 1/5/8 (rb)	Cell Signaling Technology	9511S	1:1000	1:200
Phospho-Smad 2/3 (rb)	Cell Signaling Technology	8828	1:1000	1:200
PPARγ (rb)	Abcam	ab19481	1:1000	1:100
SMA (ms)	Abcam	ab7817	1:2000	1:100

Appendix II. Table 1: Primary Antibodies Used continued

Antibody (Host Species)	Company	Catalog Number	IB Dilution	IF Dilution
SMA (rb)	Abcam	ab32575	1:2000	N.A.
Smad 1 (rb)	Cell Signaling Technology	6944S	1:1000	N.A.
Sox 9 (rb)	Millipore	ab5535	1:2000	1:100
Sox 10 (ms)	R & D Systems	MAB2864	1:1000	1:100
Sox 10 (N-20) (gt)	Santa Cruz Biotechnology, Inc.	sc-17342	1:500	1:30
Sox 17 (ms)	R & D Systems	MAB1924	1:1000	1:100
Tubulin (ms)	Santa Cruz Biotechnology, Inc.	Sc-5286	1:2000	1:2000
YAP (rb)	Cell Signaling Technology	14074	1:1000	1:200
YAP TAZ (D24E4) (rb)	Cell Signaling Technology	8418	1:500	1:200

Appendix II: Table 2. Secondary Antibodies Used

Antibody (Host species)	Company	Catalog Number	IB Dilution
Rabbit IgG-HRP (dk)	Santa Cruz Biotechnology, Inc.	sc-2313	1:2000
Mouse IgG-HRP (dk)	Santa Cruz Biotechnology, Inc.	sc-2314	1:2000
Goat IgG-HRP (dk)	Santa Cruz Biotechnology, Inc.	sc-2020	1:1000

Appendix III: Determine Whether Laminar Shear Stress Mediates Glioblastoma Tumor-Initiating Cell Differentiation to Endothelial Cell-like Fates Through Krüppel-like Factor 5

III.1 Abstract

Glioblastoma is the most common and aggressive adult brain tumor with a median survival time of 12-15 months. Glioblastoma tumor-initiating cells exhibit high self-renewal and differentiation potential in cell cultures and directly contribute to the endothelial cell layer of tumor vasculature. The cell surfaces facing the lumen of tumor vasculature are subject to laminar shear stress, a specific hemodynamic force that regulates vascular development in embryonic and adult tissues. Laminar shear stress applied to cells activates the transcription of genes involved in the differentiation of multipotent cells to endothelial cell fates. This process requires Krüppel-like transcription factors (KLFs). My project aims to investigate the role of laminar shear stress in mediating the cell fate choices of Glioblastoma tumor-initiating cells in culture. I hypothesize that laminar shear stress induces KLF5 gene expression to activate downstream gene targets that mediate the differentiation of Glioblastoma tumor-initiating cells to adopt vascular endothelial cell fates.

III.2 Introduction.

In the United States, two-thirds of malignant adult brain tumors are gliomas.[1] Glioblastoma is the most aggressive glioma characterized by large regions of necrosis, hypoxia, highly permeable and misshapen blood vessels, and a heterogeneous composition of neuronal and endothelial cells. A lineage-hierarchy of multipotent Glioblastoma tumor-initiating cells (GTICs) adopt a variety of differentiated terminal cells fates, including neuronal and endothelial cells, and exhibit high self-renewal in cell culture.[2,3]

Glioblastoma tumors are modeled through stereotactic injection of GFP-labeled primary human (Dirks, U87)[4,5] and rat (F98)[6] glioblastoma cells into the hippocampi of immune-compromised mice. Lineage-tracing studies in immune-compromised mice show that human or rat GTICs directly contribute up to 20% or 50% of the endothelial layer of the tumor vasculature, respectively.[7,8] Glioblastoma-derived endothelial cells (GDECs) express endothelial cell markers, like angiopoietin receptor 2 (TIE2) and platelet endothelial cell adhesion cell molecule (CD31) and can bind lectin, an endoethlial-specific glycoprotein.[8-11] Glioblastoma tumor-initiating cells do not express TIE2 or CD31, and do not bind lectin. These data suggest that GDECs present in tumor vasculature result from the differentaiton of GTICs to endothelial cell-like fates. This mechanism of pathological blood vessel formation in mouse models of glioblastoma will not be impaired by therapies targeting classical pathways of blood vessel formation.[12,13]

Historically research on blood vessel formation has focused on the role of pro-vascular factors (e.g., vascular endothelial growth factor (VEGF)) or cell-cell contact (e.g., Notch) signaling pathways in the adoption of endothelial cell fates.[14] The role of hemodynamic forces to promote the differentiation of GTICs to vascular cell fates has not been examined.[15] By examining parallel mechanisms of mechanical forces in normal and pathological vascular biology, this work may lead to critical insights into this process.

A cross-section of a blood vessel shows that the cells facing the lumen experience a frictional force per unit area, or laminar shear stress (τ) (Figure 1.2). This signal is critical for multipotent progenitor cells to adopt vascular cell fates.[16] Parallel-plate flow chambers reconstitute laminar shear stress in cultured cells to activate the transcription of genes required in this process.[17] The Krüppel-like transcription factors (KLFs) are required to activate downstream gene targets to signal vascular cells to remodel the vascular wall and/or form new blood vessels.[18,19] While the role of biophysical cues has been used to study the differentiation and maintenance of stem cell populations (see Chapter 1.5), the specific role of laminar shear stress to promote differentiation of GTICs to vascular cell fates has not been examined.

Gene expression profiles of glioma cell cultures were compared to identify candidate genes that may mediate cell differentiation promoted by laminar shear stress. The Wurmser lab confirmed high KLF5 transcript levels in GTICs and GDECs through quantitative reverse-transcription PCR (Wurmser lab, unpublished data).

KLF5 is a key transcription factor required for adult vascular cell remodeling.[20] Irregular laminar shear stress and/or disrupted KLF5 gene expression in rodent models and vascular cell cultures show defects in vascular wall remodeling, which results in atherosclerosis and heart failure. KLF5 knockout mice are embryonic lethal.[21] Characterization of the viable, heterozygous KLF5 littermates show decreased local inflammation and angiogenesis in wire-injured blood vessels and reduced luminal thickness in response to Angiotensin II stimulation compared to wild-type littermates. Since, direct downstream gene targets of KLF5 include soluble growth factors (e.g., early growth response-1, platelet-derived growth factors (PDGFs)) and receptor tyrosine kinases (e.g., TIE2), these data suggest KLF5 is a key mediator in the vascular cell response to cardiovascular injury and tissue remodeling.[22,23]

To determine if KLF5 is required for GTICs to contribute to tumor blood vessels, rat GTICs expressing a dominant negative KLF5 (DNKLF5) were used to initiate tumors in immune-compromised mice. DNKLF5 cell lines express only the DNA-binding domains of KLF5, which cannot recruit coactivators.[24] Engrafting DNKLF5 cells results in 33% longer survival time than engrafting with GTIC control cultures (unpublished data). At the time of surgical resection, tumors initiated with DNKLF5 cells had no obvious gross morphological changes in the vasculature or tumor size compared with tumors initiated with GTIC control cultures. Tumors initiated with DNKLF5 did reduce the frequency of GDECs in tumor blood vessels to 10-15%. These data suggest KLF5 plays a predominant role in the process of tumor vasculogenesis.

There is significant understanding of laminar shear stress in the maintenance of terminally differentiated endothelial cell fates. This project aims to broaden understanding of laminar shear stress on the differentiation capacities of GTICs-to-GDECs and the molecular mechanism(s) that regulate this process using rodent and cell culture models. I hypothesize that KLF5 mediates the differentiation response to shear stress in GTICs, and I seek to identify the molecular mechanisms and cellular components that mediate these processes.

III.3 Materials and Methods

Cell Culture

Rat F98 polyclonal GTIC (ATCC) were cultured in RPMI 1640 supplemented with 10% FBS,

1% P/S, and 1X L-Glutamate (Invitrogen). Before each shear stress treatment, sterile glass slides were coated with ~5μg cm^{-2} Rat Tail Collagen I (BD Biosciences) in 0.02N Glacial Acetic Acid for 2 hours at room temperature in a sterile tissue culture hood. Glass slides were washed twice in sterile 1X PBS. Slides were left to dry overnight in the tissue culture hood and used the following day or stored at 4ºC for up to 2 weeks. A confluent monolayer of Rat GTICs was grown overnight onto Collagen I-coated glass slides.

Assembling Parallel-Plate Flow Chamber and Shear Stress Treatment

Parallel-plate flow chambers were assembled as shown in Figure III.1.[25] For each parallel-plate flow chambers, 1 250mL Erlenmeyer flask, rubber stopper with 2 glass rods, rubber tubing, and 2 pairs of forceps were cleaned thoroughly in 70% ethanol and rinsed in distilled water. Dry sterilize for 45 minutes, followed by a 45 minutes dry cycle. Spray binder clips with 70% ethanol, wrap in tin foil and leave under UV light overnight. Submerge flow chambers in distilled water and sonicate for 30 minutes at room temperature. Submerge flow chambers in containers with 70% ethanol. Leave uncovered under UV light for 30 minutes. Aspirate all alcohol, close lid and leave chambers overnight under UV light. Submerge silicone gaskets in 70% ethanol and expose to UV light for 30 minutes. Cover gaskets and leave under UV light overnight.

Each glass slide is mounted with the cells facing the flow channel and then held together using binder clips. A sandwich is created between the glass slide and acrylic plate using a silicone gasket. Each acrylic plate has an inlet and outlet for liquid to flow over the chamber. The width of the exposed chamber is 1.70cm. The height of the silicone gasket is 0.0254 cm. The specific gravity of basal media was approximately 7.755×10^{-3} dynes sec cm^{-2}. Peristaltic pumps are used to connect tubing that allows media to flow through the chamber and across the cells. The flow rate is used to calculate the approximate shear stress, using the following equation:

$$Q = \frac{wh^2}{6} \times \frac{\tau}{\mu}$$; where Q is flow rate (mL/sec),

w is width of Silicone gasket (cm),
h is height of Silicone gasket (cm),
τ is shear stress (dynes/cm^2)
μ is specific gravity of fluid (dynes•sec/cm^2)

For shear-stress treatment of 10 dynes cm^{-2}, flow rates were approximately 5mL every 24 seconds.

Isolation of RNA and Semi-Quantitative Reverse Transcriptase PCR

In brief, static or laminar shear stress-treated samples were lysed in RNA-bee (Amsbio) after removing culturing media and washing cells twice in cold 1X PBS. Total RNA was collected following manufacturer's recommended protocol, followed by precipitation in isopropanol overnight at -20ºC. The following day, the RNA pellet was washed in 70% ethanol (-20ºC) and dried in a Speed-vac for up to 4 minutes at room temperature. The RNA pellet was resuspended in nuclease-free water. RNA concentration and purity were measured with UV spectrometry.

For cDNA synthesis, we followed the GoScript Reverse Transcriptase (Promega) protocol. Specific primers for Klf5, Klf4, Runx1, and 18S rRNA were designed as previously described.[10]

For image analysis, scanned images were quantified using ImageJ software (National Institutes of Health).[26] For each gene, relative mRNA levels were normalized to 18S rRNA, then expression was compared to static controls.

III.4 Preliminary Results

To test whether laminar shear stress promotes the differentiation of rat or human GTIC-to-GDEC fates in culture, I assembled a parallel-plate flow chamber (Figure III.1) to apply laminar shear stress to GTIC cultures, as previously described.[17,27] Endothelial cell cultures exposed to laminar shear stress exhibit time-dependent changes in inducible gene expression.[16,18]

For initial experiments, we applied a physiological laminar shear stress (10 dynes cm^{-2}) and harvested RNA at 0, 6, 12, and 14 hours. RNA harvested from rat GTICs cultured on glass coverslips, but not exposed to laminar shear stress, serve as static controls. We found that GTICs exposed to laminar shear stress in cell culture induced KLF5 transcript levels in a time-dependent manner compared to static controls (Figure III.2).

III.5 Discussion and Future Directions

Our aim was to establish a time course required for KLF5 up-regulation in physiological laminar shear stress-treated GTICs. Due to unforeseen circumstances, experiments to further characterize the role of KLF5 and identify downstream targets of KLF5 in GTIC-to-GDEC differentiation were halted.

In summary, this project aims were to determine whether GTICs exposed to laminar shear stress in cell cultures induce expression of GDEC proteins found in animal engrafting experiments. Specifically, whether laminar shear stress-treated rat or human GTIC cultures induce the expression of TIE2 and CD31, binds lectin, and can form capillary tubes in matrigel compared to static (untreated) GTIC control cultures.

If laminar shear stress-treated GTICs upregulates TIE2 and CD31 expression compared to GTIC static controls, this would demonstrate the following: (1) Applying laminar shear stress to GTIC cultures induces expression of endothelial cell and GDEC markers from mouse models of glioblastoma tumors, (2) Laminar shear stress is a specific mechanical signal that contributes to GTIC differentiation to endothelial cell fates, and (3) Applying laminar shear stress to glioblastoma cells in culture can be used to identify the molecular mechanism(s) that specifically regulate differentiation of GTICs-to-GDECs. It is possible that in addition to laminar shear stress the differentiation of GTIC-to-GDEC cell fates requires additional soluble factors and cell contacts with endothelial cells.[8,27] If so, I will use cell culture media permissive for brain microvascular endothelial cell growth in my experiments.

A critical step for normal and pathological angiogenesis is to create vascular network tubes with a lumen. Endothelial cell cultures plated on Matrigel, an artificial extracellular environment, are able to form vascular networks reminiscent of the normal vascular endothelium (Fig.1.2).[28] GDEC cultures plated in Matrigel form vascular networks reminiscent of abnormal tumor blood vessels.[7-9] To determine whether GTICs exposed to laminar shear stress adopt GDEC fates to form capillary tubes in cell culture, I will plate cell cultures in Matrigel. I expect GTICs exposed

to laminar shear stress to form capillary tubes.

Glioblastoma tumors exhibit large regions of low oxygen (hypoxia). In normal blood vessel formation, hypoxia increases active VEGF levels, which binds and signals through VEGFR2. This signaling cascade results in the local proliferation and migration of endothelial cells to form new blood vessels. If hypoxia is required, cultured cells plated on Matrigel will be placed in a sealed chamber with 1% oxygen.

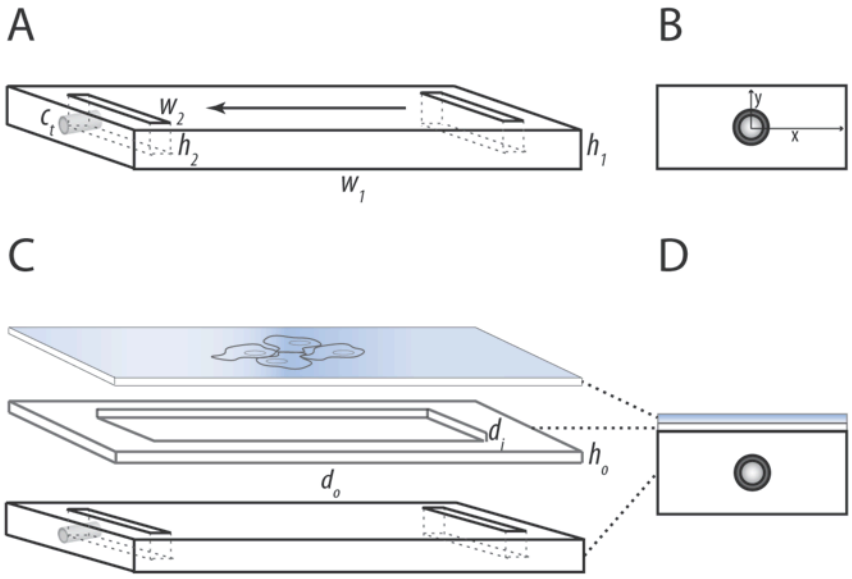

Figure III.1. Parallel-Plate Flow Chamber Used To Apply Laminar Shear Stress To Cell Cultures. A, Parallel-Plate Flow Chamber (h_1: 1.10cm, w_1: 7.60cm), Flow outlet well (h_2: 8.0cm, w_2: 1.40cm), threaded center (c_t). Arrow indicates direction of laminar shear stress. B, D Unassembled and Assembled Parallel-Plate Flow Chamber end view (threaded center, x: 1.25cm, y: 0.55cm). C, Parallel-Plate Flow Chamber Assembly with Silicone Gasket and confluent monolayer of Rat GTICs. Rat Tail Collagen I-coated glass slides were seeded with a confluent monolayer of Rat VSCs (Blue). Silicone gasket has outer (d_o: 2.90x8.80cm, h_o: 0.0254cm) and inner dimensions (d_i: 1.70x6.8cm). Binder clips on the edges of the flow chamber secure it in place (not shown). A peristaltic pump flows culturing media into the acrylic plate with an inlet and outlet through sterile tubing. All experiments are conducted in a humidified cell culture incubator set at 37ºC, 5% CO_2.

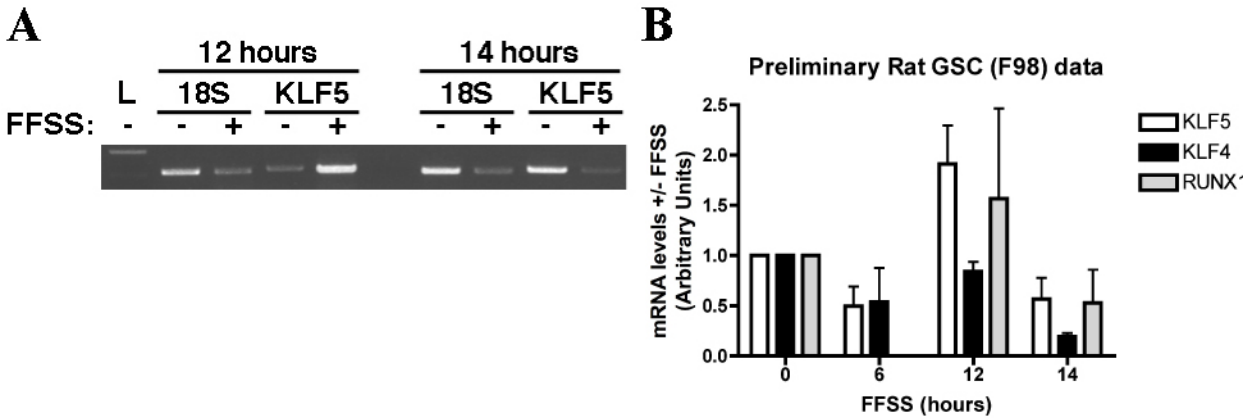

Figure III.2. *Klf5* Gene Expression Increases In Rat GTICs Exposed To 12 Hours Of Laminar Shear Stress. *A,* RT-PCR analysis of *18S rRNA* and *Klf5* in response to 12 or 14 hours of Laminar Shear Stress (10 dynes cm^{-2}); L, 1kB DNA Ladder. *B,* Densitometry results of RT-PCR for rat *Klf5*, *Klf4*, and *Runx1* of Laminar Shear Stress- or static-treated rat GTICs. *Klf5* and Runx1 show induced gene expression compared to static-treated GTIC controls. For all samples, gene expression is normalized to 18S rRNA, then normalized to static-treated samples.

Appendix III References

1. National Cancer Institute. (2011). Adult Brain Tumor Treatment. http://www.cancer.gov/cancertopics/pdq/treatment/adultbrain/Patient. Retrieved on 06-01-2011.
2. Dirks PB. (2008). Brain tumour stem cells: the undercurrents of human brain cancer and their relationship to neural stem cells. *Phil. Trans. R. Soc. B* 363: 139–52.
3. Rich JN and Eyler CE. (2008). Cancer Stem Cells in Brain Tumor Biology. *Cold Spring Harb Symp Quant Biol.* 73: 411-20.
4. Singh SK, *et al.* (2004). Identification of human brain tumor initiating cells. *Nature* 432: 396-401.
5. Silber J, *et al.* (2008). miR-124 and miR-137 inhibit proliferation of glioblastoma multiforme cells and induce differentiation of brain tumor stem cells. *BMC Medicine* 6:14
6. Barth RF and Kaur B. (2009). Rat brain tumor models in experimental neuro-oncology: the C6, 9L, T9, RG2, F98, BT4C, RT-2, and CNS-1 gliomas. *J. Neurooncol.* 94(3): 299-312.
7. Ricci-Vitiani L, *et al.* (2010). Tumour vascularization via endothelial differentiation of Glioblastoma stem-like cells. *Nature* 468: 824-8.
8. Wang R, *et al.* (2010). Glioblastoma stem-like cells give rise to tumour endothelium. *Nature* 468: 829-33.
9. Soda Y, *et al.* (2010). Transdifferentiation of Glioblastoma cells into vascular endothelial cells. *PNAS* 108(11): 4274-80.
10. Wurmser AE, *et al.* (2004). Cell fusion-independent differentiation of neural stem cells to the endothelial lineage. *Nature* 430: 350-6.
11. Pennell NA, Hurley SD, and Streit WJ. (1994). Lectin staining of sheep migroglia. *Histochemistry* 102(6): 483-6.
12. Huse JT and Holland EC. Targeting brain cancer: advances in the molecular pathology of malignant glioma and medulloblastoma. *NRC* 10: 319-31.
13. Carmeliet P and Jain RK. (2010). Molecular mechanisms and clinical applications of angiogenesis. *Nature* 473: 298-307.
14. Stolberg S and McCloskey KE. (2009). Can Shear Stress Direct Stem Cell Fate? *Biotechnol. Prog.* 25(1): 10-19.
15. Hahn C and Schwartz MA. (2009). Mechanotransduction in vascular physiology and atherogenesis. *Nat. Rev. MCB* 10: 53-62.
16. Davies PF. (1995). Flow-Mediated Endothelial Mechanotransduction. *Physiol. Rev.* 75(3): 519-60.
17. Diop R and Li S. (2011). Effects of Hemodynamic Forces on the Vascular Differentation of Stem Cells: Implications for Vascular Graft Engineering. In: Gerecht S, editor. *Biophysical Regulation of Vascular Differentiation and Assembly*. New York: Springer. pp. 227-244.
18. Dekker RJ, *et al.* (2002). Prolonged fluid shear stress induces a distinct set of endothelial cell genes, most specifically lung Krüppel-like factor (KLF2). *Blood* 100: 1689-98.
19. Suzuki T, *et al.* (2005) Vascular Implications of the Krüppel-Like Family of Transcription Factors. *ATVB* 25: 1135-41.
20. Dong J-T and Chen C. (2009). Essential role of KLF5 transcription factor in cell proliferation and differentiation and its implications for human diseases. *Cell. Mol. Life Sci.* 66: 2691-2706.
21. Shindo T, *et al.* (2002). Krüppel-like zinc-finger transcription factor KLF5/BTEB2 is a target

for angiotensin II signaling and an essential regulator of cardiovascular remodeling. *Nat. Med.* 8(8): 856-63.
22. Schwachtgen J-L, *et al.* (1998). Fluid Shear Stress Activation of Egr-1 Transcription in Cultured Human Endothelial and Epithelial Cells Is Mediated via the Extracellular Signal-Related Kinase 1/2 Mitogen-activated Protein Kinase Pathway. *J. Clin. Invest.* 101(11): 2540-9.
23. Aizawa K, *et al.* (2004). Regulation of Platelet-derived Growth Factor-A Chain by Krüppel-like Factor 5: New Pathway of Cooperative Activation with Nuclear Factor-κB. *JBC* 279(1): 70-6
24. Yang XO, Doty RT, Hicks JS, and Willerford DM. (2003). Regulation of T-cell receptor Dβ1 promoter by KLF5 through reiterated GC-rich motifs. *Blood* 101(1): 4492-99.
25. Diop R. (2013). Effects of Laminar Fluid Shear Stress on the Function of Adult Stem Cells (Doctoral Dissertation). UC Berkeley: Bioengineering. Retrieved from http://oskicat.berkeley.edu/record=b22179210~S1
26. Abramoff MD, Magalhaes PJ, and Ram SJ. (2004). Image Processing with ImageJ. *Biophotonics International* 11(7): 36-42. Retreived from http://rsb.info.nih.gov/ij/docs/menus/analyze.html#gels on 15 June 2013.
27. Frangos, JA, Eskin, SG, McIntire, LV, and Ives, CL. (1985). Flow Effects on Prostacyclin Production by Cultured Human Endothelial Cells. *Science* 227: 1477-9.
28. Koh, W, Mahan, RD, Davis, GE. (2008). Cdc42- and Rac-1 mediated endothelial lumen formation requires Pak2, Pak4, and Par3, and PKC-dependent signaling. *JCS* 121: 989-1001.